DETAILED MODELLING AND OPTIMAL DESIGN OF MEMBRANE SEPARATION SYSTEMS

James Ingram Marriott

February 2001

A thesis submitted for the degree of Doctor of Philosophy
of the University of London

Department of Chemical Engineering
University College London

To Mog

Abstract

The search for alternatives to traditional energy intensive separation methods such as distillation has led to the introduction of processes based on membranes. In this research, the use of detailed mathematical models for the optimal design of membrane systems is investigated.

Mathematical models of hollow-fibre and spiral-wound membrane modules are presented in this thesis. The models are developed from rigorous mass, momentum and energy balances and can be used to describe a generic membrane separation. This is in contrast to most existing models which are typically process specific and are only valid within a limited operating range. The generality of the new approach is demonstrated by application to gas separation, pervaporation, and reverse osmosis case studies. Simulation results for these systems show excellent agreement with published experimental data.

The thesis also introduces an optimal design strategy for membrane separation systems. This strategy is characterised by two main features: firstly, detailed models are used. This is essential if sub-optimal and inaccurate solutions are to be avoided. Secondly, an optimisation technique based on genetic algorithms is implemented. This provides multiple solutions, allowing the user to interpret the results and make a more informed decision.

The feasibility of the optimal design strategy is investigated using two realistic case studies. In the first study, the optimal design of reverse osmosis desalination plants is considered and the use of both hollow-fibre and spiral-wound modules is examined. The results of this study compare favourably with work published in the open literature and highlight the importance of using detailed models to describe membrane separation systems. In the second study, the use of pervaporation for ethanol dehydration is investigated. An existing pervaporation plant is evaluated and a significantly improved design is found.

ACKNOWLEDGEMENTS

Most importantly, I would like to express my gratitude to my supervisor Dr Eva Sørensen. Her active guidance and support have been invaluable to me. I would also like to thank Professor David Bogle for his contributions both to this research and to my general academic progress.

Numerous members of the Chemical Engineering department at UCL (too many to list, but they know who they are!) have helped me solve many of the problems that I have encountered during this research. Their help and company were gratefully appreciated. Special mention should go to Hooi Khim Teoh for helping to proof this thesis.

Thanks also to my family and friends, who all valiantly pretended to understand my work.

Finally, I would like to acknowledge financial support from the Engineering and Physical Sciences Research Council and from the Centre for Process Systems Engineering.

Table of contents

List of figures

List of tables

Chapter 1

INTRODUCTION

This chapter provides an introduction to membrane technology and to this thesis. In the first section, important background information is presented (Section 1.1). Next, the motivating factors and objectives for this research are discussed (Section 1.2). In the final section, the structure of this thesis is outlined (Section 1.3).

1.1 Background

During the last thirty years, the search for viable alternatives to traditional energy intensive methods such as distillation, has led to the introduction of separation processes based on membranes. Membrane technology often offers cheaper capital and utility costs and has displaced conventional separation techniques in many areas. Wider use is expected in the future (Ho and Sirkar, 1992). The increasing market for membrane technology has motivated interest in the development of reliable design strategies that aim to optimise the economic performance of membrane separation systems (El-Halwagi, 1992; Qi and Henson, 2000). To this end, the application of rigorous mathematical models to the optimal design of membrane separation systems is explored in this thesis.

This section presents essential background information. First, the basic definition of a membrane is given, then the various applications of membrane technology are assessed. In the final part of the section, the important types of commercial membrane unit are described.

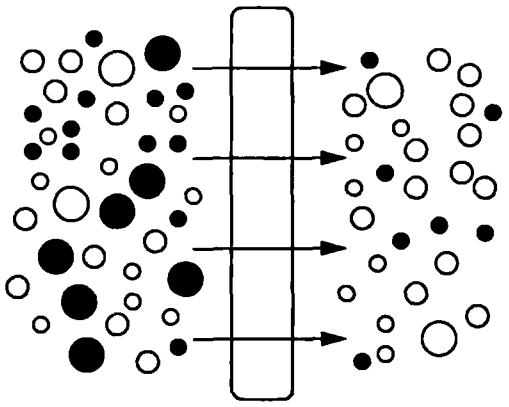

Figure 1.1 *Molecular transport through a membrane*

1.1.1 The properties of membranes

Membranes have been defined in various ways; Mulder (1996) suggests that a membrane is a "selective barrier between two phases", whereas Ho and Sirkar (1992) describe it as an "interphase between two bulk phases". Membranes can take many forms, from porous and non-porous solids to liquid phase membranes and gels. Currently, most industrial processes are based on polymeric materials. These are either microporous, with pores typically up to 20 Å, or dense with no discernible pores.

Molecules are driven across a membrane when subjected to a gradient in chemical or electrical potential. This is often the result of a concentration or pressure difference between the two phases. Selection of the correct membrane is imperative as both the speed and nature of this transport are functions of membrane structure. The speed of transfer also depends upon the physical properties of the permeating material such as its molecular size. Thus the introduction of a membrane between two phases permits the selective transfer of components and thereby facilitates their separation, Figure 1.1.

1.1.2 Membrane separation technology

In most membrane separations, the *feed* stream is split into two product streams: the *permeate* and the *retentate*. The permeate is the material that has passed through the membrane and the retentate is the material that has been rejected by the membrane. This is illustrated in Figure 1.2. Membrane technology can be applied to particle - liquid separation, liquid - liquid separation as well as gas separation. Each of these alternatives are now considered, and a summary is shown in Figure 1.3.

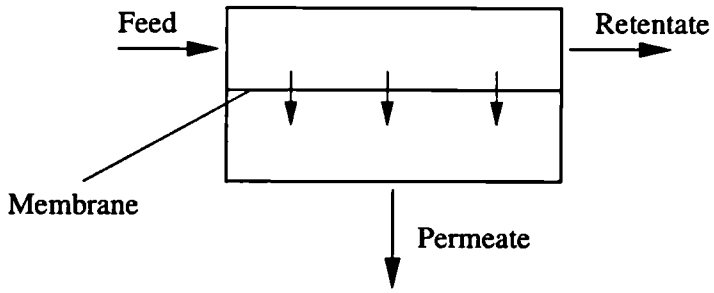

Figure 1.2 *Schematic representation of a simple membrane separation*

Particle - liquid separation

The use of membranes for the separation of particles from liquids is now firmly established. In this field, there are several well developed categories

In **dialysis**, microsolutes pass through a semi-permeable membrane when driven by a difference in concentration. A separation is achieved as smaller solutes diffuse through the membrane at a faster rate than larger macrosolutes. In **electrodialysis**, electrical potential is the driving force for mass transfer across the membrane rather than a concentration gradient.

Reverse osmosis, or *hyperfiltration*, differs from dialysis and electrodialysis in that the membrane selectively restricts the flow of solutes whilst allowing the flow of the solvent. The driving force for *solvent* transfer through the membrane is a pressure difference which must exceed the osmotic pressure of the solution. Large pressure differences (10 to 100 bar) are usually required to overcome the high resistances of reverse osmosis membranes. It is generally considered that the main mechanism for *solute* transfer through the membrane is a concentration gradient. Reverse osmosis technology can be used for particles up to about 3 x 10^{-9}m in diameter, though for the larger particle sizes (1 to 3 x 10^{-9} m) it is often referred to as *nanofiltration.*

Ultrafiltration can be used for separating larger solutes (3 x 10^{-9} to 1 x 10^{-7}m) such as sugars from their solvent. Although this method is theoretically identical to reverse osmosis, from a practical point of view the separation of larger molecules causes additional problems such as membrane fouling. The membranes used in ultrafiltration are less dense than those used in reverse osmosis and so high fluxes can be achieved using much smaller pressure differences (typically 1 to 5 bar). **Microfiltration** is used to separate micron sized particles (1 x10^{-7} to 3 x 10^{-6}m) from a suspension; it is similar to both ultrafiltration and conventional filtration. The resistance of microfiltration membranes is low and small pressure differences (0.1 to 2 bar) are usually sufficient.

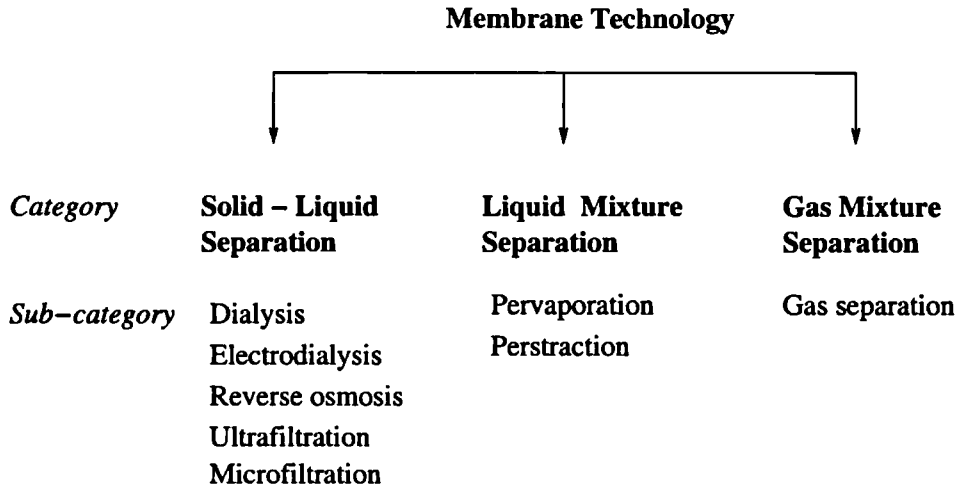

Figure 1.3 *Membrane separation technology*

Liquid - liquid separation

The constituents of a multi-component liquid feed will pass through a dense membrane when driven by a concentration gradient. The liquid - liquid separation sector divides neatly into two categories

In **pervaporation**, the membrane represents a barrier between the liquid (the feed) phase and a gaseous (permeate) phase. The permeate is pulled off, either by a sweep gas or into a vacuum. In this process, liquid molecules diffuse across the membrane and undergo a phase change referred to as permselective evaporation. In order to provide the heat of evaporation, the enthalpy of the feed stream is reduced. The resulting temperature drop can be large, particularly at the relatively high flux rates seen for concentrated systems. To compensate for this effect, interstage heaters are often employed between membrane modules.

Perstraction is different to pervaporation in that the permeating components desorb into a purge or sweep liquid rather than into a gaseous phase so unlike pervaporation, it is an isothermal process. However, fluxes are much lower and there are no current examples of industrial perstraction (Ho and Sirkar, 1992).

Gas separation

Gas molecules are driven through the membrane when subjected to a partial pressure difference. The gas that dissolves and passes through the membrane most quickly (the

fast gas) is collected as permeate. In general, only dense membranes provide a high enough degree of separation, though in some cases microporous membranes are used, such as in the separation of uranium isotopes.

Emerging processes

Growth in the use of membranes is increasing rapidly and new technologies are still being identified and developed. These processes include: **membrane distillation** - a thermally driven process; **membrane based solvent extraction** - where the membrane is used to separate the two immiscible phases; and **vapour permeation** - which is similar to pervaporation but uses an already vaporised feed stream.

A comprehensive review of membrane separation processes is given in the "Membrane Handbook" edited by Ho and Sirkar (1992). Table 1.1 shows the main characteristics and applications of commercial membrane processes.

1.1.3 Membrane modules

The large membrane area required for commercial separations is tightly packaged into membrane modules. A number of different membrane geometries have been developed for this purpose, but the same design criteria apply in each case. Firstly, for efficient mass transfer it is essential that there is good contact between the membrane and the fluids flowing through the module. Secondly, to minimise capital costs and plant size, the module must provide as much membrane area per unit volume as possible (the *packing density* of the module). Other important aspects include: the cost of manufacture, the fluid-dynamics inside the module, ease of cleaning, and the cost of replacing the membrane.

Four types of membrane module are in common use in the process industries: tubular modules, plate-and-frame modules, spiral-wound modules, and hollow-fibre modules. These are now described, with greater emphasis placed on the latter two. This thesis focuses on spiral-wound and hollow-fibre modules because of their greater commercial and technical importance. These configurations now dominate most commercial membrane processes, accounting for almost all new reverse osmosis systems (Bhattacharyya *et al.*, 1992). This is primarily because they offer much larger mass transfer areas than those provided by either tubular or plate-and-frame modules.

Table 1.1 *Characteristics and applications of industrial membrane technology (Ho and Sirkar, 1992)*

Technology	Species transported through the membrane	Driving force	Applications	Typical membrane material
Dialysis	Microsolutes	Concentration gradient	Haemodialysis Sodium hydroxide recovery in rayon processing	Microporous membrane, polymeric
Electrodialysis	Microionic species	Electro-potential gradient	Desalination of water Production of table salt	Ion exchange resin
Reverse osmosis	Solvent	Pressure gradient	Desalination of water Wastewater and hazardous water treatment	Dense membrane, polymeric
Ultrafiltration	Solution of macrosolutes	Pressure gradient	Dairy applications Fruit juice clarification	Microporous membrane, usually polymeric
Microfiltration	Particulate solution	Pressure gradient	Sterilisation of pharmaceuticals and food Antibiotic clarification	Microporous membrane, ceramic or polymeric
Pervaporation	The most volatile/smallest liquid species	Concentration gradient	Dehydration of organic solvents Removal of organics from water	Dense membrane, polymeric
Gas separation	*Fast* gas	Partial pressure gradient	H_2 or He recovery O_2/N_2 separation	Dense or microporous membrane, polymeric

Tubular module

Tubular membrane units are supported on the inside of perforated (or porous) pressure-tight tubes (12 to 25mm in diameter). Feed is usually passed through the inside of the membrane tubes. Although areas for mass transfer are not as large as in spiral-wound and hollow-fibre membranes, tubular membranes are less susceptible to fouling and are easier to clean (Brouckaert and Buckley, 1992).

Plate-and-frame module

Similar in principle to a filter press, this is perhaps the simplest and most robust type of module. Two membranes are placed one on top of another and the feed flows in flat channels between them. Packing densities for these modules vary from 100 to 400 m^2/m^3. Plate-and-frame modules are still commonly used for pervaporation.

Spiral-wound module

Spiral-wound modules are essentially flat membrane sheets separated by highly porous spacer material. The modules are relatively simple to build and have a high packing density ($> 900m^2/m^3$), but are difficult to clean.

Spiral-wound modules are constructed from a number of membrane envelopes. Two membrane sheets are glued together on three sides to form an envelope. The fourth edge is attached to a central collecting tube, around which one or more envelopes are wound. The feed flows parallel to the central tube outside the membrane envelopes (axially). Material permeates into the interior of the membrane envelopes and flows along the spiral, towards the central tube. The modules are almost always operated with a cross-current flow pattern. A spiral-wound module is illustrated in Figure 1.4.

Spiral-wound modules are housed in pressure vessels. Each vessel contains several modules connected in series. Long pressure vessels are often used to minimise capital investment, however, this can result in high pressure losses. The effect is most significant for lower pressure reverse osmosis systems, for which smaller pressure vessels are often preferred. Van der Meer *et al.* (1998) carried out a simple economic optimisation using modern high flux composite membranes and reported an optimum figure of three to four modules per pressure vessel. A pressure vessel assembly for three spiral-wound modules is illustrated in Figure 1.5.

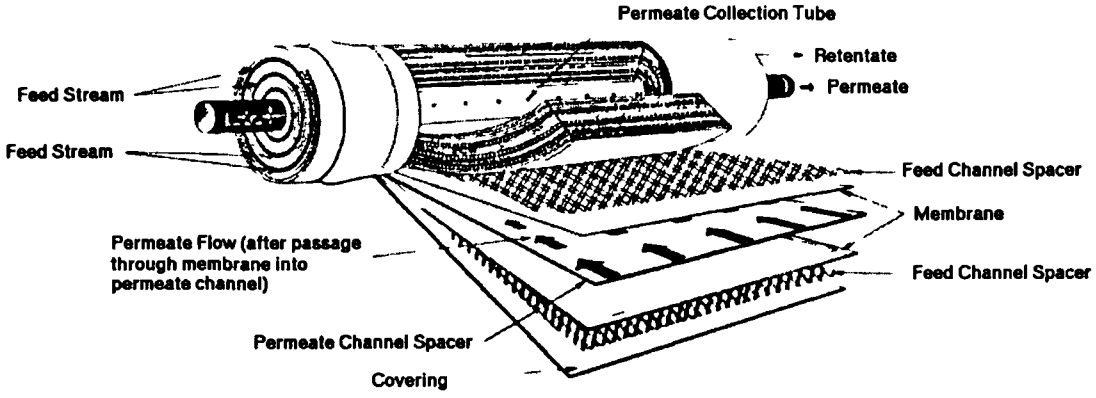

Figure 1.4 *A spiral-wound module, adapted from Bhattacharyya et al. (1992)*

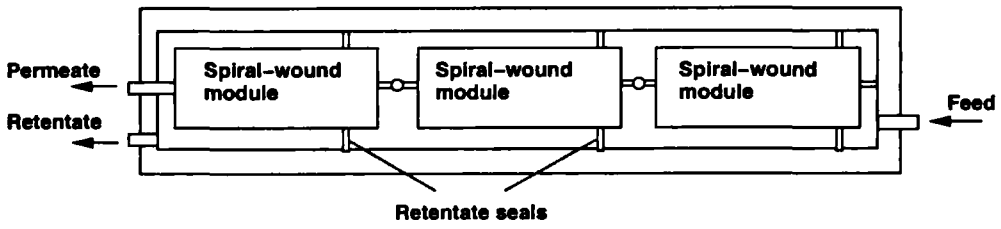

Figure 1.5 *Pressure vessel assembly for three spiral-wound modules, adapted from Bhattacharyya et al. (1992)*

Hollow-fibre module

Hollow-fibre modules contain a large number of membrane "tubes" which are housed in a module shell (or pressure vessel). This configuration has an extremely high packing density ($> 10{,}000 m^2/m^3$) due to the small diameter of the fibres ($\approx 10^{-5}$m). However, membrane permeability is usually lower than in spiral-wound modules (Bhattacharyya *et al.*, 1992) and they are also difficult to clean.

Feed is usually introduced outside the hollow-fibre with material permeating into the interior. The feed mixture may flow through the fibre bundle radially or parallel to the hollow-fibres. For gas separation, parallel (counter-current) flow modules are generally used, whereas the cross-flow pattern seen in radial flow modules is preferred for reverse osmosis (Rautenbach and Albrecht, 1989). It is equally possible to pass the feed through

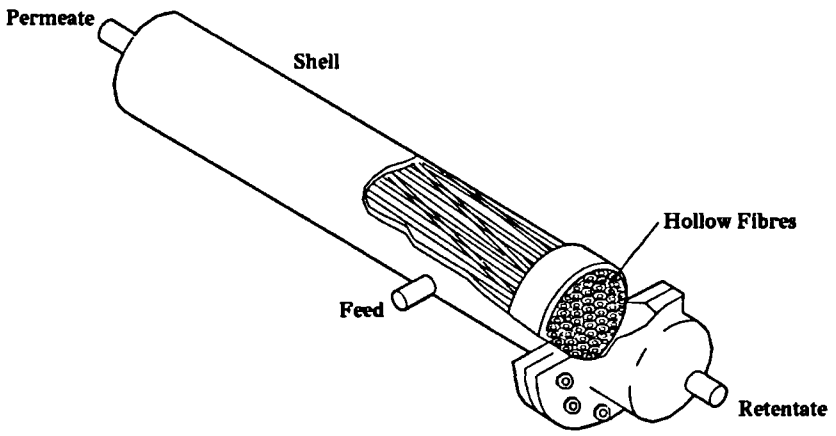

Figure 1.6 *A hollow-fibre module, adapted from Bhattacharyya et al. (1992)*

the interior of the fibres and remove the permeate from the module shell. This mode of operation is often used for pervaporation where pressure build up in the permeate stream is critical and can be avoided more easily in the module shell. A hollow-fibre module is illustrated in Figure 1.6.

1.2 Objectives and motivations

In many areas of chemical process design and operation, the use of mathematical models for process synthesis, optimisation and for control studies has shown significant benefit. These methods are beginning to be applied to the design of membrane processes (El-Halwagi, 1992; Qi and Henson, 2000) and are explored further in this thesis.

To minimise the technical risk that is inherent in the design of any new process, it is essential that unit models that accurately describe the process behaviour are used. This is particularly important for membrane systems which are usually competing with well-understood traditional separation techniques such as distillation. For membrane technology to compete, it is necessary to gain a greater understanding of the process so that better and more reliable designs can be implemented without the need for time-consuming experimental and pilot studies. This can be done through accurate and reliable simulations. *This requires a rigorous modelling approach.*

In the past two decades there has been a huge research effort developing models that characterise the separative properties of membranes (Ho and Sirkar, 1992). In compar-

ison, far fewer models describing the whole membrane module have been developed. In fact, to the best of the author's knowledge, a detailed model of a general membrane separation process is not currently available from published literature. Although a number of unit models do exist (e.g. Krovvidi *et al.*, 1992; Qi and Henson, 1997; Coker *et al.*, 1998), due to the complex nature of flow through membrane modules these usually have to rely on a variety of fixed assumptions. As a result of these assumptions, existing models are typically process specific and are only valid within a limited operating range. *The first objective of this work is therefore to develop a detailed model of a general membrane separation.*

The estimation of transport parameters for membrane modules is often achieved by fitting mathematical models to experimental data (see for example Ohya and Taniguchi, 1975). Clearly, the accuracy of the transport parameters is dependent on the validity of the model that was used to describe the membrane module. To reduce the uncertainty in the parameter values this thesis investigates the application of detailed models to *parameter estimation.*

To realise the full potential of membrane technology it is important that all the degrees of freedom are explored when a separation system is designed. Although simulation studies are useful for this purpose, they are unable to account for the interacting nature of all the design choices. Therefore, in this research, *optimisation techniques* are employed to determine the best way to design membrane separation systems.

Conventionally, optimisation problems are solved using gradient-based solution techniques. These return a single, sometimes sub-optimal, solution and provide little insight into the design problem. In reality, design engineers are often faced with a number of qualitative decisions that cannot easily be described mathematically. *This thesis establishes a solution technique which provides multiple solutions at the end of the optimisation allowing the user to interpret the results and make an informed decision.*

Although simple unit models have previously been used to optimise the operating conditions of a given membrane system (e.g. Ji *et al.*, 1994; Tessendorf *et al.*, 1999), full structural optimisation has only been carried out using approximate models (e.g. El-Halwagi, 1992; Srinivas and El-Halwagi, 1993; Qi and Henson, 2000). Unfortunately, inaccuracies in modelling the membrane modules will lead to the development of sub-optimal plant designs with the possible over (or under) prediction of plant performance and a lack of generality due to implicit assumptions. *In this research, the use of rigorous mathematical models (verified against experimental data) for the optimal design of membrane systems is explored.*

In summary, this thesis is concerned with the development of tools that help in the understanding and design of membrane systems. The objectives of the work are

1. The development of a detailed mathematical model of a general membrane separation.
2. The use of the above to determine the optimal design of membrane separation systems.

1.3 Scope of the thesis

Membrane technology is a wide and varied field, therefore this thesis concentrates on three different types of membrane separation: gas separation; pervaporation; and reverse osmosis. These are among the most important commercial membrane processes and encompass the main separation types (see Figure 1.3). From an academic point of view, these separations are also of great interest as they provide alternatives to more traditional separation techniques like distillation. The simulation of each of these separations will be investigated using a new generic modelling approach that can consider both hollow-fibre and spiral-wound modules (Chapter 3). Later in the thesis, the optimal design of reverse osmosis and pervaporation systems is given particular attention (Chapters 5 and 6).

In *Chapter 2*, a review of the important literature on membrane transport and module mathematical models is presented. Previous work that considers the optimal design of membrane separation systems is also discussed.

Chapter 3 introduces a new theoretical approach to modelling hollow-fibre and spiral-wound modules. The use of the model for gas separation, pervaporation and reverse osmosis is demonstrated and the results compared against published experimental data.

Next, in *Chapter 4*, an optimisation strategy for the structural design of membrane separation processes is described. The method is based on genetic algorithms and uses the detailed membrane model introduced in the previous chapter.

In *Chapter 5*, the optimal design of a reverse osmosis system is considered. The detailed model is verified against experimental data for hollow-fibre and spiral-wound modules. Then, using the detailed model and the design methodology outlined in the previous chapter, a well established desalination case study is considered. The use of approximate design models for membrane system design is also assessed and is shown to lead to inferior results.

The design of pervaporation systems is considered in *Chapter 6*. An existing pervaporation plant for ethanol dehydration is evaluated using the detailed model. The methodology presented in Chapter 4 is applied to the case study and a significantly improved design is found. The study is also used to compare the optimisation strategy with a more conventional gradient-based solution technique.

Finally, in *Chapter 7*, conclusions are presented and possible directions for future work are discussed.

Chapter 2

LITERATURE REVIEW

This chapter presents a critical review of the published literature on the use of mathematical models for membrane system design. The review is presented by subject area (rather than chronologically) because of the diversity of material covered.

2.1 Introduction

There are three aspects to consider when modelling membrane separation processes: the transport of material across the membrane; the flow of material through the membrane module; and the design of the complete separation system. These aspects are all considered in this chapter.

Section 2.2 is concerned with the mass transport of material through porous and dense membranes. The following issues are addressed in detail

- Molecular transport through porous membranes
- Molecular transport through dense membranes (the solution-diffusion model)
- General transport models that describe both porous and dense membranes
- Other resistances to mass transport (such as concentration polarisation and fouling)

Mathematical models of the whole membrane module are reviewed in Section 2.3. This considers

- Restrictive assumptions used in the development of membrane module models
- Unit models of hollow-fibre modules
- Unit models of spiral-wound modules
- Approximate models used for quick design calculations
- Available numerical solution techniques

In Section 2.4, previous work that considers the optimal design of reverse osmosis, pervaporation and gas separation systems is assessed.

Finally, conclusions on the use of mathematical models for the design of membrane systems are presented in Section 2.5.

First, however, an initial definition of some important terms and parameters is required for an understanding of the material reviewed in this chapter.

Definitions

The driving force for mass transport across the membrane is the chemical potential gradient. As discussed in Section 1.1, this is usually generated by imposing a pressure or concentration gradient. For example, in pervaporation, the driving force is generally regarded as being a concentration difference, for gas separation it is a partial pressure difference and in reverse osmosis it is the hydrostatic pressure difference. Although in the last case, the osmotic pressure difference (discussed below) must also be considered.

In general terms, for porous and dense membranes, the specific rate of transport (or flux, J_i) can be written

$$J_i = Q_i \frac{d(driving force)}{dz^m} \tag{2.1}$$

The permeability, Q_i, cannot always be modelled as a constant, although in some cases, particularly for gas separation, this may be adequate. It should be noted that as the driving force for mass transport can vary, so will the units of permeability.

The ability of a membrane to distinguish between two species can be measured in a number of ways. A common definition is the *separation factor*, α, which is written

$$\alpha = \frac{x_{2i}/x_{1i}}{x_{2j}/x_{1j}} \tag{2.2}$$

Additionally, the *ideal separation factor*, α^*, which is commonly used to determine the maximum separation efficiency, is defined as

$$\alpha^* = \frac{Q_i}{Q_j} \tag{2.3}$$

In most reverse osmosis systems, the *osmotic pressure* difference across the membrane must be taken into account. This is the pressure difference that must be imposed across a membrane (porous or dense) to prevent solvent molecules passing from a dilute phase to a concentrated phase. The osmotic pressure of a mixture is given by

$$\Pi = (\rho_i^m R'T) ln(a_i) \tag{2.4}$$

However, in most cases, it is assumed that the osmotic pressure is proportional to the solute concentration and is thus described by the van't Hoff relationship (Rautenbach and Albrecht, 1989)

$$\Pi = gR'Tc_i \tag{2.5}$$

For non-dissociated solutions (organic compounds), the empirical constant, g, has a value close to one. However, for electrolytes this is not the case: e.g. for sodium chloride solutions $g \approx 1.86$.

2.2 Characterisation of membranes

This thesis is mainly concerned with the performance of the membrane modules that make up the separation process. Thus, the focus is on developing accurate descriptions of the flow either side of the membrane. Nevertheless, if the performance of the module is to be predicted correctly, an accurate characterisation of the membrane itself is critical. Therefore, in this section, the transport of liquids and gases through porous and

dense membranes is discussed in some detail. In-line with the rest of the thesis, we will concentrate on pervaporation, gas separation and reverse osmosis processes.

This section commences with a look at the transport of liquids and gases through porous membranes. This is followed by a review of models used to characterise liquid and gas transport through dense membranes. Next, general approaches to modelling both types of membrane are discussed. Finally, other resistances to mass transport such as concentration polarisation and fouling are considered. The main transport models described here are summarised at the end of this section in Table 2.1.

2.2.1 Porous membranes

Gas and liquid transport through porous membranes are somewhat different and hence are now considered separately.

Gas systems

Gas molecules are driven through a porous membrane by a pressure gradient. There are two main mechanisms of capillary flow through membrane pores: Knudsen diffusion, where molecules interact with the pore walls more frequently than with each other; and viscous flow. In both cases, the flux of molecules through a single pore, J_i, is expressed

$$J_i = Q_i \frac{\Delta P}{\delta m} \tag{2.6}$$

Where for Knudsen diffusion (Rangarajan *et al.*, 1984), the permeability can be given by

$$Q_i = \frac{4R^p}{3}\left(\frac{2}{\pi M_i R' T}\right)^{1/2} \tag{2.7}$$

and for viscous flow, the Hagen-Poiseuille model (Bird, *et al.*, 1960) is used

$$Q_i = c_i\left(\frac{(2R^p)^2}{32\mu}\right) \tag{2.8}$$

The dominant flow mechanism is generally regarded as a function of the mean free molecular path, λ, and of the pore radius, R^p. Knudsen flow is predominant when the pore radius is much smaller than the mean free path and viscous flow when much larger. Rangarajan *et al.* (1984) use the following criteria

$R^p/\lambda < 0.05$ Knudsen flow dominates

$R^p/\lambda > 50$ Viscous flow dominates

The transition region between the different flow mechanisms is difficult to model, various authors (Schofield *et al.*, 1990; Lawson and Lloyd, 1996) have used correlations to combine the Knudsen and viscous flow models. However, as viscous flow is generally non-separative, porous membranes are usually designed to operate in the Knudsen region. The ideal separation factor for Knudsen separation, calculated from Eq. 2.3 is

$$\alpha^K = \sqrt{\frac{M_j}{M_i}} \tag{2.9}$$

The ratio M_i/M_j is usually small and so the separability of porous membranes is generally much lower than those of dense membranes. Thus, the use of porous membranes for gas separation is rare.

Solvent - solute systems

The transport of liquids through porous membranes is more complicated as the osmotic pressure (Section 2.1) of the feed and permeate solutions is usually significant. Hence, the flux of solvent (J_i) through ultrafiltration and reverse osmosis membranes is usually written

$$J_i = \frac{Q_i}{\delta^m}(\Delta P - \Delta\Pi) \tag{2.10}$$

For microporous membranes, viscous forces tend to dominate and the Hagen-Poiseuille model is again used to characterise the resistance of the membrane (Eq. 2.8). The rejection of solute particles by the membrane must also be characterised. A number of models are used to describe particle rejection by microporous ultrafiltration membranes; these are reviewed by Deen (1987). However, ultrafiltration is outside the scope of this thesis and will be not be discussed further.

Reverse osmosis membranes do not generally contain pores. Hence, models for dense membranes are usually used to describe solute rejection in reverse osmosis, these are discussed in the following section.

2.2.2 Dense membranes

The majority of models for dense membranes consider mass transport to be a three stage process: sorption of the components into the membrane; transport or diffusion through the membrane; and then desorption on the downstream side. Such models are referred to as *solution-diffusion* type models (Greenlaw *et al.*, 1977).

The solution-diffusion model

This model is used widely to describe gas permeation, pervaporation and reverse osmosis systems. The premise for such processes is that the transport is driven by a concentration (or activity) gradient in the membrane. Thus the simplest and widest used model describing the transport of components across a membrane is Fick's law, where the flux is proportional to the concentration gradient

$$J_i = D_i \frac{dc_i^m}{dz^m} \tag{2.11}$$

This simple diffusion model can be used to describe gas, liquid and solute transport through the membrane. In many cases, the concentration gradient across the membrane can even be assumed to vary linearly (Hickey and Gooding, 1994), reducing the equation to a simple form

$$J_i = D_i \frac{c_{i1}^m - c_{i2}^m}{\delta^m} \tag{2.12}$$

Equilibrium is generally assumed at the phase boundaries (Greenlaw *et al.*, 1977). To describe the equilibrium relationship between the concentration in the bulk (c_i) and in the membrane (c_i^m), several sorption isotherms have been proposed. These include the dual sorption model (Koros, 1980) and the UNIQUAC model (Heintz and Stephan, 1994). However, most commonly, ideal behaviour is assumed (Henry's law). In this case, the solution-diffusion model is simply written

$$J_i = Q_i \frac{c_{i1} - c_{i2}}{\delta^m} \tag{2.13}$$

The application of Fick's law to membrane characterisation assumes that any pressure gradient has negligible effect on mass flux. Mulder *et al.* (1985) suggest that the solution-diffusion model in its most general form is expressed

$$J_i^v = Q_i \frac{d\psi_i}{dz^m} \tag{2.14}$$

This simplifies back to Fick's law if the pressure gradient is neglected and if ideal solution behaviour is assumed (Mulder *et al.*, 1985; Mason and Lonsdale, 1990). Furthermore, Muldowney and Punzi (1988) demonstrate how this reduces to Equation 2.10, which describes solvent flux, if a number of simplifying assumptions are made.

Unfortunately, permeability is often a strong function of concentration. This dependence is often described empirically by a two parameter exponential relationship (Mulder *et al.*, 1985)

$$Q_i = Q_{i0} e^{(\kappa_i c_i)} \tag{2.15}$$

Mulder *et al.* (1985) state that the constant κ represents the plasticising effects of the penetrant on the membrane.

There has also been considerable work, by among others Mulder *et al.* (1985) and Soltanieh and Zaare-Asl (1996), adapting the solution diffusion model to account for driving force coupling. This effect is especially apparent in the pervaporation of ethanol and water where it is believed to occur due to the creation of ethanol-water dimmers which travel through the membrane together (Soltanieh and Zaare-Asl, 1996).

Pore-flow models

A contrasting approach to those based on a solution-diffusion type mechanism has been to consider dense membranes to contain straight cylindrical pores. Much of the work using this model has been carried out by Sourirajan, Matsuura, and co-workers (e.g. Matsuura and Sourirajan, 1981; Farnand *et al.*, 1987) in relation to reverse osmosis. More recently, several authors (Okada and Matsuura, 1991; Tyagi *et al.*, 1995) have applied a similar approach to other permeation processes. However, Muldowney and Punzi (1988) have shown that for reverse osmosis, the model predictions are similar to those from a solution-diffusion approach.

2.2.3 General membrane models

Most of the mass transport models described previously suffer from non-constant parameters and are unable to predict some of the complex phenomena inherent to membrane separations (such as flux coupling). In response, attempts have been made to develop more theoretical models. There are two detailed approaches which incorporate a greater understanding of the nature of flux thorough a membrane: the dusty gas model and the frictional model. The results of the two theories are in fact very similar, and both reduce to other models such as Fick's law if simplifying assumptions are made (Mason and Lonsdale, 1990; Heintz and Stephan, 1994). The models can be used to describe flux through both microporous and dense membranes for all membrane separation processes. A third approach applied to a variety of membrane processes is to characterise membrane performance using the thermodynamics of irreversible processes (e.g. Molina *et al.*, 1997).

Dusty gas model The dusty gas model has gradually been developed by Mason and co-workers (Mehta *et al.*, 1976; Mason and Lonsdale, 1990) over a number of years from a statistical-mechanical approach. The original model first derived for gas systems has been developed further to describe a general separation using chemical potential as the driving force. The main feature of the model is that viscous and diffusional effects are considered separately. The dusty gas model for isothermal flux in the absence of external forces can be written

$$\sum_{j=1}^{n} \frac{(x_i J_j - x_j J_i)}{c_\Sigma D^D_{i,j}} - \frac{J_i}{c_\Sigma D^D_{im}} - \frac{\alpha^D_i B_o}{\mu D^D_{im}} \nabla P = \frac{x_i}{R'T} \nabla_{T,P} \psi_i + \frac{x_i}{c_\Sigma R'T} \nabla P \qquad (2.16)$$

Frictional model The Stefan-Maxwell equation (Kerkhof, 1996) equates frictional resistances to driving forces. It was first used to characterise membrane performance by Lightfoot (1974) and can be written (Kerkhof, 1996)

$$\sum_{j=1}^{n} \frac{(x_i J_j - x_j J_i)}{c_\Sigma D^F_{i,j}} - \frac{J_i}{c_\Sigma D^F_{im}} = \frac{x_i}{R'T} \nabla_{T,P} \psi_i + \frac{\phi_i}{c_\Sigma R'T} \nabla P \qquad (2.17)$$

The model parameters (D^F) can either be interpreted as frictional resistances or as diffusional coefficients.

The difference between the dusty gas and frictional models is in the approach to viscous

effects. The dusty gas model incorporates an additional term to account for viscous flux. Mason and Lonsdale (1990) showed that the models are algebraically equivalent if the frictional coefficients are regarded as "augmented diffusion coefficients" incorporating viscous effects. However, Kerkhof (1996) contends that they are in fact real diffusion coefficients and that the differences in the model are errors in the dusty gas model which provides double counting of the viscous terms.

In general, the dusty gas model requires five parameters to describe isothermal flux through a membrane for a binary mixture, whereas a frictional approach requires four. In both cases, experimental data is still required, although some of the parameters can be predicted from standard diffusional and membrane data (Lawson and Lloyd, 1996).

Irreversible thermodynamics This classical theory assumes that the flux of any species is a linear relationship of the generalised forces. The membrane performance is then simply characterised by the values of phenomenological coefficients. The main advantage of the theory is that it does not require any knowledge of the transport mechanisms involved and is therefore applicable to any membrane permeation process (Molina *et al.*, 1997). It also automatically accounts for any coupling of the various fluxes through the membrane. The disadvantage is that the phenomenological coefficients cannot be derived and so must be investigated experimentally over a range of conditions for a given separation to create a useful model.

A number of variations on the model have been developed for a range of different membrane systems by making several simplifications. An important example is the widely used Kedem-Katchalsky model (Solantieh and Gill, 1981) which considers the use of reverse osmosis for desalination. This can be written

$$J_W = Q_W \left[(P_1 - P_2) - \sigma \left(\Pi_1 - \Pi_2 \right) \right] \tag{2.18}$$

$$J_s = (1 - \sigma)\, \bar{c}_{s,lm} \frac{J_W}{c_{w1}} + Q_s \left(c_{s1} - c_{s2} \right) \tag{2.19}$$

Although this model suffers from concentration dependent parameters, Solantieh and Gill (1981) report that the dependence is not as great as that using solution-diffusion based models.

2.2.4 Other resistances to mass transfer

The membrane itself is not the only resistance to mass transfer, for example many membranes are supported on a porous material. Although the effect of the support is often neglected, it can be modelled in a similar manner to a porous membrane (Singh *et al.*, 1995). The resistances (reciprocal of the permeability) can be summed using a resistance-in-series approach analogous to the that used for electrical resistances in series (Zolandz and Fleming, 1992)

$$\Omega_{total} = \Omega_{porous} + \Omega_{memb} \tag{2.20}$$

thus,

$$\frac{1}{Q_{total}} = \frac{1}{Q_{porous}} + \frac{1}{Q_{memb}} \tag{2.21}$$

Furthermore, the flux of material can be much slower than expected due to additional resistances such as fouling and as a result of concentration boundary layers. These are now considered.

Concentration polarisation

When a mixture passes through a membrane there will usually be a build up of the slower penetrant towards the interface and a depletion of the faster penetrant. This is referred to as *concentration polarisation* and is illustrated in Figure 2.1. Excessive concentration polarisation not only retards the productivity of a membrane plant, it can also cause precipitation (scaling) and thus reduce the life of the membrane. Although the effect of concentration polarisation on the overall mass transfer coefficient in gas systems is usually negligible (Mulder, 1996; Narinsky, 1991), it can have a considerable effect on the overall resistance in solvent systems such as reverse osmosis.

To measure the severity of this effect, the concentration polarisation factor is used. It is defined as the ratio of concentration at the membrane surface to that in the bulk flow. For reverse osmosis, membrane manufacturers recommend maximum values between 1.2 and 1.4 (Taylor and Jacobs, 1996).

The effect of concentration polarisation is generally reduced at higher velocities when mixing effects (such as turbulence) are greater. For many membrane systems this creates an interesting trade-off between concentration polarisation and pressure drop. The

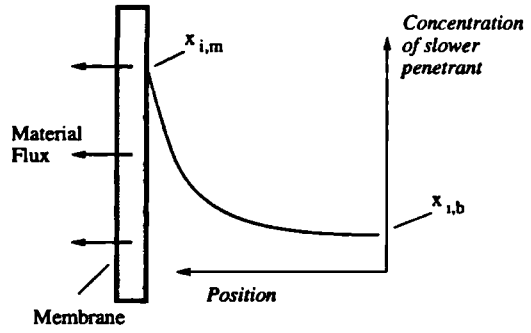

Figure 2.1 *Build up of the slower penetrant (concentration polarisation)*

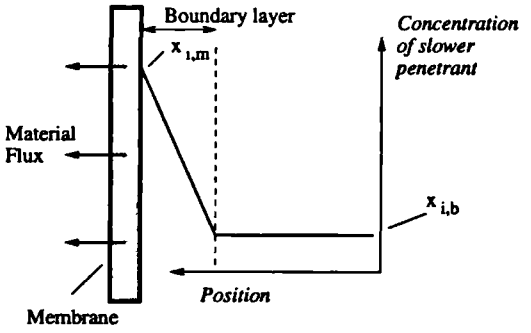

Figure 2.2 *Stagnant film model for concentration polarisation*

latter *increases* with velocity which, like concentration polarisation, detrimentally effects membrane performance. This is further investigated later in this thesis when the optimal design of a reverse osmosis system is examined (Chapter 5).

Concentration polarisation is often described by the **stagnant film model** (Brouckaert, 1992; Zydney, 1997). This model assumes that there is a thin (liquid) film, or boundary layer, next to the membrane of thickness δ. The distance δ is controlled by the flow conditions such as the fluid velocity and the diffusion coefficient D. Across the boundary layer, the concentration changes from $x_{i,b}$ (the bulk concentration) to $x_{i,m}$ (the concentration at the membrane surface), this is illustrated in Figure 2.2. From a simple one-dimensional mass balance, the stagnant film model can be written (Kulkarni *et al.*, 1992)

$$x_{i_m} = \frac{J_i}{J_\Sigma} + \left(x_{i_b} - \frac{J_i}{J_\Sigma}\right) exp\left(\frac{-J_\Sigma}{\rho k}\right) \tag{2.22}$$

where k ($=\frac{D}{\delta}$) is the mass transport coefficient. This is usually calculated from empirical correlations such as that used by Winograd *et al.* (1973).

Fouling

Over the life cycle of an industrial membrane a significant decrease in flux is often seen (see Figure 2.3). This is mainly a result of fouling and is usually irreversible. Processes using porous membranes such as microfiltration and ultrafiltration are much more sus-

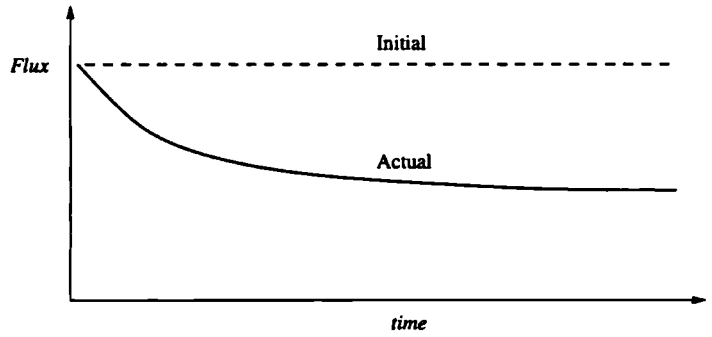

Figure 2.3 *The effect of fouling on the flux of material through the membrane*

ceptible to fouling than those based on dense membranes such as reverse osmosis. Mulder (1996) states that fouling is complex and is difficult to describe theoretically. Nevertheless, several models have been developed to describe membrane fouling (e.g. Al-Ahmad and Aleem, 1993; Bacchin *et al.*, 1995).

Many membrane processes will require some form of feed pre-treatment in order to minimise the degree of fouling and prevent contaminants from damaging the membrane. Pre-treatment is both membrane and feed specific (Taylor and Jacobs, 1996) and usually involves a large number of steps. Pre-treatment will often include microfiltration, pH adjustment, the addition of antiscalent, and both chlorination and dechlorination stages.

2.2.5 Summary

Numerous models with different theoretical backgrounds have been proposed to describe the transport of material through membranes. The main model types are summarised in Table 2.1. Currently, the choice of the correct model is determined primarily by the availability of experimental data and also by the type of mixture being separated.

Of primary concern when selecting a characterisation model is whether the parameter values are independent of the operating point. This is particularly evident in the solution-diffusion model: Mulder *et al.* (1985) suggest that aqueous solutions cannot be modelled accurately with concentration independent permeabilities. However, more theoretical models also suffer from non-constant flux coefficients: El-Halwagi *et al.* (1996) describe water desalination using the Kedem-Katchalsky model and correlate each of the three model parameters (Q_w, Q_s, σ) against concentration, temperature and pressure.

Table 2.1 *Comparing different membrane characterisation approaches*

Model	Membrane	Species transported through the membrane	Main assumptions	Main references
Knudsen diffusion/ viscous flow model	Porous	Gas	Non separative viscous flow Negligible diffusion through body of membrane Negligible surface diffusion	Schofield *et al.* (1990), Rangarajan *et al.* (1984), Bandini *et al.* (1997)
Solution-diffusion model	Dense	Liquid, gas or solute	Membrane pressure is equal to the feed pressure Equilibrium at the phase boundaries No phase change in the membrane Isothermal flux Ideal mixture/Fick's law	Greenlaw *et al.* (1977), Mulder (1996), Rautenbach *et al.* (1988)
Pore-flow model	Dense	Liquid, gas or solute	Isothermal flux Phase boundaries inside membrane Ideal mixture Darcy's equation for flow through pores	Sourirajan and Matsuura (1982), Tyagi *et al.* (1995)
Dusty gas model	Dense and porous	Liquid, gas or solute	Laminar flow through membrane pores Fluxes are proportional to gradients Variations at the molecular level are ignored Viscous and diffusive fluxes are additive	Mason and Lonsdale (1990)
Frictional model	Dense and porous	Liquid, gas or solute	Stefan-Maxwell equation Variations at the molecular level are ignored	Kerkhof (1996), Schaetzel *et al.* (1993)
Irreversible thermodynamics model	Dense and porous	Liquid, gas or solute	Fluxes are proportional to driving forces Equilibrium at the phase boundaries	Soltanieh and Gill (1981), Molina *et al.* (1997)

In conclusion, there is little consensus in the published literature as to the best membrane transport model and a wide range of approaches are currently in use. However, the main focus of this research is not on the membrane itself. Instead, we are interested in the performance of membrane modules and the design of the complete separation system. Therefore, in this work we introduce a modelling structure that is suitable for use with any membrane characterisation. Indeed, a number of different characterisation strategies are implemented in this thesis.

2.3 Modelling of membrane modules

A range of mathematical models that describe the performance of membrane modules have been developed over recent years. The level of detail in the model has usually depended on the application. Generally module models can be said to fall into two categories: either *approximate models* used for quick design calculations (e.g Evangelista, 1985 and Malek *et al.*, 1994); or more detailed *simulation models* that are required for more accurate simulation studies (e.g. El-Halwagi *et al.*, 1996; Ben-Boudinar *et al.*, 1992). The former category are generally intended for quick calculations and typically assume averaged conditions either side of the membrane, whereas the latter attempts to characterise the spatial variation in fluid properties throughout the module. In this section, both approximate and simulation models are assessed.

This thesis concentrates on hollow-fibre and spiral-wound membrane modules (refer to Section 1.1). Consequently, in this section we only consider mathematical models of these two types of module. In the first part of this section, general modelling issues are addressed. This is followed by a review of simulation models of hollow-fibre and then spiral-wound modules. Next, approximate design models for these modules are considered. Finally, available solution techniques for the simulation models are investigated.

2.3.1 General considerations

Many of the published models described later in this section (such as those developed for sea-water desalination) assume binary mixtures. In contrast, membranes are often used to separate multicomponent mixtures (sea-water is itself a multicomponent mixture). It is also common to assume constant physical and thermodynamic fluid properties. However, changing concentrations, temperatures and pressures all effect properties such as fluid viscosity and density. For example, assuming constant density is clearly inappropriate for gas separations where significant pressure changes are observed.

Transient response

Nearly all published models assume steady state conditions and the dynamics of membrane processes are rarely considered. However, chemical plants rarely operate at steady state and so a dynamic model is required for steady-state transitions and plant start-up and shut-down simulations.

Temperature gradients

In processes without a phase change such as reverse osmosis and gas separation, isothermal conditions are reasonably assumed. However, in pervaporation (Section 1.1) the heat supplied to vaporise the permeating material often results in a significant feed stream temperature drop. The assumption of isothermal conditions can lead to large inaccuracies due to an exponential relationship between temperature and permeability. Furthermore, the heat lost usually needs to be re-supplied by a heat exchange system.

Rautenbach and Albrecht (1985) circumvent the problem by assuming infinite feed flowrates or fixed temperature drops. More recent models calculate the temperature gradient by coupling an energy balance with the mass and momentum balance equations. Ito *et al.* (1997) use a simplified energy balance with constant enthalpies and feed liquid heat capacity to estimate the temperature change

$$\frac{dT}{dA} = \frac{\sum_{i=1}^{N^c} \left(H_i^v \frac{dm_i}{dA} \right)}{C_p \sum_{i=1}^{N^c} (m_i)} \tag{2.23}$$

Membrane characterisation

Despite the quantity of work on accurate membrane characterisation, most published module models use simplistic local transport equations. For gas separation, constant permeabilities are invariably assumed (Pan, 1986; Tessendorf *et al.*, 1996), however, Pan (1986) suggests that this approach may not be appropriate for the whole concentration range.

Pervaporation models tend to rely heavily on experimental measurements to describe the concentration dependence and the coupling effects (Tsuyumoto *et al.*, 1997). The use of averaged parameter values in pervaporation is likely to result in high errors due to the

strong dependence of the diffusional parameters on temperature and concentration.

The complexity of characterisation strategies for reverse osmosis varies widely; common approaches include the solution-diffusion model and the Kedem-Katchalsky model. A number of authors assume constant water and salt permeabilities (e.g. Ohya and Taniguchi, 1975). However, in several cases this has been found to be inadequate, and the effect of concentration, pressure and temperature has been included (Ben-Boudinar *et al.*, 1992; El-Halwagi *et al.*, 1996) .

Summary

All the published models discussed in the remainder of this section make at least one of the assumptions identified above. The primary motivation for the introduction of these assumptions is to minimise computational requirements. This is of course an important consideration as a large model may take a very long time to solve and will therefore be unsuitable for computationally intensive uses such as dynamic optimisation. However, computational power has increased dramatically over recent years and better solution algorithms are now available. Therefore, many of these assumptions are unnecessary and can severely restrict the generality of the model.

2.3.2 Simulation models of hollow-fibre modules

Hollow-fibre modules are commonly used for a number of membrane separations including pervaporation, gas separation and reverse osmosis (Rautenbach and Albrecht, 1989). A number of simulation models have been presented over the last thirty years to describe the performance of these modules. The features of the principal models are summarised in Table 2.2. The different approaches implemented in these models are now reviewed.

Hollow-fibre modules were described in Section 1.1. In these modules, feed can be introduced either on the inside or outside of the fibres. The fibres are usually considered to be long thin cylindrical tubes with material injection or removal at the tube walls (the former is illustrated in Figure 2.4). The shell side is treated as a continuous phase with axial and/or radial flow through the porous fibre bundle.

Table 2.2 *Comparing detailed mathematical models of hollow-fibre (HF) modules*

Description	Mass balances	Momentum balances	Membrane characterisation
Reverse osmosis			
Dandavati *et al.* (1975) develop a simple model of a radial flow HF module suitable for describing water desalination.	A one dimensional mass balance is used to describe radial flow through the fibre bundle and only a solvent mass balance is used on the fibre side.	An empirical relationship is used to predict shell-side pressure drop (Sullivan and Hertel, 1940) and fibre side pressure changes are described by the Hagen-Poiseuille relationship.	The solution-diffusion imperfection model is used. A maximum concentration polarisation factor of 1.014 is predicted and thus the effect of any boundary layer is neglected.
Soltanieh and Gill (1984) present the complete-mixing model which describes the behaviour of radial flow HF modules.	The mass balance is simplified by neglecting radial variations in both feed side and permeate side concentration.	The Hagen-Poiseuille relationship is used to describe fibre side pressure build up. Shell side pressure drop is neglected.	The model can be used with a range of membrane transport models but concentration polarisation is assumed to be minimal.
Sekino (1993) develops a model of a Hollosep module. In this module the hollow-fibres are cross-wound onto a central tube.	A one dimensional mass balance describes radial flow through the fibre bundle and an axial mass balance is used on the fibre side.	The Ergun equation is used to describe pressure drop resulting from the fibre bundle and the Hagen-Poiseuille relationship is again used for flow inside the fibres.	The solution-diffusion model is used. A concentration boundary layer is considered.
El-Halwagi *et al.* (1996) develop a detailed model of a radial flow HF module suitable for water desalination.	Two dimensional shell-side flow is considered, however, diffusive flux is neglected. Plug flow is assumed through the fibre bore.	A "modified" Navier-Stokes method is used to describe shell-side pressure drop and the Yuan and Finkelstein analysis (1956) is used for fibre side pressure changes.	The Kedem-Katchalsky model is used with concentration, temperature and pressure dependent parameters. Concentration polarisation is neglected.

Table 2.2 *(continued)*

Description	Mass balances	Momentum balances	Membrane characterisation
Gas separation			
Pan (1986) develops a model of a parallel flow hollow-fibre module for multicomponent gas separation. The model is solved using an iterative shooting method.	One dimensional (axial) mass balances are solved either side of the membrane.	The Hagen-Poiseuille relationship is used to determine the pressure drop on the fibre side. Shell-side pressure drop is neglected.	The membrane is characterised using a simple constant permeability model. Concentration polarisation is not considered.
Tessendorf *et al.* (1996) develop a module model which is almost identical to that of Pan (1986). However, their model is solved using orthogonal collocation.	As above	As above	As above
Pervaporation			
Rautenbach and Albrecht (1985) develop a model to describe pervaporation in HF modules. The model assumes a fixed temperature drop.	A one dimensional (axial) mass balance is solved on the fibre side of the membrane, but shell side conditions are not considered.	As with the gas separation models, the Hagen-Poiseuille relationship is used to determine the pressure drop on the fibre side. Shell-side pressure drop is neglected.	The membrane is characterised using a solution-diffusion model. Concentration polarisation is not considered.
Ito *et al.* (1997) develop a model describing pervaporation in HF modules. A simple energy balance is solved to calculate the temperature change in the module (Eq. 2.23).	A one dimensional (axial) mass balances is solved on the fibre side of the membrane and perfect mixing is assumed on the shell side.	Both fibre side and shell side pressure drop are neglected.	The membrane is characterised using a vapour phase driving force model (Ito *et al.*, 1995). Concentration polarisation is not considered.

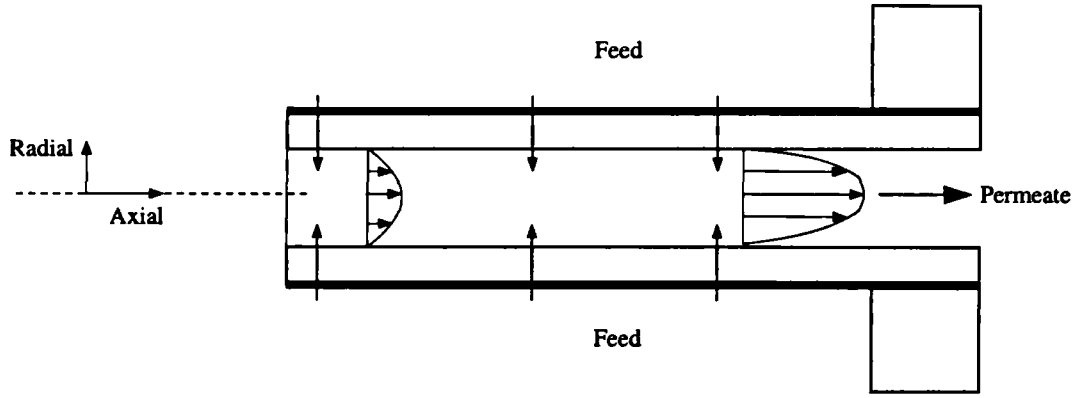

Figure 2.4 *Flow through a hollow-fibre with material injection at the fibre wall*

Hollow-fibres

All recent simulation models, including among others, the works of Pan (1986), Sekino (1993), and El-Halwagi *et al.* (1996), assume plug flow when describing the flow of either the feed or permeate streams through hollow-fibres. Concentration and velocity distributions along the length of the fibre are then obtained by the solution of an axial mass balance. Conventionally, it is assumed that each fibre in the module has identical specifications. Nevertheless, some variation in fibre properties can be expected and Lemanski and Lipscomb (2000), recently demonstrated a strategy that investigated the effect of fibre uncertainty on module performance. However, the scope of their work is somewhat restricted as knowledge of the actual uncertainty in fibre properties (such as inside diameter) is usually unavailable.

Plug flow can be a highly inaccurate assumption. In many pervaporation and reverse osmosis systems there are significant radial concentration variations inside each fibre (concentration polarisation - Section 2.2.4). Cote and Lipski (1988) account for concentration polarisation using the stagnant film model (Eq 2.22). Later in this thesis, we will evaluate this assumption and introduce a more rigorous two dimensional approach that can predict both axial and radial variations inside each fibre.

Pressure build-up inside the fibre pore can be significant and will effect the mean driving force for mass transport through the membrane. The pressure change inside the fibres can be calculated from the solution of an axial momentum balance. Most published models simplify this to the Hagen-Poiseuille relationship (refer to Table 2.2) which is used to calculate pressure drop for steady laminar flow. However, the flow is not laminar due to fluid injection or removal rates at the fibre walls. El-Halwagi *et al.* (1996) consider this effect, using the Yuan and Finkelstein (1956) analysis. They suggest that this only

reduces to the Hagen-Poiseuille relationship when the permeation velocity is "vanishingly small". Clearly, therefore, the validity of the Hagen-Poiseuille relationship depends on the rate of transport through the membrane. The use of a more detailed momentum balance avoids this concern, and is therefore used in this work (Chapter 3).

Module shell

Radial distributions are neglected when describing parallel flow hollow-fibre modules. This is reasonable as a constant permeation rate can be expected in the radial direction if identical fibres are used throughout (see earlier). Hence, the spatial variation of velocity and concentration in the module shell is calculated from an axial mass balance (Chern *et al.*, 1985; Pan, 1986; Tessendorf *et al.*, 1996; Coker *et al.*, 1998). An alternative approach is to assume complete-mixing on the shell side which greatly simplifies the model equations (Ito *et al.*, 1997).

In radial flow modules, the feed stream enters on the shell side and flows radially outward across the fibre bundle. Varying permeation rates are seen both axially and radially due to pressure build up and concentration changes inside the modules. A number of models have been developed to describe these two-dimensional flow patterns. The least complex approach is the complete-mixing model proposed by Soltanieh and Gill (1984) which assumes uniform shell side concentration. In complete contrast, Dandavati *et al.* (1975) assume plug flow (in the radial direction) with no radial mixing. A similar approach was used by Kabadi *et al.* (1979). More recently, El-Halwagi *et al.* (1996) developed a rigorous approach that describes axial and radial flow through the fibre bundle. Again however, the mixing effects (dispersion) are neglected. Nevertheless, all these authors report good agreement with experimental data.

Due to the difficulty of calculating the superficial area and complicated flow patterns, shell-side pressure drop is often neglected (Soltanieh and Gill, 1984; Tessendorf *et al.*, 1996). However, a number of techniques have been introduced to account for shell side pressure drop: Sekino (1993) uses the Ergun equation; and El-Halwagi *et al.* (1996) solve a two-dimensional steady state momentum balance and account for the drag exerted by the porous fibre bundle using a theoretical friction factor (Happel, 1959).

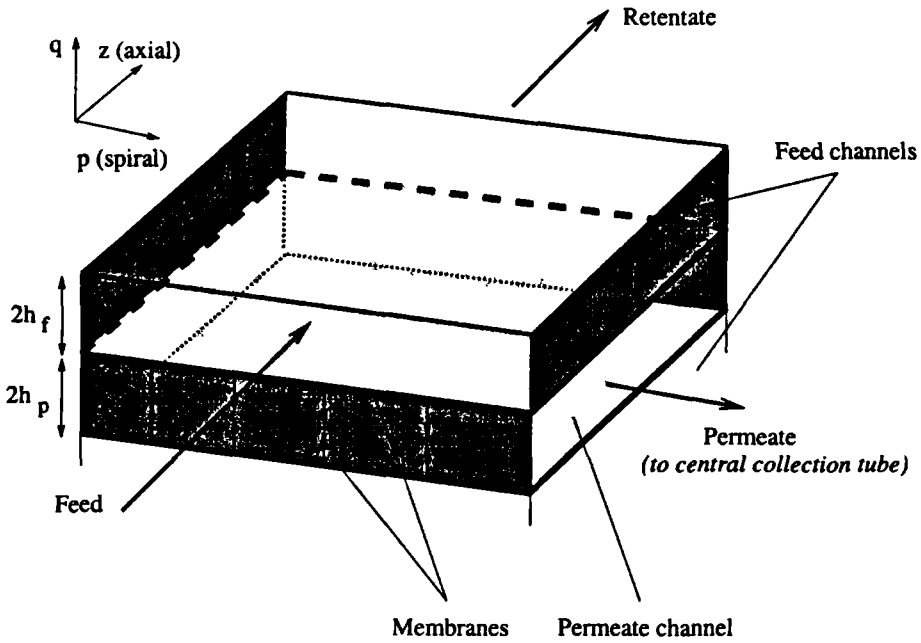

Figure 2.5 *The feed and permeate channels of a spiral-wound module*

2.3.3 Simulation models of spiral-wound modules

Spiral-wound modules were described in Section 1.1. For many membrane systems, such as reverse osmosis, spiral-wound modules are more widely used than hollow-fibre modules. This is because they have traditionally offered much higher permeation rates and easier cleaning than their hollow-fibre counterparts (Bhattacharyya and Williams, 1992). Therefore, it is somewhat surprising that few detailed models of spiral-wound modules have been presented in the open literature. One reason for this may be that accurate modelling must take into account the two-dimensional nature of velocity, pressure and concentration distributions due to the fluid cross-flow inside the membrane modules (Rautenbach and Albrecht, 1989). Selected models of spiral-wound modules are summarised in Table 2.3. The main features of these models are now discussed.

The classic approach is to neglect the curvature of the channels and to consider flow through two flat spacer-filled channels either side of the membrane (see Figure 2.5). Rautenbach and Albrecht (1989) state that this assumption can be justified because the ratio of channel height to the mean module diameter is small. In-line with common industrial practice, constant flow areas are usually assumed. However, tapered flow channels have also been proposed and Evangelista (1988) develops a model that can consider variable flow areas.

Table 2.3 *Comparing detailed mathematical models of spiral-wound modules*

Description	Mass balances	Momentum balances	Membrane characterisation
Reverse osmosis			
Ohya and Taniguchi (1975) describe a binary model of a spiral-wound module. The model is used to describe water desalination.	Plug flow is assumed through the feed channel and averaged properties are used for the permeate side of the membrane.	Pressure drop is neglected on both sides of the membrane.	The Kimura-Sourirajan two parameter model is used to characterise the membrane. Concentration polarisation is described using the stagnant film model.
Ben-Boudinar *et al.* (1992) present a binary model of a spiral-wound module. The model is used to describe water desalination.	Perpendicular one dimensional mass balances are carried out on the feed and permeate channels.	Darcy's law is used to predict pressure drop in both the feed and permeate channels.	The solution-diffusion model is used with concentration, temperature and pressure dependent parameters. Concentration polarisation is again described using the stagnant film model.
Gas separation			
Pan (1983) presents a model of a spiral-wound module for multicomponent gas separation.	Perpendicular one dimensional mass balances are carried out on the feed and permeate channels.	Pressure drop is neglected in the feed channel but pressure drop for the permeate stream is calculated using Darcy's law.	The membrane is characterised using a simple constant permeability model. Concentration polarisation is not considered.
Pervaporation			
Hickey and Gooding (1994) describe a model for the pervaporative separation of VOCs from water. Isothermal conditions are assumed.	A perpendicular one dimensional mass balance is used to describe flow through both the feed and permeate channels, but the total flowrate through the feed channel is assumed to be constant.	As with the gas separation model, pressure drop is neglected in the feed channel and pressure drop for the permeate stream is calculated using Darcy's law.	The resistance-in-series approach proposed by Cote and Lipski (1988) is used to describe the membrane and concentration polarisation.

There are essentially two types of model developed to describe spiral-wound modules: one dimensional plug flow models that assume constant values on either the feed or the permeate side of the membrane; and two dimensional models that describe the true cross-flow nature of the flow. The former category includes the Ohya and Taniguchi (1975) model which assumes a constant concentration in the permeate channel (Table 2.3). The membrane module is then described by an axial mass balance for the feed channel assuming plug flow.

More recent two-dimensional models disregard this assumption. Important examples of this include the works of Pan (1983), Evangelista and Jonsson (1988), and Ben-Boudinar *et al.* (1992). These models allow concentration and permeation variation in both the axial and spiral directions, but neglect the component of feed flow in the spiral direction and permeate flow in the axial direction. Flow through the modules is then described by the solution of two perpendicular one-dimensional balances on either side of the membrane. This approach was also implemented in models developed by Rautenbach and Dahm (1987) and Rautenbach and Albrecht (1989).

Fluid is conducted through the feed and permeate channels in spiral-wound modules in porous spacer material. The mixing effect of the spacer materials means that the concentration variations toward the membrane (in the q-direction, see Figure 2.5) cannot be described theoretically. Consequently, the stagnant film model (Section 2.2.4) is used to describe concentration polarisation where necessary (refer to Table 2.3). A good spacer material should promote mixing in order to reduce the effect of concentration polarisation but should not result in a large pressure drop[1]. Pan (1983) and Ben-Boudinar *et al.* (1992) among others, describe pressure drop through spacer materials using Darcy's law in conjunction with a friction factor.

2.3.4 Design models

For both hollow-fibre and spiral-wound modules concentration, velocity, and pressure distributions are obtained by the solution of appropriate mass and momentum balance equations. A number of approximate models have been proposed for the purpose of quick design calculations. These generally transform the differential equations into non-linear algebraic equations which can be solved relatively easily, often analytically. A number of approaches have been suggested for this purpose

[1] An experimental study on different spacer materials has previously been carried out by Hickey and Gooding (1994).

1. Ideally mixed volumes can be assumed on either or both sides of the membrane (Evangelista, 1985). This is a continuous stirred tank approach where concentration is uniform. The validity of the assumption depends on the dispersive properties of the fluid and the module geometry.

2. Alternatively, the concentration gradient can be assumed to follow either a linear or log-mean model (e.g. Krovvidi *et al.*, 1992; Pettersen and Lien, 1994; Qi and Henson, 1996; Smith *et al.*, 1996).

In Table 2.4, the main features of selected approximate design models are discussed. The validity of the assumptions made in each model will vary greatly from one system to the next; which clearly reduces the generality of the model. It also makes a general assessment of each model difficult. However, the accuracy of several of these design models for specific case studies is assessed later in this thesis.

2.3.5 Solution methods

The simulation models described in Sections 2.3.2 and 2.3.3 consider variations with spatial position, and are often termed *distributed models.* They consist of mixed sets of partial differential and algebraic equations (PDAEs). The partial differential equations arise from the mass, momentum and energy balances. Algebraic equations are needed to represent fluid property and thermodynamic relationships. This type of problem is usually solved by numerical integration of the partial differential equations due to the absence of analytical solutions.

Early distributed models were solved using an iterative shooting method (e.g. Pan, 1983). However, such methods are often computationally expensive and in certain cases lead to numerical difficulties (Kaldis *et al.*, 1998). These difficulties have provided a significant motivation for the development of approximate models using assumed concentration gradients (discussed in Section 2.3.4).

Distributed models are now usually solved by discretising the spatial domain using a finite difference (e.g. Ben-Boudinar *et al.*, 1992) or orthogonal collocation (e.g. Tessendorf *et al.*, 1996) approach. The result is a set of non-linear algebraic equivalents which are solved using efficient Newton type methods[2]. The two discretisation methods are now outlined.

[2]For dynamic models, the partial differential equations are converted into a set of ordinary differential equations (as a function of time) which can also be solved relatively easily using implicit numerical integration techniques.

Table 2.4 *Comparing approximate mathematical models of hollow-fibre (HF) and spiral-wound (SW) modules*

Description	Mass balances	Momentum balances	Membrane characterisation
Reverse osmosis			
Evangelista (1985) describes a simple model to predict the performance of reverse osmosis HF modules.	The mass balance is simplified by using mean feed and permeate side concentrations in the calculations.	A geometric correction factor is introduced into the calculations to account for the changing pressures inside the modules.	A two parameter membrane model is used. Concentration polarisation is neglected.
Evangelista (1985) also describes a simple model to predict the performance of reverse osmosis SW modules.	Again, the mass balance is simplified by using mean feed and permeate side concentrations in the calculations.	Pressure drop in both the feed and permeate channels is neglected.	A two parameter membrane model is used. Concentration polarisation is described by the stagnant film model with a constant mass transfer coefficient.
Malek *et al.* (1994) develop a lumped transport model which describes a radial flow HF module.	Shell side concentration is assumed to vary linearly with radial position and there is no fibre side mass balance.	Constant shell side pressure drop; negligible permeate pressure.	The solution-diffusion model is used. Concentration polarisation is neglected.

Table 2.4 *(continued)*

Description	Mass balances	Momentum balances	Membrane characterisation
Gas separation			
Krovvidi *et al.* (1992) present a model that describes binary gas mixture separation in HF and SW modules.	The mass balance is simplified by assuming a relationship between the feed-side and permeate side concentrations (both linear and quadratic relationships are considered).	Pressure drop on both sides of the membrane is neglected.	Constant gas permeability is assumed.
Smith *et al.* (1996) also present a model for binary gas mixture separation in HF modules.	The mass balance is simplified by assuming a uniform permeate concentration.	As in the Krovvidi *et al.* (1992) model, pressure drop on both sides of the membrane is neglected.	Constant gas permeability is assumed.
Qi and Henson (1997) present an approximate model of a SW module developed from a simplification of the simulation model described by Pan (1983) - see Table 2.3.	The one dimensional mass balances are simplified by assuming that the flowrate in the feed channel is constant in the spiral direction.	Pressure drop is neglected in the feed channel but pressure drop for the permeate stream is calculated using Darcy's law.	The membrane is characterised using a simple constant permeability model. Concentration polarisation is not considered.
Pervaporation			
Srinivas and El-Halwagi (1993) present an approximate model of a HF module that describes isothermal pervaporation.	A log mean concentration difference is used to represent the concentration changes on the feed-side.	Feed-side pressure drop is calculated using the Hagen-Poiseuille relationship, permeate pressure drop is neglected.	The membrane is characterised using a simple constant permeability model. Concentration polarisation is described by the stagnant film model using a non-constant mass transfer coefficient.

Orthogonal collocation methods Orthogonal collocation methods assume that the spatial variation of distributed variables can be approximated by Lagrangian polynomials. The approximations are enforced at discrete points within the spatial domain; N+1 points are needed for polynomials of order N. Increasing the order of the polynomials improves the accuracy of the approximation. However, high order polynomials exhibit multiple maxima and minima (Pantelides, 1998) so an alternative approach is to partition the domain into a number of finite elements. Orthogonal collocation is then carried out for each element independently with continuity of variables and derivatives at element boundaries. This is the orthogonal collocation on finite elements (OCFE) method - for further details refer to Pantelides (1998) and Rice and Duoung (1995).

Finite difference methods Finite difference methods also divide the spatial domain into a number of elements for which the derivatives are approximated by linear approximations derived from the Taylor series. The error in finite difference methods is a function of the neglected second order derivative terms and the number of elements used.

In Appendix C, the relative merits of these two methods are assessed for the models developed in this thesis.

2.3.6 Summary

It would seem that a rigorous general approach to membrane module simulation has not yet been attempted. Much of the published work has limited application due to simplifying assumptions such as plug flow; constant temperature; constant pressure; binary mixture; steady-state conditions; and constant physical properties. Approximate design models have been proposed for particular case studies to enable quick membrane area calculations. However, with improved CPU performance and better solution algorithms, such approaches are no longer necessary. Thus, in this thesis, a rigorous general model is advocated.

The advantages of a rigorous approach to module simulation are greater generality, a wider range of application, and higher accuracy. Detailed models should account for all different membrane systems and be able to utilise a range of local mass transport equations. Furthermore, in a rigorous model, averaged physical and thermodynamic properties cannot be assumed as in reality they vary with concentration, temperature and pressure. A modelling approach that addresses all of these concerns is presented in Chapter 3 of this thesis.

2.4 Design of membrane separation systems

In this section, the use of mathematical models for the design of membrane separation systems is considered. In the design of a general membrane separation plant, there are several factors to take into account, these include: the required membrane area; the module type and size; the process configuration; the positioning of additional equipment items such as heat exchangers and pumps; and the operating point of the plant (temperatures, pressures, etc.). Therefore, selecting the best design values involves many complicated and interacting choices. Two general approaches are prevalent in the literature

1. To consider each choice separately making use of existing experimental data, simulation results and known heuristics. Each choice can be reconsidered iteratively if initial solutions are deemed to be uneconomic. However, even with an iterative approach there is no guarantee that the best design is found because of interacting, and often conflicting, decisions.

2. The second approach is to consider the problem as a whole. Over recent years, several authors have considered the use of optimisation algorithms to do this. The main advantages of this method are that assumptions of the nature of the process are not required, and interacting decisions are fully taken into account *if* accurate models have been used. These works are now discussed.

2.4.1 Optimal membrane process design

The use of an optimisation approach for the full structural design of membrane separation systems has been considered in a limited number of cases. However, in each instance, approximate models are used to determine the membrane area and the operating parameters.

Reverse osmosis

Several papers based on a state space approach originally developed by El-Halwagi (1992), have calculated the optimal design of reverse osmosis networks (Zhu *et al.*, 1997, Voros *et al.*, 1997). The method is based on a superstructure including pumps and energy recovery devices. Zhu *et al.* (1997) also considered cleaning cycle scheduling as part of the optimisation problem. In all these works, the number of modules is determined using the approximate module model proposed by Evangelista (1985) - refer to Table 2.4.

Pervaporation

The optimisation of pervaporation systems has also been examined in several instances. Ji *et al.* (1994) have carried out an optimisation study on the removal of volatile organics from water. However, an assumed structure (excluding a heat exchanger) was used and only an operating point study was carried out. A simplistic module model was applied with constant permeability parameters.

Srinivas and El-Halwagi (1993) used the state space approach to determine the optimal design of a pervaporation network for the removal of organics from waste-water. They use a representation which includes heat exchangers, condensers and compressors. However, their approach applies a simple design model (Table 2.4) which assumes isothermal flow through the modules. Consequently, the model is particularly unsuitable for pervaporation systems with large temperature changes (see Section 1.1).

Gas separation

Qi and Henson (1998, 2000) have considered the optimal design of gas separation systems. They have demonstrated their methodology for both binary gas mixtures (carbon dioxide/methane) and multicomponent gas mixtures (the removal of acid gases from crude natural gas). However, their work is also based on a simplified design model: the approximate spiral-wound model which is assessed in Table 2.4 (Qi and Henson, 1997).

2.4.2 Summary

Unless rigorous models incorporating accurate local mass flux and flow models are used, then high inaccuracies will be incorporated into the results of design studies. In none of the studies identified above, is an assessment made of the effect of the simplifying assumptions on the process design. In fact, errors in modelling the performance of the modules will lead to the development of sub-optimal plant designs, possible over (or under) prediction of plant performance and lack of generality due to implicit assumptions. The use of simplified models for pervaporation is particularly inappropriate due to the high dependence of permeability on temperature which, if ignored, may cause large inaccuracies.

2.5 Conclusions

The importance of developing a greater technical understanding of membrane systems in order to obtain better and more reliable designs was discussed in Section 1.2. A prerequisite for this is a rigorous mathematical model that can accurately describe whole membrane systems and their building blocks - membrane modules. Thus, published literature concerned with the modelling and design of membrane systems has been assessed in this chapter.

Much of the recently published modelling work has concentrated on a range of different approaches to describe the transport of material through membranes. Although in many cases, membrane selectivities and fluxes can now be determined with high accuracy, a large number of experimental parameters are still required. Consequently, much work is still needed if these models are to be realistically applied to multicomponent separations. It is particularly important to reduce the number of experimentally measured parameters that are required.

Accurate membrane characterisation is of little value if it is only incorporated into an approximate module model. So far, the use of detailed models for membrane separation system simulation and design has hardly been considered. Existing work has focused on specific separations and a general approach has not been attempted. Until recently, solution difficulties have limited the accuracy of membrane models, however, the use of improved solution strategies combined with increased computational power, facilitates the implementation of more detailed models. Therefore, in this research, many typical assumptions are discarded and the development of a rigorous model for a *general* membrane separation is investigated (Chapter 3).

Optimisation design studies of membrane separation systems have rarely been carried out, and are based on simple models that make a large number of assumptions. The low accuracy of these models means that the designs advocated are unreliable and that the conclusions presented are highly questionable. The use of detailed models will increase confidence in the proposed designs. Further confidence will be gained if the models have been validated experimentally over a wide range of conditions. In this thesis, these points are addressed. Hence, a new optimal design strategy that incorporates a rigorous mathematical model of a membrane module is proposed in Chapter 4.

Chapter 3

DETAILED MATHEMATICAL MODELLING OF MEMBRANE MODULES

This chapter details the development of a mathematical model used to describe the separation of a general mixture in hollow-fibre and spiral-wound membrane modules. An appropriate numerical solution technique is also introduced. The use of the model for gas separation, pervaporation and reverse osmosis is then demonstrated.

3.1 Introduction

The objectives of this chapter are to describe a detailed approach to modelling a general membrane separation and to illustrate its use for different systems.

In the next section, a rigorous modelling approach that can consider both hollow-fibre and spiral-wound membrane modules is presented. A suitable numerical solution technique is described in Section 3.3. Following this, the generality of the detailed model is demonstrated when pervaporation, gas separation and reverse osmosis case studies are investigated (Section 3.4). Some conclusions on the suitability of the model for describing membrane systems are presented in the final section.

3.2 Mathematical model

A complete description of a membrane module requires that local mass transport equations describing the membrane itself are solved simultaneously with conservation and continuity equations that model the flow of material through the module. There has

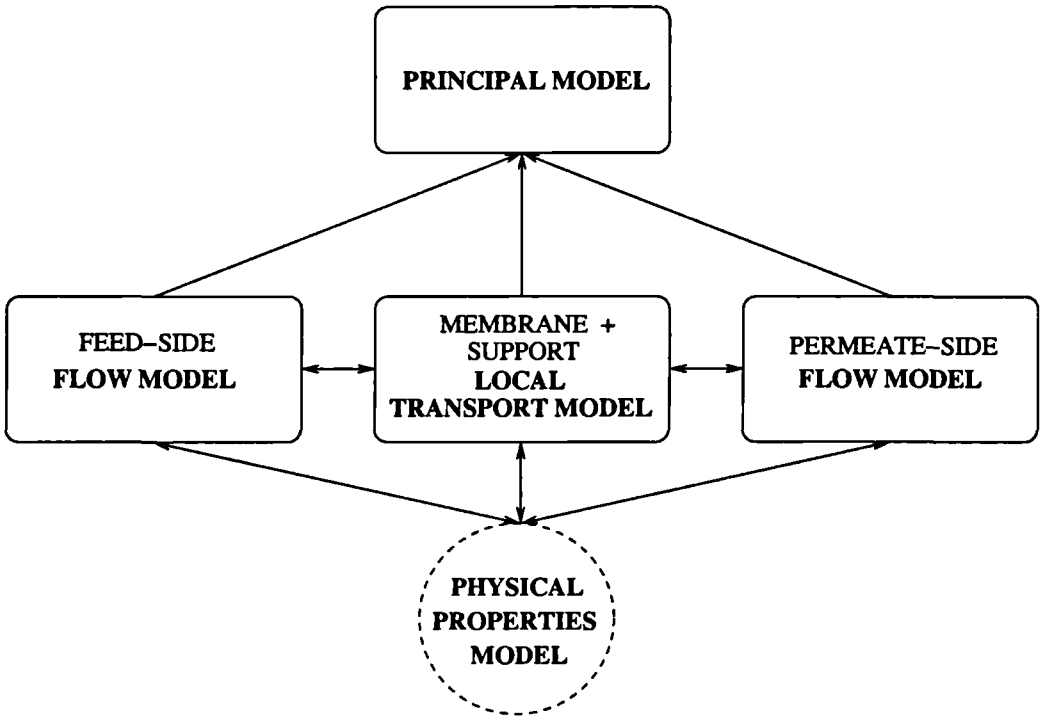

Figure 3.1 *Model structure*

been a substantial amount of published research (Section 2.2) on developing equations that describe the flux characteristics of different membranes. Therefore, in this work, we concentrate on modelling the flow patterns inside different membrane modules.

To describe the behaviour of a membrane module, three sub-models are required; two which describe the flow on either side of the membrane and a third model which characterises the separative properties of the membrane and any porous support material. In this work, a number of flow sub-models have been developed to account for flow through different module geometries. All of the sub-models are developed from rigorous dynamic mass, momentum and energy balances, and thus are applicable to *any* membrane separation. The structure of the model is controlled by a principal model that simply links the three sub-models. This is illustrated in Figure 3.1.

The literature review showed that membrane systems have mainly been studied using simplified models that are based on a number of restrictive assumptions (Section 2.3). In contrast, the models developed in this work can all consider

1. *Two-dimensional flow patterns.* In most flow models presented in the literature, one-dimensional plug flow is assumed (refer to Section 2.3). This means that con-

centration variations perpendicular to the bulk flow direction are neglected. In this section, the development of two-dimensional flow models will show that this assumption is unnecessary.

2. *Steady-state and dynamic simulations.* To ensure that the model can be used for a range of applications from steady-state simulation and process synthesis to investigating control issues and dynamic optimisation, it is important that steady-state conditions are not assumed. However, it should be noted that although the model developed in this work is dynamic, only steady-state simulation and optimisation of membrane systems has been considered in the case studies. Steady-state simulation is easily achieved using a dynamic model by setting all time derivatives to zero.

3. *Multi-component systems.* Many of the models presented in the literature are restricted to binary systems (see Section 2.3). A truly general model, such as the one developed in this work, must be able to consider multicomponent systems.

4. *Both viscous and dispersive flow mechanisms.* A concentration profile usually develops as a fluid flows through a membrane module. However, due to the effect of diffusion and turbulent eddies, a degree of back mixing may help promote a uniform concentration (dispersion). Whilst most membrane flow models neglect the effect of dispersion, this is not the case here. A study of the effect of dispersion on the flow pattern inside membrane modules is presented in Appendix B.

5. *Non-isothermal flow.* Many membrane processes, such as reverse osmosis and gas separation, are isothermal. However, large temperature changes are seen in some pervaporation processes (see Section 1.1). The simulation and optimisation of a non-isothermal pervaporation process is investigated in Chapter 6 of this thesis.

6. *Accurate physical properties.* Most of the models described in Section 2.3 assume constant physical properties. When significant temperature, pressure or concentration changes occur, this may significantly effect model accuracy. In all the work presented in this thesis, accurate physical and thermodynamic properties (such as densities, viscosities and enthalpies) are provided by external software.

Based on the above principles, models that describe flow patterns inside hollow-fibre and spiral-wound modules are now presented. Brief consideration is also given to the local transport sub-model. All the model equations are given in Appendix A.

3.2.1 Hollow-fibre modules

As introduced in Section 1.1, a hollow-fibre module contains a large number of membrane fibres housed in a module shell. Feed can be introduced on either the fibre or the shell side. Permeate is usually withdrawn in a co-current or counter-current manner, with the latter being generally more effective. The flow pattern in a parallel flow hollow-fibre module where fluid is introduced on the fibre side, is illustrated in Figure 3.2.

Radial flow hollow-fibre modules are also used, and are particularly common for reverse osmosis systems. In these modules, feed is introduced into the shell side using a central porous tube from which fluid flows across the fibre bundle. A radial flow module is illustrated in Figure 3.3.

Fibre flow and shell flow models are now presented. These can be used to describe both parallel flow and radial flow hollow-fibre modules.

Fibre flow sub-model

A two-dimensional sub-model that considers liquid or gas flow inside the fibres of a hollow-fibre module has been developed from dynamic mass, momentum and energy balances.[1] As well as describing axial variations in concentration, velocity, pressure and temperature, the model yields full radial concentration and velocity profiles.

To limit the size of the model so that it can be solved with reasonable computational expense, and to avoid having to obtain values for parameters that cannot accurately be estimated, the following simplifying assumptions have been made

1. It is assumed that each fibre is of identical specifications and can be modelled as a thin horizontal pipe of uniform diameter. Lemanski and Lipscomb (2000) have recently demonstrated a strategy that determines the effect of fibre uncertainty on module performance. A similar approach could be adopted here to investigate the effect of uncertainty if desired.
2. Radial variations in temperature and pressure will be neglected. This is reasonable due to the very small diameter of hollow fibres.

The state balance equations and the appropriate boundary conditions are presented in Section A.2.1 (Appendix A).

[1] Although not considered in this thesis, the fibre flow sub-model can easily be adapted to describe tubular membrane modules.

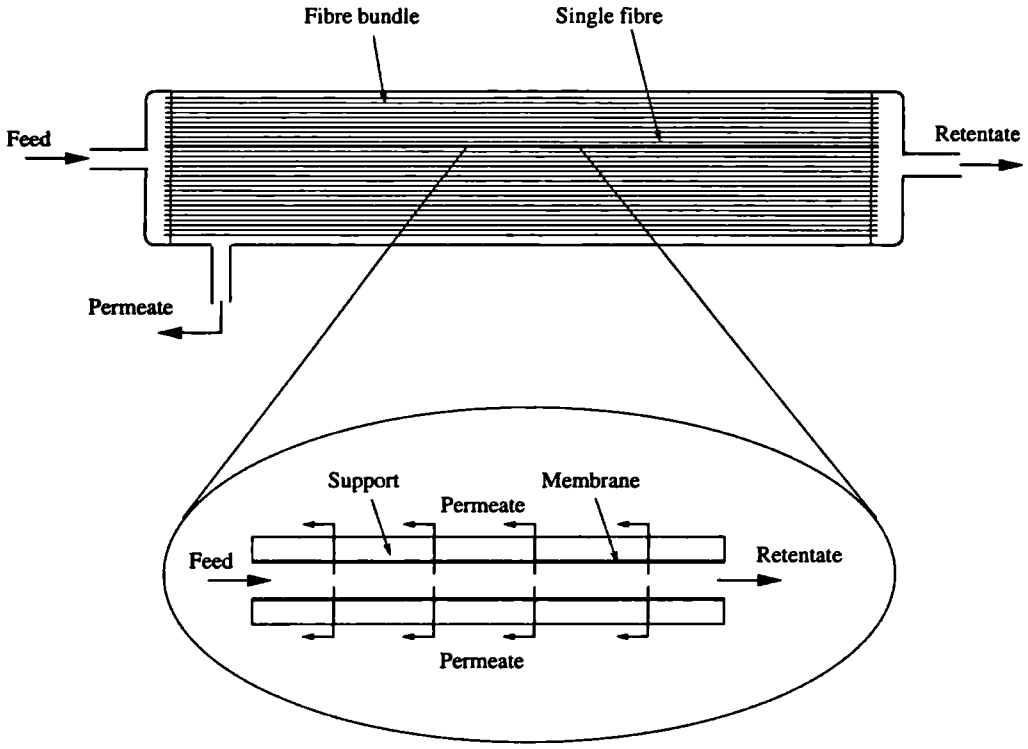

Figure 3.2 *Flow pattern in a parallel flow hollow-fibre module (fibre side feed)*

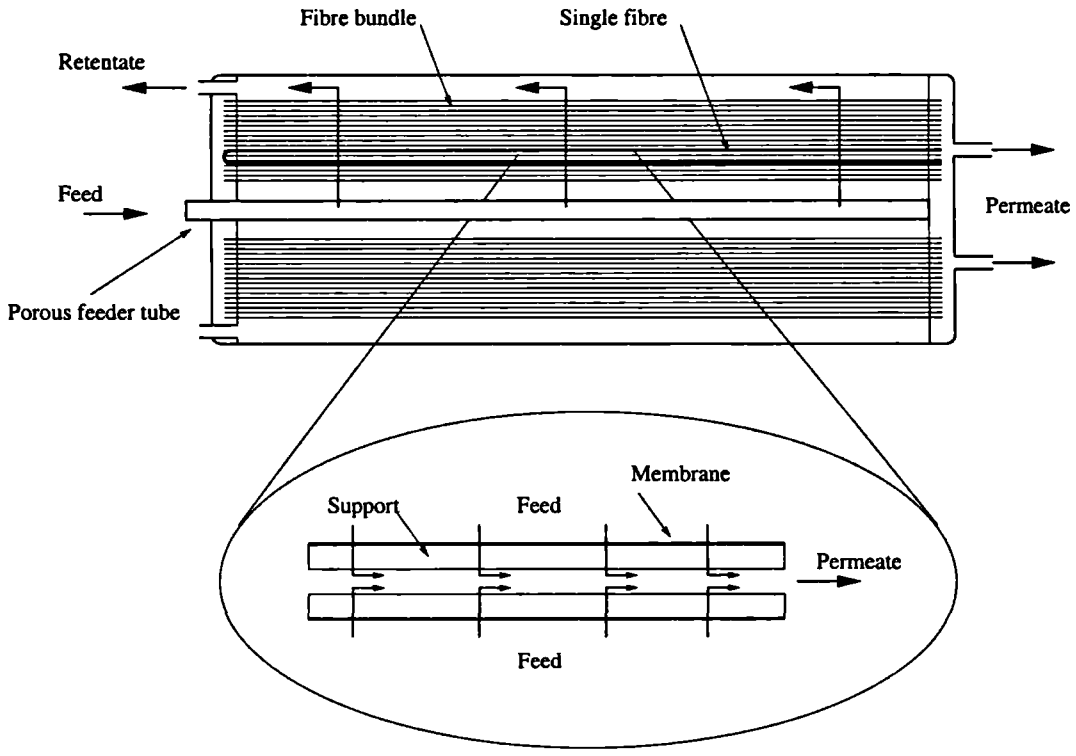

Figure 3.3 *Flow pattern in a radial flow hollow-fibre module (shell side feed)*

In some cases, radial concentration variations inside the hollow-fibre are negligible (i.e. no *concentration polarisation*). Therefore, to minimise computational expense, a simpler one-dimensional model has also been developed (Section A.2.1, Appendix A). The one-dimensional model is identical to the two-dimensional model except that radial concentration and velocity variations are neglected (i.e. plug flow is assumed). Concentration polarisation is considered in more detail later in this chapter.

Shell flow sub-model

The shell side of a hollow-fibre module contains a large number of hollow-fibres (typically of the order of 10^5). Fluid flows around or across each fibre. Considering each fibre individually would clearly be impossible, so in this work, the fibre bundle is treated as a continuous radially symmetric porous medium.

The model is derived from dynamic two-dimensional mass, momentum and energy balances, and is therefore able to predict both axial and radial fluid property variations (see Figure 3.4). In order to limit model size, the following assumptions have been made

1. The pressure drop for flow through the fibre bundle is characterised using a friction parameter. The value of the parameter can be obtained from either experimental or theoretical studies (e.g. Happel, 1959).

2. The effect of localised concentration changes around each fibre (concentration polarisation on the transport of material through the membrane can be described using the stagnant film model (see Section 2.2.4).

The equations for the model are presented in Section A.2.2 (Appendix A). The boundary conditions for the shell side define the module flow pattern (i.e. parallel flow or radial

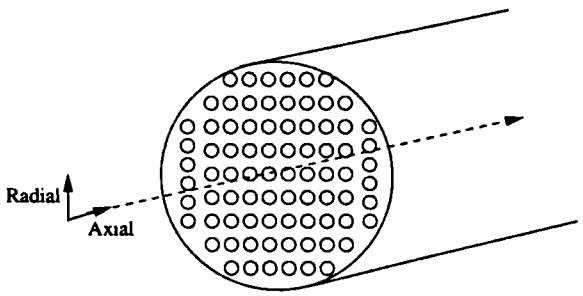

Figure 3.4 *Flow directions inside the shell of a hollow-fibre module*

flow) - appropriate boundary conditions for the radial flow module are given in Section A.2.2.

For parallel (co- or counter-current) flow modules, radial variations on the shell side can usually be neglected as each fibre will behave in an identical manner. Therefore, a one-dimensional (plug flow) model has also been developed to describe shell side conditions. This model is similar to the two dimensional flow model but is based on one-dimensional dynamic mass, heat and momentum balances (again see Section A.2.2).

3.2.2 Spiral-wound modules

Spiral-wound modules were also introduced in Section 1.1. The modules are made from flat membrane envelopes, wrapped around a central tube. Feed passes along the length of the module and the permeate passes into a membrane envelope and then out via the central tube. Both the feed and the permeate are transported through the module in fluid-conductive spacer material. Modern modules tend to contain multiple membranes that are all attached to the same central tube. A diagram of a flat membrane envelope is shown in Figure 3.5.

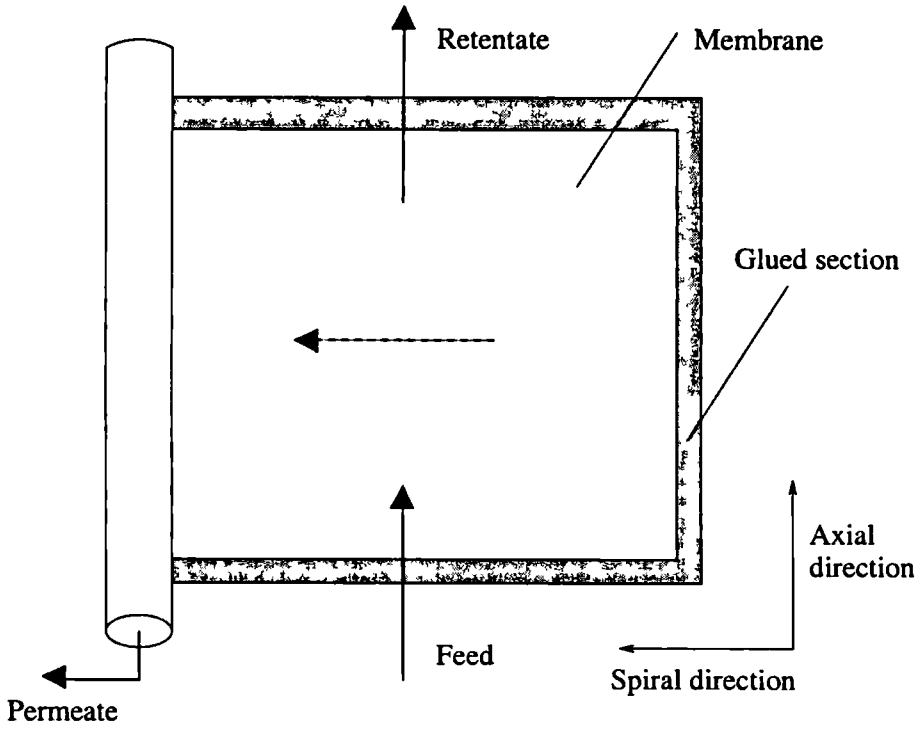

Figure 3.5 *An unwound spiral-wound module*

Usually in spiral-wound membrane modules the size of the feed channel is greater than the active membrane area. This is a result of the method of manufacture where membrane sheets are glued together to form permeate envelopes. In particular, the feed channel spacer is typically about 20% wider (see for example Ben-Boudinar *et al.*, 1992) than the membrane envelope. This additional width may promote flow perpendicular to the bulk flow (along the spiral). Whilst in published studies flow perpendicular to the main flow direction is neglected (see Section 2.3), in this work no such simplification is necessary and the full channel width is easily incorporated.

Feed and permeate channel flow models

A two-dimensional flow model has been developed that can describe flow in the axial and spiral directions in both the feed and permeate channels. In mathematical terms the model is very similar to the shell flow sub-model presented earlier. Once again, a number of assumptions have been made in order to limit model size

1. It has been shown in several studies (e.g. Schock and Miquel, 1987) that the bent channel does not significantly effect the flow behaviour in the module. Hence, in this work channel curvature is neglected and the membrane is treated as a flat sheet with cross-current flow channels either side.

2. Localised concentration variations toward the membrane (*concentration polarisation*) are described by the stagnant film model (see Section 2.2.4).

3. The pressure drop for flow through the porous spacer material is characterised using a friction parameter. The value of the parameter will vary for different spacer materials but can easily be estimated from pressure drop measurements.

4. Constant flow area is assumed (i.e. the flow channel is not tapered). This assumption can be disregarded if necessary - this has been considered by Evangelista and Jonsson (1988).

5. All membranes in the module are identical.

The two-dimensional model is derived from dynamic mass, heat and momentum balances. The boundary conditions for both the feed and permeate channels are presented along with the model equations in Section A.3 (Appendix A). Solution of the model equations yields full two-dimensional pressure, temperature, concentration and velocity profiles inside each channel.

As before, a simplified one dimensional plug flow model has also been developed (Section A.3, Appendix A). This model assumes a uniform concentration in the permeate channel and hence variations in the spiral direction are neglected. This is the same principal assumption used by Ohya and Taniguchi (1975) - refer to Section 2.3.3.

3.2.3 Local transport sub-model

The membrane material and any porous support can usually be characterised by a flux equation of the form given in Section 2.2. This describes the rate of transport of material (and energy) between the two phases either side of the membrane. This will usually be a function of concentration, activity, and temperature. No assumptions on the performance of the membrane are made at this stage as a number of case studies, each with different membranes, are considered in this thesis.

The temperature of the membrane itself is assumed to be constant at the upstream value. This assumption can only be removed if the thermal conductivity of the fluids and the membrane are known.

3.2.4 Summary

The model is formed by linking two flow sub-models using an appropriate local transport model. Three different two-dimensional (2-D) flow sub-models have been developed. Each sub-model can describe the axial and radial (spiral) variations in fluid properties as material passes through the module. Simplified one-dimensional (1-D) flow sub-models have also been developed as plug flow is a reasonable assumption for certain systems. The main features of the 2-D flow sub-models are summarised in Table 3.1.

The application of the detailed model to a range of different separations will be considered later in this chapter. In these case studies we will also contrast a two-dimensional approach with more conventional one-dimensional models.

3.3 Numerical solution

A spatial discretisation technique is necessary for the solution of the distributed sub-models that were described in the previous section. Discretisation converts a system of partial differential and algebraic equations (PDAEs) into a set of ordinary differential and algebraic equations (DAEs) - see Section 2.3.5. The latter can be solved relatively

Table 3.1 *Characteristics of the flow sub-models*

Model characteristics	Fibre flow (HF)	Shell flow (HF)	Channel flow (SW)
Steady-state and dynamic simulation	✓	✓	✓
Multi-component systems	✓	✓	✓
Viscous and dispersive flow	✓	✓	✓
2-D mass balance	✓	✓	✓
2-D momentum balance	1-D	✓	✓
Non-isothermal flow	✓	✓	✓
Accurate physical properties	✓	✓	✓

easily using implicit numerical integration techniques. A variety of spatial discretisation methods are available (Oh, 1995), and in this research, the use of both finite difference and orthogonal collocation on finite element methods has been considered.

Selection of the most appropriate discretisation strategy is essential if computational effort is to be minimised whilst maintaining sufficient accuracy. Generally, for both finite difference and orthogonal collocation on finite element methods, increasing the number of discretisation points results in more accurate solutions. However, this must be balanced against longer solution times. Throughout this thesis, the orthogonal collocation on finite element methods is found to be the most efficient approach. The reason for this is discussed in Appendix C using a simple reverse osmosis case study.

3.4 Model assessment

The detailed model is now applied to several case studies. The purpose of this section is two-fold. Firstly, we will contrast the model with other approaches used to describe membrane systems in the literature. Secondly, the generality of the approach will be demonstrated by considering a range of membrane systems. In particular, simulation results are presented for pervaporation, gas separation and reverse osmosis. These case studies are outlined in Table 3.2.

All of the calculations reported in this section are performed on an IBM RISC System/6000 workstation running under the AIX 4.3.2 operating system.

Table 3.2 *Simulation case studies considered in this chapter*

	Pervaporation (Section 3.4.1)	**Gas separation** (Section 3.4.2)	**Reverse osmosis** (Section 3.4.3)
Separation considered	Removal of trichloroethylene from waste-water	Hydrogen and nitrogen separation	Brine water desalination
Module	Hollow-fibre	Hollow-fibre	Spiral-wound
Feed sub-model	2-D fibre	1-D shell	2-D channel
Permeate sub-model	1-D shell	1-D fibre	2-D channel

3.4.1 Pervaporation simulation example

In this section, we consider the removal of organics from waste-water - a potentially important application of pervaporation. This system is usually characterised by low flux rates through the membrane due to very low organic concentrations. Hence, only a small fraction of the feed needs to be evaporated and the system is nearly isothermal. In a later study (Chapter 6), we will discuss how the detailed model accounts for non-isothermal flow. Whilst temperature changes are not significant for the removal of organics from waste-water, concentration polarisation is a considerable problem. This will now be examined in detail.

Concentration polarisation inside hollow-fibres is usually modelled using a plug flow model coupled with an empirical mass transfer coefficient (Brouchaert and Buckley, 1992) - the stagnant film approach.[2] The effect of assuming a stagnant boundary layer was illustrated earlier in Chapter 2 of this thesis (see Figures 2.1 and 2.2). However, the development of the 2-D fibre model enables this effect to be described more rigorously, as it does not assume a boundary layer and instead considers full radial variations in both concentration and velocity (Section 3.2.1).

Description of the system

Experimental results for the removal of trichloroethylene from waste-water by pervaporation using lab-scale silicone rubber hollow-fibre modules have been presented by Psaume

[2]Note that the use of the stagnant film approach is necessary when describing the shell side of hollow-fibre modules and for flow inside spiral-wound membranes due to the uncertainty in describing flow through porous media.

Table 3.3 *Pervaporation simulation example (Psaume et al., 1988)*

et al. (1988). System details are given in Table 3.3. The authors calculate the experimental mass transfer coefficient for a range of feed flows from the overall trichloroethylene flux rate.

The resistance of the membrane to trichloroethylene flux has been shown to be insignificant in comparison to the resistance created by the concentration boundary layer (Cote and Lipski, 1988). Therefore, for this study, a very simple membrane characterisation model is used: the resistance of the membrane to trichloroethylene is neglected; and in line with the experimental results (Psaume *et al.*, 1988), a constant water flux rate of $3.89 \times 10^{-6} kg/m^2 s$ is assumed.

In this study, both the 2-D and 1-D fibre flow models (Section A.2, Appendix A) are used to simulate the liquid feed flow through the fibre bore. The models are solved using the g*PROMS* simulation software (Process Systems Enterprise Ltd, 1999). The spatial variation of the distributed variables in the axial and radial domains is approximated using 4th order orthogonal collocation on two elements for both domains (see Appendix C). With this strategy, typical solution times are 0.4 CPUs using the 1-D fibre sub-model and 2 CPUs using the 2-D fibre sub-model.

Concentration boundary layer

The boundary layer is formed due to slow diffusion of trichloroethylene to the membrane surface. The Wilke correlation (Bird *et al.*, 1960) can be used to estimate the diffusion coefficient for a dilute non-disassociating solute, with a typical accuracy of ±10%. For diffusion through water, the correlation is written

$$D_i = 1.86 \times 10^{-18} \frac{(2.6 M_W)^{0.5} T}{\mu \rho_i^{-0.6}} \tag{3.1}$$

Hence the diffusion coefficient for trichloroethylene at 20 ^oC is estimated as $D_i = 9.6 \times 10^{-10} m^2/s$ (where $M_W = 18.015 g/mol$, $\mu = 1 \times 10^{-3} Pas$, $\rho_i = 1.05 \times 10^5 mol/m^3$).

The stagnant film approach (Eq. 2.22) is used to calculate the interface concentration, x_{i_m}, for the 1-D fibre flow model. This requires an empirical mass transfer coefficient, k. In this work, the Leveque correlation (Cote and Lipski, 1988) will be used to estimate the mass transfer coefficient

$$k = 1.62\frac{D}{2R}\left(\frac{\rho v 2R}{\mu}\right)^{\frac{1}{3}}\left(\frac{\mu}{\rho D}\right)^{\frac{1}{3}}\left(\frac{2R}{L}\right)^{\frac{1}{3}} \tag{3.2}$$

Simulation results

The accuracy of the simulation results for the two sub-models is assessed against experimental data (Psaume *et al.*, 1988) in Table 3.4. The results are also plotted in Figure 3.6 which shows the mean mass transfer coefficient, k_{ov}, as a function of Reynolds number. In this case, as the selectivity of the membrane with respect to trichloroethylene is extremely high, the overall mass transfer coefficient represents the resistance of the liquid boundary layer (Cote and Lipski, 1988). The average mass transfer coefficient can therefore be calculated from the ratio of trichloroethylene flux to mean feed-side concentration

$$\frac{\bar{J}_i}{\bar{c}_f} \approx k_{ov} = \frac{D_i}{\delta} \tag{3.3}$$

For comparison, Figure 3.6 also shows experimental results that have been presented by Cote and Lipski (1988) for the same system.

Both models predict the experimental results reasonably well and the predictions of the two models show a close correlation with each other. Unfortunately, uncertainty in the value of the diffusion coefficient and in the experimental results, which show a wide degree of scatter, limits further analysis. However, at low Reynolds numbers it is seen that the 2-D model correlates better with the experimental results whereas at higher Reynolds numbers, the results are very similar.

Radial concentration profiles for a single data point ($Re = 46$) calculated using the 1-D and 2-D models are compared in Figure 3.7. Whilst both approaches suggest that the concentration at the membrane wall is significantly different to the bulk concentration, the assumption of a boundary layer is seen to be inappropriate. In fact, the 2-D model demonstrates that the trichloroethylene concentration varies across the whole diameter of the fibre rather than just at the wall. This actually concurs with boundary layer theory (see Section 2.2.4). The boundary layer thickness, δ, can be calculated from Equation 3.3 - approximately $100\mu m$ ($0.1mm$), which is $\frac{2}{3}R_f$. For this reason, a boundary layer approach cannot be recommended.

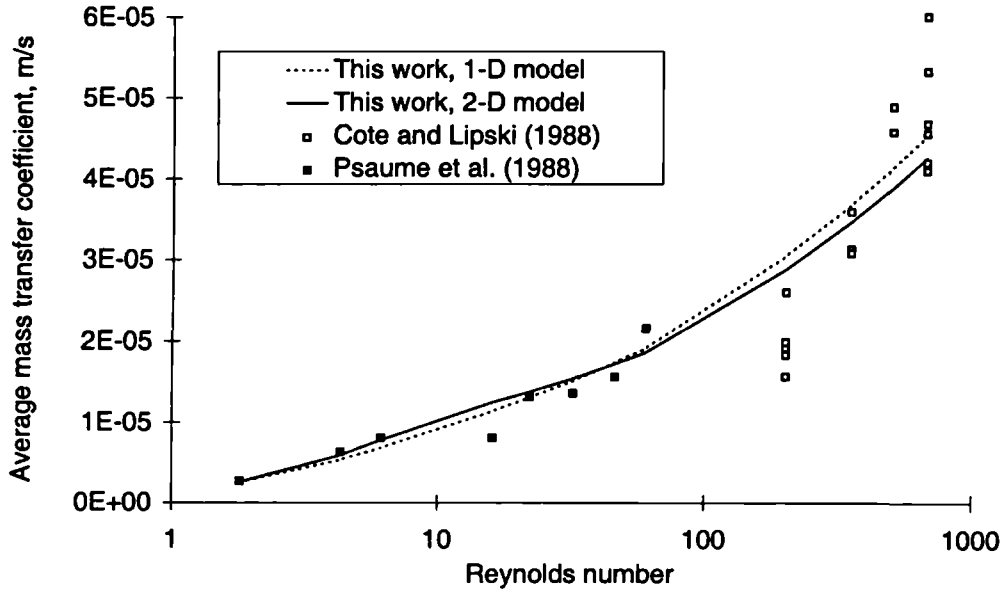

Figure 3.6 *Average mass transfer coefficient as a function of Reynolds number*

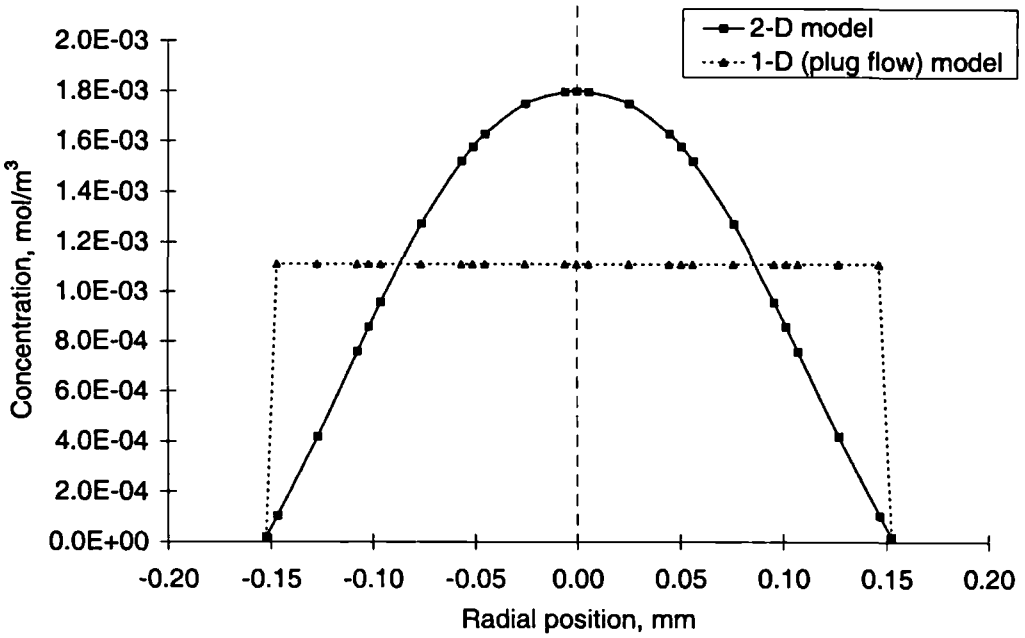

Figure 3.7 *Radial concentration profile for trichloroethylene at the fibre outlet (Re = 46)*

Table 3.4 *Comparison of experimental and calculated results for the removal of trichloroethylene from water*

Feed		Permeate conc. (ppm)		
Reynolds no.	**Conc. (ppm)**	**Experimental Psaume *et al.* (1988)**	**1-D model This work**	**2-D model This work**
1.8	0.200	70	65.5	66
4.3	0.210	176	154	163
6.1	0.212	233	208	224
16	0.241	337	472	499
22	0.270	650	642	664
32	0.255	675	745	755
46	0.251	803	886	877
64	0.222	1060	890	871

Summary

The 2-D detailed model has been used to accurately describe the removal of trichloroethylene by pervaporation. This case study highlights the importance of modelling concentration polarisation accurately. In fact, the effect of the membrane on trichloroethylene flux can be neglected due to the slow rate of transport through the boundary layer to the membrane surface. In other words, the resistance due to concentration polarisation is much larger than the resistance in the membrane.

The results of the two different modelling approaches are similar in this case. However, although the 2-D fibre flow model is computationally more expensive, it provides a rigorous and more general approach to describing concentration polarisation than the 1-D model. Furthermore, an empirical mass transfer coefficient does not need to be estimated for the 2-D flow model.

In Chapter 6 of this thesis, a second pervaporation case study is investigated. In this study, the simulation and optimal design of an existing ethanol dehydration plant will be considered. Here, the use of a detailed non-isothermal model is essential, as the removal of water from ethanol is usually accompanied by large temperature drops.

3.4.2 Gas separation simulation example

Membrane technology is commonly used to separate gas mixtures - important examples of this include: hydrogen and helium recovery, air separation, and the removal of acid gases from light hydrocarbons. In this process, the membrane forms a barrier between a high pressure feed gas and a low pressure permeate gas. To aid in the design of gas separation systems, Smith *et al.* (1996) and Krovvidi *et al.* (1992) have recently proposed two approximate models that describe the separation of a binary gas mixture in a hollow-fibre module. In this section, we evaluate the accuracy of these approximate models by comparing them with the detailed model presented earlier in this chapter. First, however, the detailed model is verified for gas separation using experimental results for a multicomponent system that has previously been simulated by Pan (1986).

Description of the system

Parallel flow hollow-fibre modules (Figure 3.2) are often used for gas separation. Here, feed enters on the shell-side and the penetrant passes first through the membrane and then through the porous support before being withdrawn as permeate on the fibre-side. 1-D flow sub-models (Section A.2) are used for both upstream and downstream flows, as concentration polarisation in gas separation can usually be neglected. The model is solved in less than 0.2 CPUs using the g*PROMS* simulation software and 4th order orthogonal collocation on a single finite element.

For this study, a simple solution-diffusion model (see Section 2.2) is applied to describe the cellulose acetate membrane. As the effect of concentration on gas permeabilities is small, constant permeability, Q, is often assumed. Pan (1986) states that resistance of the porous support is such that the downstream concentration is independent of the bulk concentration - the so called *cross flow model.* This is due to the slow rate of Knudsen diffusion (see Section 2.2) through the porous support. Thus the mass flux through the membrane is given by

$$J_i = \frac{Q_i}{\delta}(x_{1i}P_1 - \frac{J_i}{J_\Sigma}P_2) \tag{3.4}$$

Multicomponent gas separation

For this study, the detailed model is used to describe the removal of hydrogen from a multicomponent gas mixture containing 51.78% hydrogen, 24.69% nitrogen, 19.57%

Table 3.5 *Multicomponent gas separation simulation example (Pan, 1986)*

methane and 3.96% argon. Module and operating details are given in Table 3.5. The calculated results for this study are in excellent agreement with the experimental data (Pan, 1986) over the whole operation range. This is seen in Figure 3.8 which shows the hydrogen purity in the permeate stream as a function of the total product recovery.

Comparison with approximate model results

Having verified the model against experimental data, we will now use this case study to illustrate the problems associated with using approximate models to describe membrane systems. Over recent years, a number of approximate models have been proposed for a range of different membrane systems. We will consider two approximate design models that have been developed for gas separation by Smith *et al.* (1996) and Krovvidi *et al.* (1992).

To accurately describe gas separation, mass and momentum balances must be calculated on both sides of the membrane. The momentum balances are solved to yield the pressure profile along the length of the module, and the mass balances to yield concentration profiles. Approximate models generally disregard the momentum balance, and often also simplify the mass balances. Smith *et al.* (1996) assume that the permeate concentration is constant along the entire length of the module, whereas Krovvidi *et al.* (1992) assume a linear relationship between the feed-side and permeate-side concentrations - the operating line method [3].

[3]Krovvidi *et al.* (1992) have also described a second model. The authors report that though it does not perform well for co-current operation, it is a better model for counter-current operation. Unfortunately, there appear to be a number of mistakes in the equations given in the paper, and it was impossible to reproduce the authors' results.

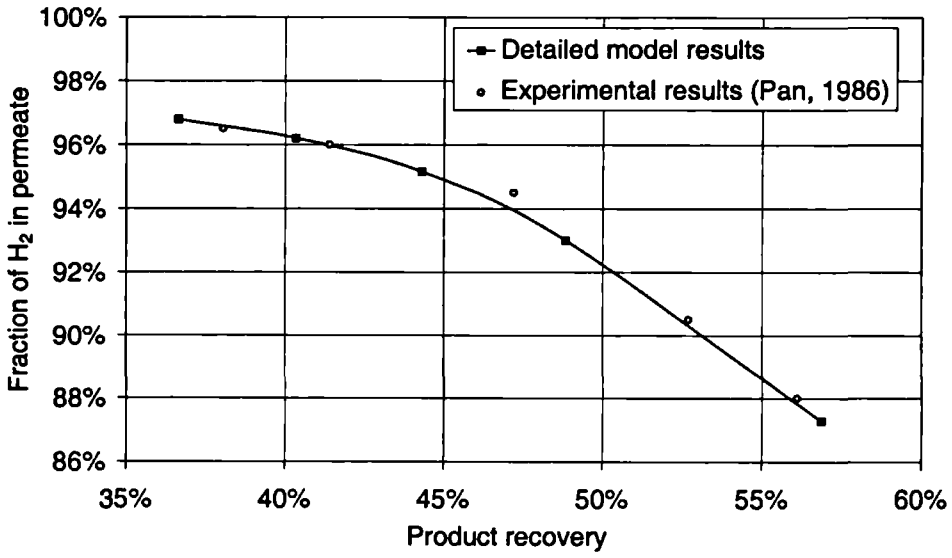

Figure 3.8 *Calculated permeate purity as a function of total product recovery*

Smith *et al.* (1996) use their model to describe the separation of hydrogen and nitrogen in a shell fed hollow-fibre module. This system will also be used in this work. Two cases with different operating conditions, membrane selectivities and feed compositions are considered. For each study, the retentate purity and the total product recovery are calculated for a range of feed flows. System details are given in Table 3.6.

Simulation results from the two approximate models for Case A are compared with the results from the detailed model in Figure 3.9. This shows the retentate product purity as a function of the product recovery. The approximate model results are generally poor, showing a significant deviation from the detailed model results over the entire operating range. This error is primarily due to the effect of neglecting the pressure profile, when in fact, there is a significant pressure build up on the fibre side.

The simulation results for Case B are shown in Figure 3.10. The permeate pressure is higher than in Case A, and as a result, the relative pressure drop is much lower. Consequently, the approximate model results show a good agreement ($\pm$ 1-2%) with those from the detailed model, particularly at high feed rates (i.e. low product recoveries). This is because the concentration profiles along the length of the module are relatively constant. However, at high product recoveries, the Krovvidi *et al.* (1992) model predicts an infeasible (greater than 100% H_2) permeate concentration, and the results from the

Table 3.6 *Approximate model gas separation system (Smith et al., 1996) Hollow-fibres: 0.76m length, 50 μm i.d., 100 μm o.d.*

Smith *et al.* (1996) model diverge significantly from the detailed model results (Fig. 3.10). The likely explanation for this is that the Smith *et al.* (1996) model assumes constant permeate concentration down the length of the module. This assumption is particularly invalid at high recovery rates, when there are significant concentration changes along the length of the module. Even for this simple system (ideal gas and constant membrane permeability), the approximate model results are unreliable, showing relatively poor agreement with the detailed model. It is seen that only at high permeate pressures and low product recoveries do the approximate models provide a reasonable level of accuracy. In contrast, hollow-fibre modules are usually connected in parallel (Zolandz and Fleming, 1992), with high recoveries, and low pressure operation will often be optimal. It should also be pointed out that one of the main disadvantages of most approximate models presented in the literature is that, unlike the detailed model, they are limited to binary separations.

Summary

The detailed model presented in this work can also be used to describe gas separation and excellent agreement is found with experimental data for a multicomponent gas mixture. The detailed model was used to highlight problems with two approximate models recently presented in the open literature. Later in this thesis (Chapter 4), a design method based on the detailed model is presented. This will be used to show that the use of approximate models for design purposes is unnecessary and can lead to sub-optimal and inaccurate designs.

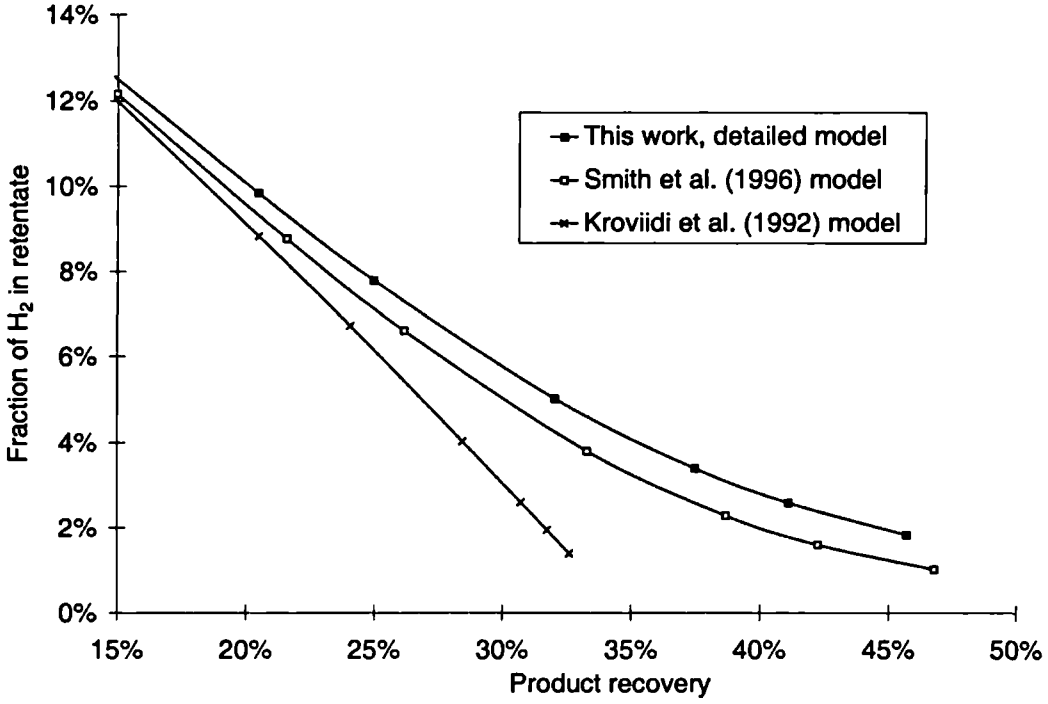

Figure 3.9 *Calculated retentate purity (Case A)*

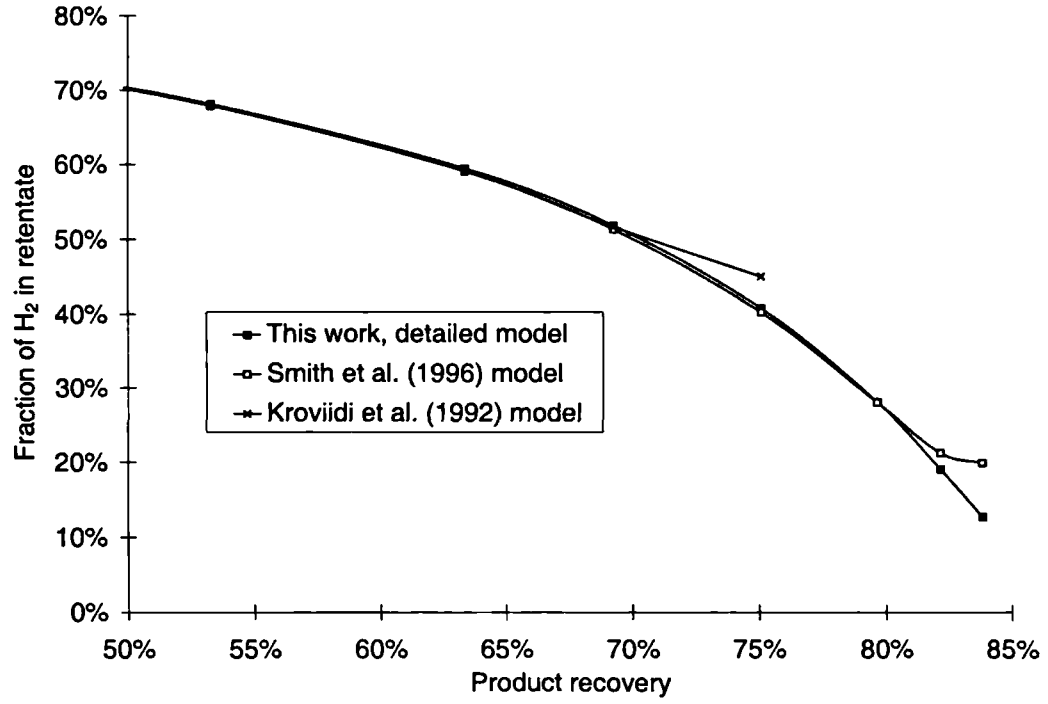

Figure 3.10 *Calculated retentate purity (Case B)*

3.4.3 Reverse osmosis simulation example

The model has now been tested for both pervaporation and gas separation systems in hollow-fibre modules. The use of the model to describe reverse osmosis in spiral-wound modules is now considered. This case study is also used to illustrate the application of the model for parameter estimation.

Description of the system

Ohya and Taniguchi (1975) have presented experimental results for a reverse osmosis spiral-wound module (ROGA-4000). The module is used for the desalination of brine water, where the product water preferentially permeates through the membrane. System details are given in Table 3.7.

Material flux through the membrane is characterised using a solution diffusion approach (Section 2.2). This is written

$$J_W = Q_W c_W \left(\Delta P - \Delta \Pi\right) \tag{3.5}$$

$$J_s = Q_s \left(\Delta c_s\right) \tag{3.6}$$

The effect of concentration polarisation is approximated using the stagnant film model (Equation 2.22) which introduces the mass transfer coefficient, k. In total three parameters, Q_W, Q_s and k, must be known. These have been determined by Ohya and Taniguchi (1975) from their experimental data using an analytical approach and a simple plug flow model. Initially, we will consider the simulation of the module for four operating conditions using these parameters.

In this study, the detailed 2-D channel flow sub-model (Section A.3, Appendix A) is used to describe flow through the feed and permeate channels of the ROGA-4000 spiral-wound module. The orthogonal collocation on finite elements method (4th order) is used to discretise both the axial and spiral spatial domains. A single element is used for the axial domain, whereas two elements are used for the spiral domain - this is to cope with the additional width of the feed channel spacer ($W^G = 0.15m$). For comparison purposes, the 1-D (plug flow) model has also been used to simulate flow through both the feed and permeate channels of the module. For the 1-D model, orthogonal collocation on a single element is used.

The model is solved using g*PROMS* (Process Systems Enterprise Ltd, 1999), taking approximately 0.4 CPUs for the 1-D model and 0.8 CPUs for the 2-D model.

Table 3.7 *Reverse osmosis simulation example (Ohya and Taniguchi, 1975)*

Simulation results

The use of the one and two-dimensional channel flow models to describe the ROGA-4000 module is now considered. The simulation results are presented in Table 3.8.

The results from the one and two-dimensional models are similar (within 1%). This suggest that assuming plug flow is reasonable in this case (i.e. variations in the spiral direction are low). To assess the validity of such an assumption, the concentration profile on the feed side of the membrane is plotted for Run C in Figure 3.11. This shows that there are significant concentration variations in the spiral direction, but these are mostly confined to the region where there is no membrane (0 - 0.15m). Over the membrane itself (0.15 - 1.65m), the concentration is relatively constant and therefore, plug flow can be assumed without significant penalty. However, Rautenbach and Albrecht (1989) suggest that in many cases, a greater difference can be expected between the results of the two approaches (Section 2.3.3). That the results of the two-dimensional approach are only a slight improvement on the simpler one-dimensional (plug flow) model can be attributed to the low pressure build up in the permeate stream in this particular case.

The simulation results from the detailed model over-predict the salt concentration in the permeate (Table 3.8). This concurs with the results of an earlier study by Sirkar *et al.* (1982), suggesting that the parameter estimation method used by Ohya and Taniguchi (1975) is inadequate. In response, a method based on the detailed model is described in the following section.

Table 3.8 *A comparison of experimental and calculated results for brine-water desalination - based on Ohya and Taniguchi's (1975) parameters*

Run	Feed				Permeate concentration (ppm)		
	Temp	Conc	Press	Rate	Exper.	Detailed model	
	^oC	ppm	psig	m/min	Ohya (1975)	1-D flow	2-D flow
A	20.0	2600	500	3.2	260	310.9	309.4
B	21.0	2600	415	4.98	260	270.6	270.0
C	21.85	2100	500	3.14	198	215.2	213.9
D	22.5	2100	415	4.96	198	212.2	211.7

Parameter estimation

Ohya and Taniguchi (1975) present permeate flow and concentration data for the desalination of brine water at several different feed conditions. They calculate the water permeability, Q_W, from pure water flux runs. The same value is also used here ($Q_W = 1.96 \times 10^{-12} m/sPa$). However, the salt permeability, Q_s, and feed side mass transfer coefficient, k, cannot be calculated directly. The use of the detailed (2-D) model to determine the parameter values is now investigated as an alternative to the parameter estimation method used by Ohya and Taniguchi (1975).

The values of the two parameters can be estimated by minimising the deviation of the model predictions from the experimental results (permeate flow rate and salt concentration). This can be done automatically within the g*PROMS* simulation environment (Process Systems Enterprise Ltd, 1999), using the g*EST* parameter estimation tool.

To determine the values of the parameters, all four runs will be considered simultaneously. It will be assumed that the salt permeability is independent of concentration, temperature and pressure (i.e. it is constant). The mass transfer coefficient is usually a function of velocity (see Section 2.2.4). A large number of correlations have been developed to estimate the mass transfer coefficient in spiral-wound modules (e.g. Winograd *et al.*, 1973; Chiolle *et al.*, 1978). In this work, the mesh step model (Winograd *et al.*, 1973) is used. From this, the mass transfer coefficient, k can be expressed as $k = bv^{\frac{1}{2}}$.

The estimation of the membrane characterisation parameters took 710 CPUs (just under twelve minutes). The results are presented in Table 3.9. These show much better agreement with the experimental results than those in Table 3.8 which were generated using the models presented in this thesis but with parameters derived by Ohya and Taniguchi. The slight discrepancy between the new results and the experimental data is most likely

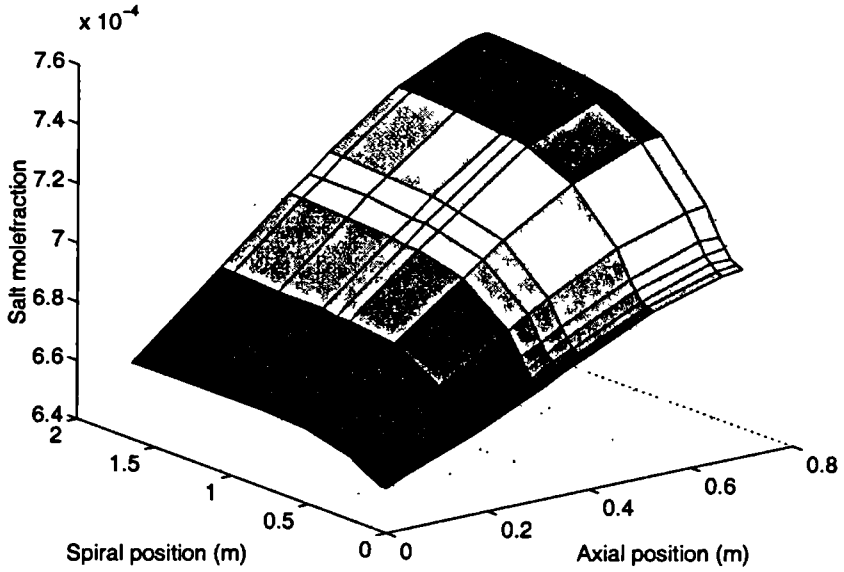

Figure 3.11 *Calculated salt concentration in the feed channel*

due to the assumption of constant salt permeability across the four runs. In fact, the permeability will change with the slightly different feed temperatures and concentrations (also see Section D.2, Appendix D).

Summary

The detailed modelling approach described in Section 3.2 has been successfully applied to reverse osmosis for a spiral-wound module case study. The use of the model for parameter estimation has also been demonstrated and simulations with the new parameters show much better agreement with the experimental data than those published previously for this case study.

In this case, the use of a one-dimensional (plug flow) approach was shown to lead to only small discrepancies in the product purity when compared with results from a two-dimensional model. Nevertheless, the two-dimensional approach provides greater information about the flow patterns inside the module (see for example Figure 3.11), making it more appropriate for a wider range of applications, such as module design. Furthermore, whilst the assumption of plug flow is reasonable here, in other cases, particularly when pressure build up in the permeate stream is significant, this may not be true.

The application of the detailed model to reverse osmosis modules is investigated further in Chapter 5. In this study, the use of radial flow hollow-fibre and spiral-wound modules for sea-water desalination is considered.

Table 3.9 *Parameter estimation results for brine-water desalination example*

Run	Salt permeability, Q_s $(10^{-7}m/s)$	Mass transfer coefficient, k $(10^{-6}m/s)$	Permeate concentration (ppm)	
			Experimental (Ohya, 1975)	Calculated (This work)
A	5.15	$144\,(v)^{\frac{1}{2}} = 33$	260	258
B	5.15	$144\,(v)^{\frac{1}{2}} = 41$	260	255
C	5.15	$144\,(v)^{\frac{1}{2}} = 33$	198	203
D	5.15	$144\,(v)^{\frac{1}{2}} = 41$	198	201

3.5 Conclusions

A detailed modelling approach has been described in this chapter. The model is developed from rigorous mass, momentum and energy balances and disregards many common assumptions such as: plug flow; constant pressure; constant temperature; binary mixture; steady-state conditions; and constant physical properties. The high accuracy of the results presented in Section 3.4 demonstrates the importance of such an approach. Furthermore, the lack of fixed assumptions made in the development of the model enables a wide range of different separations to be tackled.

The model has also been compared with two approximate design models that have been presented in the literature for gas separation (Section 3.4.2). The approximate model results differ significantly from the detailed model results over the entire operating range. As a result, the use of approximate models for system design cannot be recommended. This point will be further explored in Chapter 5, where optimal design strategies based on detailed and approximate models are compared using a reverse osmosis example.

The aim of Section 3.4 was to demonstrate the generality of the detailed model by considering a range of different membrane systems. This objective was successfully achieved. However, it should be noted that only a small fraction of the possible uses of the detailed model have been investigated in this chapter, and it is hoped that in future work, an even wider range of applications can be considered, such as investigating operating point and control issues - for which a dynamic model is essential (see Chapter 7). The remainder of this thesis concentrates on the application of the detailed model to the optimal design of membrane systems.

Chapter 4

Optimisation strategy

In this chapter, a new strategy for the optimal design of membrane separation systems is outlined. A superstructure for a generic membrane process, that enables all design choices to be considered simultaneously, is developed. The approach focuses on the balance between the number of membrane units and the driving forces for mass transport through the membranes. The problem is formulated as an MINLP optimisation problem and a solution technique based on genetic algorithms is described.

4.1 Introduction

The performance of a membrane process is limited by the magnitude of the chemical potential driving force for mass transfer. This driving force can be maximised by manipulating the temperature or pressure of the feed stream as well as the pressure of the permeate outlet. In a pervaporation plant, it is usual to control the permeate pressure and feed temperature; whereas for reverse osmosis and gas separation plants, it is the feed pressure which is generally controlled.

The manipulation of stream pressures and temperatures can demand significant energy and is costly. When designing a membrane separation system, this expenditure must be balanced against other costs, such as the cost of the membranes and other capital outlay. The interactive nature of all these choices is complex and, consequently, formal optimisation techniques are required to determine the best values for the various design parameters.

An optimisation strategy which considers both the structural configuration and the oper-

ating point of membrane separation systems is presented in this chapter. The approach is based on the optimisation of a process superstructure using a genetic algorithm and utilises the detailed model presented in the previous chapter (though in principle, any module model could be used). In the next section, various solution techniques for solving this type of problem are discussed. In Section 4.3, a methodology for developing a superstructure of a general membrane system is presented. Following this (Section 4.4), a solution technique based on genetic algorithms is introduced. In the last section (Section 4.5), conclusions on the viability of this new optimisation strategy are given.

4.2 Solution alternatives

To consider a design problem in its entirety, a formulation that enables all decision choices to be considered simultaneously must be produced. This is done by generating a superstructure of design alternatives.

A process can be simulated by a set of individual unit models connected in the correct sequence by information streams. Therefore, a process superstructure can be rigorously generated by considering all possible units and allowing stream connections between all of these units. Generally, both discrete and continuous variables are required: discrete variables may describe whether a unit exists in a process, and continuous variables may describe unit operation and stream flowrates.

An optimisation problem requires that the value of a given objective function be maximised or minimised, subject to equalities such as those derived from mass and energy balances, and to inequalities such as product specifications. The objective of a design problem is usually to select the process flowsheet with the minimum annualised plant cost. The annualised plant cost incorporates both capital and operating costs. In this section, we explore a range of techniques that can be used to solve this type of optimisation problem.

4.2.1 Gradient-based approaches

In general, superstructure optimisation problems require the solution of equations containing both linear and non-linear functions in discrete and continuous variables. This is referred to as a Mixed Integer Non-Linear Programming (or *MINLP*) problem. The solution of *MINLP* optimisation problems is complex. Conventional *MINLP* solution methods involve disassociating the integer and binary variables from the continuous variables and

solving the resulting *NLP* sub-problems using a gradient-based approach. Three solution methods are now discussed, further details can be found by reference to Biegler *et al.* (1997).

- Enumeration of all possible integer values: solving each *NLP* sub-problem to find the optimal value of the continuous variables (Smith, 1996). The result of this search is an optimal solution for each possible combination of the integer variables, the best of these is the solution to the *MINLP* optimisation problem.
- Branch and bound method: the integer variables are relaxed to continuous values and the *MINLP* transformed to a relaxed *NLP*. The *rNLP* is solved using an *NLP* solver to give the lower bound on the problem. The values of the integer variables are fixed using a branching method. If all of the integer variables at a given node have obtained integer values or the current upper bound has been exceeded, the branch is terminated. The search space has been fully explored when all branches are terminated (Biegler *et al.*, 1997).
- Generalised Benders Decomposition/Outer-Approximation methods (Geoffrion, 1972; Duran and Grossmann, 1986): the *MINLP* is solved for fixed values of the binary variables (therefore reducing to an *NLP* problem). This solution yields an upper bound on the optimum. A lower bound is generated by solving an *MILP* master problem[1]. When the two solutions agree (or are within a specified tolerance), an optimum has been found.

The *NLP* sub-problems are usually solved using successive quadratic programming methods or reduced gradient methods (Biegler *et al.*, 1997), for which many commercial algorithms are available. In many cases, the *NLP* problems involve non-convexities that may give rise to a number of local optima. Currently, whilst there have been considerable recent advances (Grossmann and Daichendt, 1996; Adjiman *et al.*, 1997), a method that guarantees a global optimum solution is not yet available. Therefore, several optimisations at different starting points must be carried out to determine whether the global optimum has indeed been identified.

If a large number of integer variables are present, the enumeration approach requires too many *NLP* evaluations to be a feasible option. However, Smith (1996) has successfully applied such an approach to design studies involving distillation columns and reactor sequences for problems with only a small number of integer variables. The branch

[1]The *MILP* is a global approximation to the *MINLP* problem which increases in accuracy following each iteration.

and bound method is similar but eliminates many of the alternatives by bounding the solution, again, a large number of *NLP* evaluations may be required. The Benders Decomposition/Outer-Approximation approach is much more efficient for problems containing a larger number of integer variables. However, the first two methods have the advantage of higher transparency and they enable the user to handle the non-convexity of the problem. This allows the user to subjectively repeat the optimisation if it is felt that a sub-optimal solution has been returned. Whereas when using automated algorithms, non-convexities can result in feasible solutions being cut-off.

Unfortunately, many design problems are highly non-convex and gradient-based methods will only converge to the closest local optimum. Furthermore, gradient-based methods are unable to handle discontinuities correctly and can be computationally expensive as they require derivative information (Androulakis and Venkatasubramanian, 1991).

The application of genetic algorithms to the design of process plants has only been explored in a limited number of cases (such as Androulakis and Vekatasubramanian, 1991; Fraga and Senos Matias, 1996; Garrard and Fraga, 1998) and has not previously been considered for the design of membrane systems. Genetic algorithms are generally slower than gradient-based solution techniques when used for solving simple optimisation problems. However, they potentially offer a number of important advantages over gradient-based approaches

- They do not require a smooth search space - i.e. discontinuous functions can easily be handled as derivative information is not required.
- Multiple solutions are available at the end of the optimisation.
- They perform a global search and are less likely to get trapped in local optima.
- They can cope with both continuous and discrete variables.

For these reasons, the use of genetic algorithms for the optimal design of membrane systems is explored in this work.

4.2.2 Genetic algorithms

Genetic algorithms are used for a range of purposes from solving practical optimisation problems to providing computational models of natural evolutionary systems (Mitchell, 1996). The basics of genetic algorithms are now discussed.

Genetic terms

Many of the terms used to describe biological systems are also used by analogy in the description of the components of a genetic algorithm - though of course their artificial counterparts are much simpler. The following definitions are based on the work of Mitchell (1996)

Genome: the collective name for all the genetic material of an organism is genome - all of the chromosomes taken together.

Chromosomes: all living organisms are known to consist of cells, each cell containing the same set of chromosomes, these are DNA strings that form the "blueprint" for the organism as it develops.

Genes: chromosomes are made up of functional blocks, these blocks are termed genes and are believed to encode many of the traits of the organism, such as eye colour. The different possible settings for the trait form the *allele* of the gene.

Optimisation problems

Genetic algorithms are stochastic optimisation methods, based on the principles of natural selection. These were first investigated by Holland (1975) who devised methods to introduce the mechanisms of natural adaption into computer systems.

In a genetic algorithm, genes are used to encode optimisation decision variables. A genome is the set of genes which uniquely encodes a candidate solution to the optimisation problem. The genes are of variable type, so they can hold continuous values, be selected from an allele set or even be complex data structures such as graphs.

A genetic algorithm is usually initialised by filling the population with randomly generated genomes. Each subsequent generation is populated by applying genetic operators, such as *mutation* and *crossover*, to the best individuals from the previous generation. Essentially, genetic operators stochastically adjust the value of one or more genes in order to generate a new set of optimisation decision variables. Mutation is used to introduce new information and crossover combines information from two existing solutions. The algorithm can continue **evolving** the population in this manner indefinitely. However, often stopping criteria such as a maximum number of generations or population convergence are used.

The genetic algorithm uses the fitness of each individual to determine which individuals should survive, which should reproduce and which should die. The fitness is usually the objective function of the optimisation problem.

4.3 Methodology

A membrane separation process consists of a large number of membrane units as well as ancillary equipment which may include heat exchangers, pumps and compressors. The purpose of the ancillary equipment is to control the transport of material through the membrane. This is done by changing the state (i.e. pressure or temperature) of the process streams.

A process superstructure of design alternatives is rigorously generated by considering all possible units and allowing stream connections between all of these units (Section 4.2). Such an approach usually leads to very large problems. Therefore, it is necessary to formulate the problem carefully, in order to minimise computational expense.

In previous work (see also discussion in Section 2.4), El-Halwagi (1992) considered the optimal design of reverse osmosis networks. He represented the design problem using the so-called "state space approach" which has been developed for the synthesis of mass, heat and distillation networks (El-Halwagi and Manousiouthakis, 1990; Manousiouthakis *et al.*, 1990; Manousiouthakis and Bagajewicz, 1990). This representation provides a powerful means of considering all potential process configurations and has been used for the optimal design of a number of membrane systems (e.g. El-Halwagi, 1992; Srinivas and El-Halwagi, 1993; Voros *et al.*, 1997). However, it suffers from a number of disadvantages

- There are a very large number of potential stream connections as the ancillary equipment items (such as pumps) are introduced independently to the membranes with this approach. In contrast, in this research, the driving force for mass transport across the membrane is optimised directly. The position of any ancillary equipment items is deduced from the required change in state (e.g. stream pressurisation) of the process streams. This greatly reduces the number of potential stream connections and hence, the problem size.

- Two variables are used to describe the fixed and variable nature of the cost of ancillary equipment items: a binary variable determines whether the unit actually exists and a second, continuous, variable describes the state change across the unit. This is necessary when using gradient-based solution techniques to avoid

discontinuous functions. However, genetic algorithms do not require a smooth search space (see Section 4.2.1) and only a single continuous variable describing the state change of any stream is used: the unit simply does not exist when a state change is not required. This approach also avoids a large number of inequality constraints that are otherwise necessary (e.g. to prevent stream pressurisation when no pump is selected) and are often difficult to implement with genetic algorithms.

An alternate methodology for the representation of membrane processes is presented in this section. This new approach concentrates on the interacting choices between the number of modules and the driving force for transport across the membrane. The detailed membrane unit model presented in Chapter 3 is used throughout this work, and models which can be used to describe the ancillary equipment are presented in Section A.4 (Appendix A).

4.3.1 Process superstructure

The process is conceptualised using separation stages. A **separation stage** is defined simply as a number of identical membrane modules connected in parallel (see Section 4.3.2).

The process superstructure is then built from three unit types: N^s separation stages, N^f feed points and N^p product points. The features of each unit type are shown in Table 4.1. Most membrane systems contain a single feed and two (permeate and retentate) product points. A superstructure for a process containing two separation stages is illustrated in Figure 4.1.

To define the superstructure we must allow for all possible network choices, this is done using streams. These allow a flow of material from a unit outlet to any unit inlet. The thermodynamic state, S, (temperature and/or pressure) of the fluid is manipulated to

Table 4.1 *The unit types used to build a superstructure for a membrane separation process*

Unit type	No.	No. inlets per unit	No. outlets per unit
Separation stage	N^s	1	2
Feed point	N^f	0	1
Product point	N^p	1	0

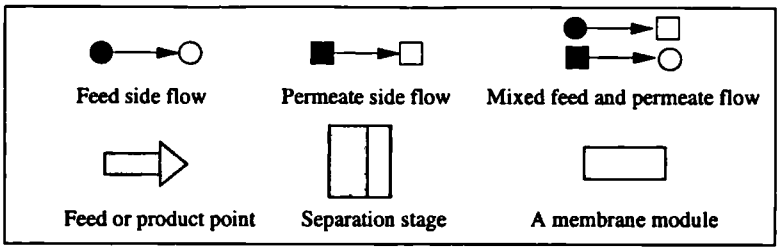

Key to the figures in this chapter

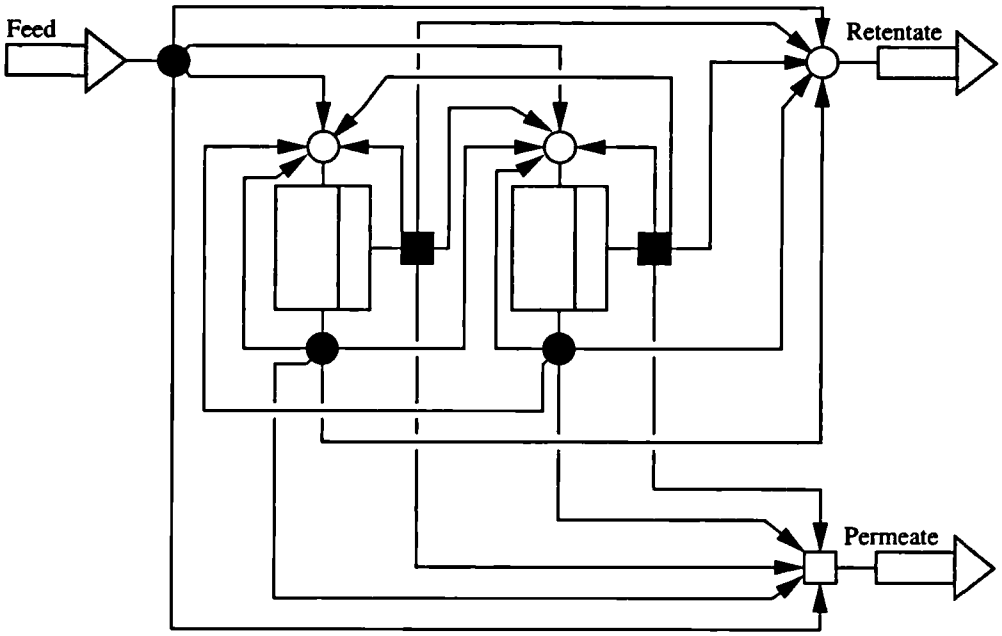

Figure 4.1 *A process superstructure for two separation stages*

the conditions of the destination unit. The minimum cost (C) for this transformation is calculated using the ancillary equipment models (Section A.4, Appendix A)

$$C^{fixed} = f_1(\Delta S) \tag{4.1}$$

$$C^{op} = f_2(\Delta S) \tag{4.2}$$

The functions can be in any form - this is specified by the ancillary equipment models. For example, the fixed cost may be a step function: 0 if $\Delta S = 0$ and 10 if $\Delta S > 0$. In this work, two types of ancillary equipment are considered: pressurisation/depressurisation devices; and heating/cooling devices - see Table 4.2.

Table 4.2 *The main ancillary equipment requirements for different membrane processes*

Separation process	Main driving force for mass transport	Main ancillary equipment
Gas separation	Pressure	Compressors
Reverse osmosis	Pressure	High pressure pumps
		Energy recovery devices
Pervaporation	Concentration	Heaters
		Vacuum compressors

As the ancillary equipment models are embedded in the stream model, the number of potential stream connections that are required is greatly reduced. Furthermore, it is not necessary to introduce constraints to forbid two manipulators operating on the same stream - El-Halwagi (1992) prevents pressurisation and depressurisation of the same stream using an inequality constraint. This is not required here, as the thermodynamic state (temperature and/or pressure) of each stream, S, can only be adjusted once.

4.3.2 Separation stage

A separation stage consists of a number of identical membrane modules connected in parallel. This is shown for a general system in Figure 4.2. A single instance of the detailed model can be used to describe the set of parallel membrane modules in each stage. This is possible as the modules will all perform in an identical manner if the feed is distributed evenly between them. This approach requires a significantly smaller computational effort than if a separate mathematical model was used to describe each module. For each stage, the state (pressure or temperature) of the feed stream and pressure of the permeate product must be specified. This enables the driving force across the membrane to be controlled.

For each stage, the optimiser is free to manipulate the state (S) of the feed and permeate streams and the number of membrane modules (N^m). These can be optimised directly or selected from an allele set. Each choice may have associated capital and operating cost implications. For example, changing the pressure of a stream will introduce the unit cost of a pump as well as the cost of pressurising the fluid.

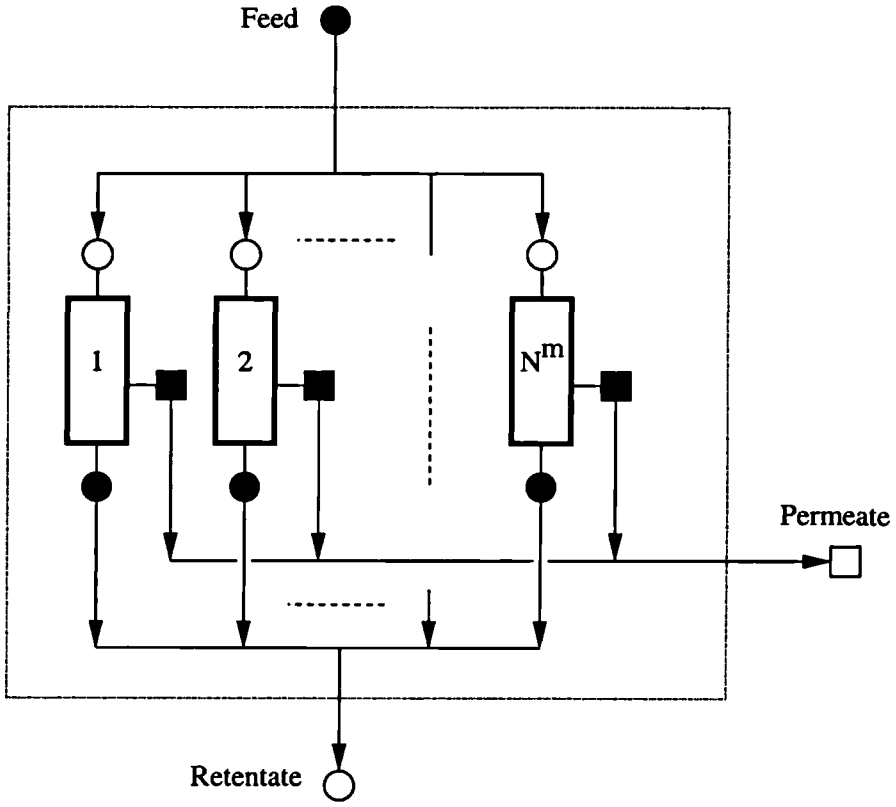

Figure 4.2 *A separation stage*

4.3.3 Network choices

As each unit outlet can potentially send flow to any unit inlet, the total number of streams from a unit outlet is equal to the total number of unit inlets ($N^1 = N^p + N^s$). If each unit outlet is assigned a number a and each unit inlet a number b, we can define the split fraction, $\sigma_{a,b}$. This is the fraction of material leaving unit outlet a that goes to unit inlet, b, and is calculated

$$m_{a,b}^{in} = \sigma_{a,b} m_a^{out} \tag{4.3}$$

However, as the mass balance must hold at each unit outlet, a, we can write

$$\sum_{b=0}^{N^1-1} \sigma_{a,b} = 1 \tag{4.4}$$

The structure of the system is fixed by specifying the split fractions (σ) for each unit outlet. It is clear that despite using separation stages, a large number of choices must

Table 4.3 *Number of optimisation decision variables for different superstructure sizes*

System size	Number of stage variables	Number of network variables	
		Full	Simplified*
One stage	3	6	2
Two stages	6	15	6
Three stages	9	28	12
Four stages	12	45	20

*Simplified network: assumes that the permeate and retentate streams cannot be mixed.

be taken. This was illustrated earlier in Figure 4.1. For a general superstructure $\{(N^f + 2N^s) \times (N^p + N^s - 1)\}$ network decisions are required. The number of optimisation decision variables for one, two, three, and four stage systems is shown in Table 4.3. Fortunately, in many cases, it is possible to reduce the number of network decisions by making a few reasonable assumptions: for example in pervaporation, the vapour permeate stream cannot be mixed with the liquid retentate stream. Simplifying the network by preventing permeate and retentate mixing is seen to greatly reduce the number of network choices.

4.3.4 Summary

A superstructure for the optimal design of membrane systems has been described in this section. It provides a neat and efficient framework, yet, is able to encompass all design alternatives. This new methodology enables the number of modules as well as the driving force for mass transport to be optimised directly. The structure of the system can also be optimised by manipulating the stream flows leaving each unit.

The use of this methodology for the optimal design of a reverse osmosis process is investigated in Chapter 5 and the design of a pervaporation system is considered in Chapter 6. In the next section, a solution technique based on genetic algorithms is presented.

4.4 Implementation

An optimisation strategy using genetic algorithms has been implemented in a C++ program. This is based on the genetic algorithm library GAlib (version 2.4) which provides a set of genetic algorithm tools. The main components of the program are the genetic algorithm and the genome - these are described in this section. The best values for

important parameters which control the performance of the genetic algorithm are also investigated.

4.4.1 The genome

The process superstructure is fixed by specifying the values of all the optimisation decision variables. The list of decision variables (i.e. the genome) for a two separation stage system is illustrated in Table 4.4. The decision variables are encoded using two chromosomes, these are described below. However, it should be noted that it is easy to add extra decision variables (genes) at any position in the genome. For example, if one wanted to optimise the module size, an extra gene representing the membrane area could be introduced into the primary chromosome (Chromosome 1).

Primary chromosome

The first chromosome is concerned with the stage decision variables. These are the number of modules (discrete), the feed stream pressure or temperature (continuous) and the permeate stream pressure (continuous). In this work, the operating state variables (temperature or pressure), S, are normalised between 0 and 1 using the following linear mapping of the decision variable (D^S)

$$S = D^S \left(S^{max} - S^{min}\right) + S^{min} \tag{4.5}$$

Secondary chromosome

The second chromosome is concerned with the full structural layout of the membrane system and therefore holds the values of the network decision variables. These are essentially the flow split fractions ($\sigma_{a,b}$) bounded to ensure that Equation 4.4 is not violated (also see Table 4.4)

$$0 \leq \sigma_{a,b} \leq max\left(\left(1 - \sum_{b=0}^{b=N^t-2} \sigma_{a,b}\right), 0\right) \tag{4.6}$$

It should be noted that the split fraction to the permeate product cannot be adjusted independently as this would over specify the problem - instead the fraction of material to the permeate product point is calculated from Equation 4.4.

Table 4.4 *Genome encoding the decision variables for a two separation stage system*

Decision variable	Lower bound	Upper bound
Chromosome 1 (stage decision variables)		
Number of modules, Stage 1	N_m^{min}	N_m^{max}
Normalised feed state, Stage 1	0	1
Normalised permeate state, Stage 1	0	1
Number of modules, Stage 2	N_m^{min}	N_m^{max}
Normalised feed state, Stage 2	0	1
Normalised permeate state, Stage 2	0	1
Chromosome 2 (split fractions)		
Feed to stage 1, $\sigma_{0,1}$	0	1
Feed to stage 2, $\sigma_{0,2}$	0	$1 - \sigma_{0,1}$
Feed to retentate product, $\sigma_{0,3}$	0	$1 - (\sigma_{0,1} + \sigma_{0,2})$
Stage 1 retentate to stage 1, $\sigma_{1,1}$	0	1
Stage 1 retentate to stage 2, $\sigma_{1,2}$	0	$1 - \sigma_{1,1}$
Stage 1 retentate to retentate product, $\sigma_{1,3}$	0	$1 - (\sigma_{1,1} + \sigma_{1,2})$
Stage 1 permeate to stage 1, $\sigma_{2,1}$	0	1
Stage 1 permeate to stage 2, $\sigma_{2,2}$	0	$1 - \sigma_{2,1}$
Stage 1 permeate to retentate product, $\sigma_{2,3}$	0	$1 - (\sigma_{2,1} + \sigma_{2,2})$
Stage 2 retentate to stage 1, $\sigma_{3,1}$	0	1
Stage 2 retentate to stage 2, $\sigma_{3,2}$	0	$1 - \sigma_{3,1}$
Stage 2 retentate to retentate product, $\sigma_{3,3}$	0	$1 - (\sigma_{3,1} + \sigma_{3,2})$
Stage 2 permeate to stage 1, $\sigma_{4,1}$	0	1
Stage 2 permeate to stage 2, $\sigma_{4,2}$	0	$1 - \sigma_{4,1}$
Stage 2 permeate to retentate product, $\sigma_{4,3}$	0	$1 - (\sigma_{4,1} + \sigma_{4,2})$

4.4.2 The genetic algorithm

All of the work in this thesis is based on a steady-state genetic algorithm. This algorithm is initiated using a population of randomly generated genomes. It selects a new population of genomes based on the best individuals from the current population and applies the crossover and mutation operators to these genomes (discussed in the next section). The probability of an operator being applied to any genome is determined by the crossover and mutation rates, and these are also discussed later (Section 4.4.5.)

Each new population is merged with the existing population and the worst individuals removed to keep the size of the population constant. This method ensures that the best solutions encountered are not lost from one generation to the next. The algorithm is terminated when the population converges to a single genome.

The genetic algorithm used in this thesis is illustrated in Figure 4.3.

4.4.3 Genetic operators

The key characteristics of the genome are the crossover and mutation methods that the genetic algorithm uses to create the new generations.

Crossover

The crossover operator defines the procedure for generating two children from two parent genomes. In these studies, the operator simply randomly mixes the parent genes. Consequently, the two children are opposing mixtures of their parents' genes. This is illustrated for the primary chromosome of a two stage superstructure in Table 4.5.

Table 4.5 *Example of crossover operator (primary chromosome only)*

Decision variables	Parent 1	Parent 2	Child 1	Child 2
Number of modules, Stage 1	54	19	19	54
Feed pressure, Stage 1	0.85	1	0.85	1
Permeate pressure, Stage 1	0	0	0	0
Number of modules, Stage 2	20	18	20	18
Feed pressure, Stage 2	0.6	0.7	0.7	0.6
Permeate pressure, Stage 2	0	0	0	0

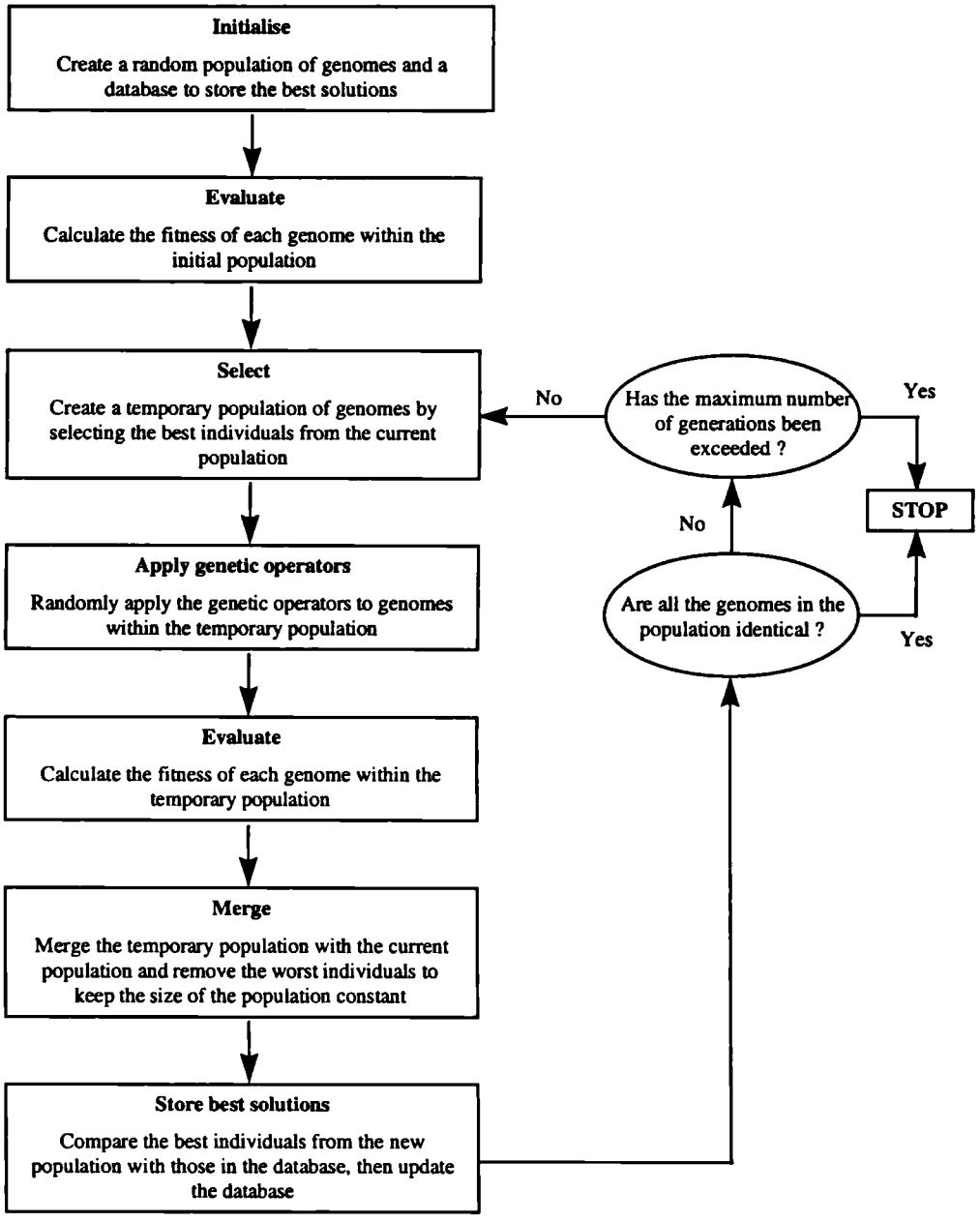

Figure 4.3 *The steady-state genetic algorithm used in this thesis*

Table 4.6 *Example of mutation operators (primary chromosome only)*

Decision variables	Original	Gaussian mutation	Stage mutation
Number of modules, Stage 1	54	29	20
Feed pressure, Stage 1	0.85	0.85	0.6
Permeate pressure, Stage 1	0	0	0
Number of modules, Stage 2	20	20	54
Feed pressure, Stage 2	0.6	0.6	0.85
Permeate pressure, Stage 2	0	0.05	0

Mutation

Mutation is used to introduce new genetic material or to move existing genetic material around the genome. The type of mutation that takes place will depend on the data type: a binary genome is usually mutated by randomly flipping some of the genes; whereas a Gaussian distribution around the current value is often used to mutate a real number gene. In this work, the genome is mutated in one of two ways, as described below. The application of both mutation operators to the primary chromosome of a two stage superstructure is illustrated in Table 4.6.

Gaussian mutation Each gene can be individually mutated: the value of the gene is changed using a Gaussian distribution around the current value. If the gene can only take discrete values then it is rounded to the nearest feasible value. However, if the gene reaches either of its bounds then it is reset to that bound. It is important that the algorithm explores the boundary possibilities as this enables units to be either deselected or operated at maximum power.

Stage mutation The genes for one stage are swapped with genes that represent another stage. This is illustrated in Table 4.6 where the genes for Stage 2 are swapped with those representing Stage 1. This enables information to be passed around the genome which is a powerful feature of genetic algorithms.

4.4.4 Fitness

The likelihood of selecting a member of the population is based on its fitness. The fitter the genome the more likely it is to be selected. There is no limit on the number of times

a certain genome can be selected.

Each time the genetic algorithm makes a call to calculate the fitness of a genome, a simulation is executed. The current values of the optimisation decision variables are passed to the simulator. After the simulation has been executed, the value of the objective function is returned. The fitness is usually a simple (often linear) function of the objective function.

4.4.5 Parameter values

There are four main parameters that control the performance of the genetic algorithm. These are: 1) the population size, 2) the percentage of the population to replace from one generation to the next, 3) the crossover rate and 4) the mutation rate. The choice of suitable parameter values is crucial to the success of a genetic algorithm, where both high quality solutions and short computational times are desired. The best values for these parameter are now discussed.

Population size

The size of the population should be large enough to provide sufficient diversity at the start of the evolution. Unfortunately, "sufficient diversity" is difficult to quantify. However, Lewin *et al.* (1998) report that genetic algorithms are insensitive to the population size provided that it is not very small. In this work, a population size of fifty genomes will be used for small one-stage problems. This will be increased to one hundred-and-fifty for larger problems.

Replacement percentage and crossover rate

The maximum number of genomes that are replaced in each generation (the replacement policy) and the rate of crossover must be specified. Garrard and Fraga (1998) found good results for mass exchanger synthesis using a 75% replacement policy and a crossover rate of 75% [2], these values will also be used here.

[2] A crossover rate of 75% indicates that 25% of children are clones of their parents (subject to any later mutation).

Table 4.7 *The effect of mutation rate on genetic algorithm performance for a two stage pervaporation system*

Mutation rate, %	Best solution, $/day	Generations required
0	19.4	37
1	20.8	33
5	21.7	46
15	21.7	37
20	22.1	81
40	21.8*	>300

*40% mutation rate run was incomplete and terminated after 300 generations.

Mutation rate

The mutation rate is the likelihood that a gene in a newly born individual will mutate. It is an important parameter used to control the rate of introduction of new genetic material into the population. A high value overrides the effect of crossover, but a value set too low forces the genetic algorithm to converge prematurely.

The best mutation rate is heavily dependent on the type of problem. A mutation rate of 10% is used by Garrard and Fraga (1998) for mass exchanger network synthesis. However, for heat exchanger networks, Lewin *et al.* (1998) use a value of 0.1% and Androulakis and Venkatasubramanian (1991) use 30%. Androulakis and Venkatasubramanian (1991) also investigate the use of variable *or generation dependent* mutation rates.

To determine a suitable value for the type of problem studied in this thesis the effect of mutation rate on both solution quality and computation time has been investigated using a population of two stage genomes and the pervaporation case study detailed later in Chapter 6. Figure 4.4 shows the results for a mutation rate of 5%. It is seen that the mean objective function score and the best-of-generation score converge at generation 46. At this point, the population is filled with identical genomes - population convergence. This is used to terminate the genetic algorithm in these studies (Section 4.4.2). Although random mutation may enable further improvement beyond this point, it is highly unlikely.

The mutation study results are presented in Table 4.7. This shows the effect of different mutation rates on the best solution found by the genetic algorithm and the number of generations required for population convergence. It is seen that similar solutions are found when there is even a small amount of mutation. However, a high rate of about 20% is required to find what is believed to be the global optimum (22.1 $/day) and prevent

premature convergence to sub-optimal values - most apparent for the zero mutation case. Unfortunately, population convergence takes much longer at higher mutation rates, and at a rate of 40% population convergence did not occur within 300 generations.

The results are also plotted in Figure 4.5 which shows the effect of various mutation rates on population evolution.

4.4.6 Summary

In this section, a technique for the solution of the superstructure optimisation problem posed in Section 4.3 has been described. The technique, which is based on a genetic algorithm, has been implemented in a C++ program.

In order to determine the best mutation rate for the genetic algorithm, a series of optimisation runs were carried out using a pervaporation example (Section 6.2). In line with published studies (e.g. Garrard and Fraga, 1998), it is seen that with no mutation, the genetic algorithm quickly finds a sub-optimal solution. However, with even a small amount of mutation, the runs converge to similar solutions. Based on these experiences, throughout this work, a mutation rate of 20% is used in conjunction with a crossover rate of 75%; a replacement rate of 75%; and a population size from 50 to 150 (depending on the problem size).

4.5 Conclusions

A new optimal design methodology has been presented in this chapter. In this approach, a genetic algorithm is used to solve a superstructure optimisation problem. The design methodology focuses directly on the balance between the number of membrane units and the driving forces for mass transport through the membranes. However, the structure of the system can also be optimised by manipulating the stream flows leaving each unit. In the following two chapters, the application of this method to the design of reverse osmosis (Chapter 5) and pervaporation (Chapter 6) systems is assessed.

The application of detailed models to the optimal design of membrane systems is advocated in this research (Section 1.2). Therefore, the optimal design methodology will be coupled with the detailed mathematical model presented in Chapter 3. However, if desired, it could equally be coupled with an approximate design model (Section 2.3.4). These two approaches will be contrasted in Chapter 5.

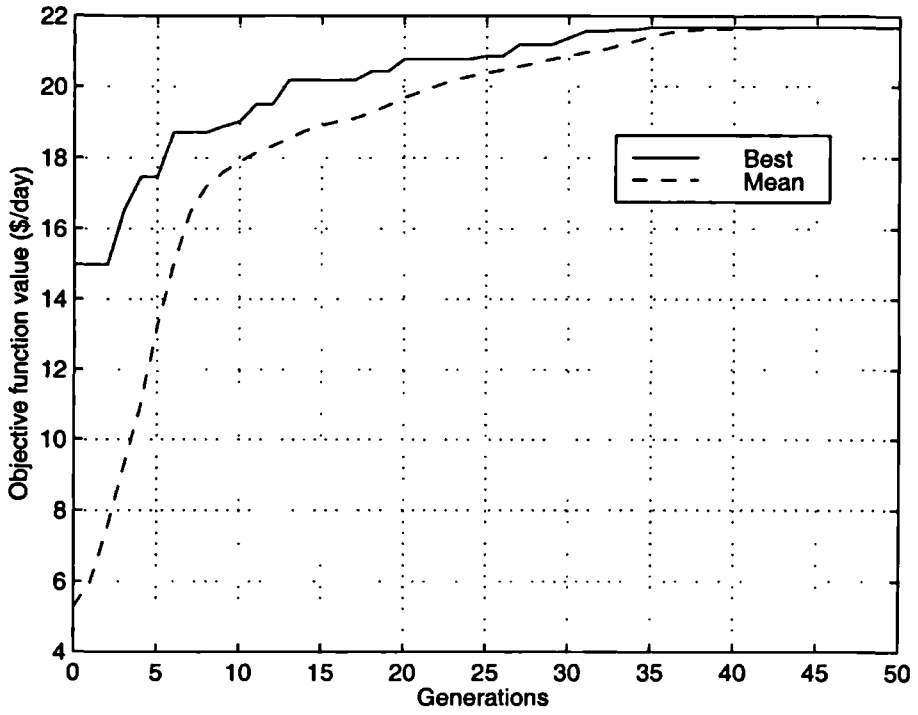

Figure 4.4 *Objective function profile at a mutation rate of 5%*

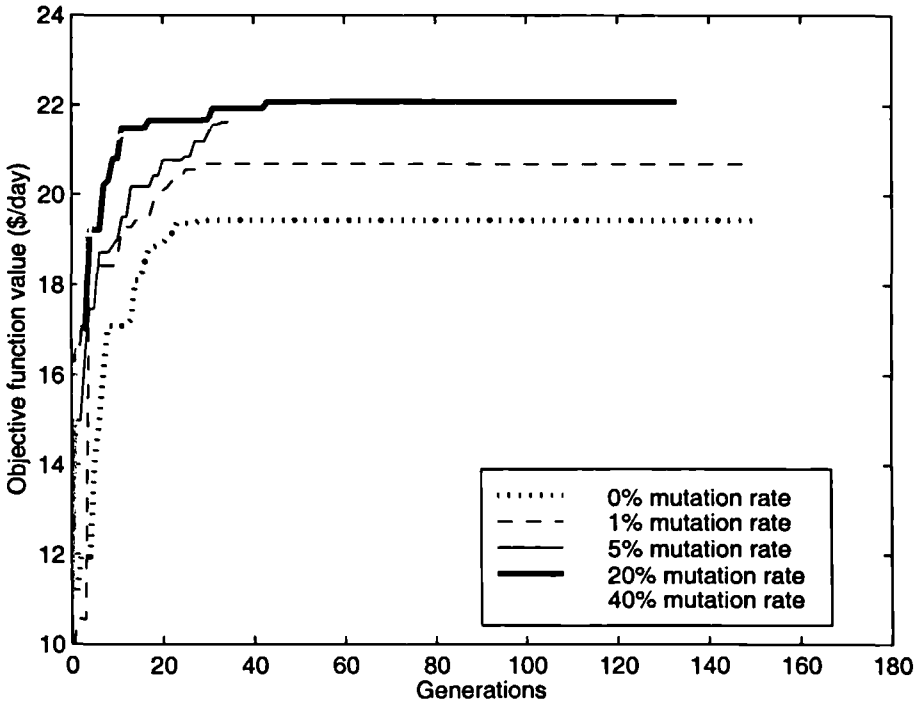

Figure 4.5 *Objective function profile for different mutation rates*

A considerable advantage of the solution technique introduced in this chapter is that multiple solutions are available at the end of the optimisation, thereby allowing the user to interpret the results and make an informed decision. This contrasts to more conventional gradient-based optimisation methods which return a single (sometimes sub-optimal) solution and little insight. In Chapter 6, the optimisation strategy presented in this chapter will be evaluated against a conventional (branch and bound) *MINLP* solution strategy.

Chapter 5

Optimal design of reverse osmosis systems

The optimal design methodology outlined in Chapter 4 is demonstrated using a well established reverse osmosis case study. This work differs from published studies by the incorporation of a rigorous membrane unit model into the design procedure. The use of both hollow-fibre and spiral-wound modules is considered. Further information on the work presented in this chapter can be found in Appendix D.

5.1 Introduction

At present, reverse osmosis is the best established industrial membrane separation process. It is used to separate low molecular weight solutes from a solvent (usually water). Sea-water desalination is the most mature application of reverse osmosis; others include brine-water desalination and waste-water treatment. Whilst in theory, reverse osmosis may also be used to separate mixtures with high organic concentrations, in practice the high osmotic pressure of such mixtures somewhat limits its feasibility. An alternative membrane process for separating such organic mixtures is pervaporation (see Chapter 6).

Several authors (e.g. El-Halwagi, 1992; Voros *et al.*, 1997; Zhu *et al.*, 1997) have investigated the use of optimisation techniques for the full structural design of reverse osmosis separation plants. A good review of the early work concerned with the design of reverse osmosis networks is provided by El-Halwagi (1992). In much of this early work, the design strategies focussed on the configuration of the reverse osmosis modules but gave little attention to pumps and energy recovery devices which can significantly effect

the economic performance of the system. Similarly, the potential benefits of by-pass and recycle streams were usually neglected. In response, El-Halwagi (1992) developed a state space approach (see Section 4.3) to calculate the optimal design of reverse osmosis networks. He claims that it accounts for all network configurations and provides the necessary degrees of freedom for optimally designing reverse osmosis networks. He, and later Voros *et al.* (1997), then applied this method to the design of desalination systems based on hollow-fibre modules.

However, all of the literature studies concerned with the design of reverse osmosis systems are based on approximate module models, such as those proposed by Evangelista (1985). Approximate models do not accurately describe the performance of either hollow-fibre or spiral-wound modules. In response, the application of the detailed model (Chapter 3) to the design of hollow-fibre and spiral-wound reverse osmosis processes is explored in this chapter. The validity of using approximate models for system design will also be assessed by a comparison with the detailed model results.

In the next section, a methodology for the optimal design of reverse osmosis systems is presented. This is followed by a description of a well established desalination case study (Section 5.3). The accuracy of the detailed model for this case study is assessed in Section 5.4 by comparison with experimental data. Then, in Section 5.5, the optimal design of a reverse osmosis system based on hollow-fibre modules is considered. In Section 5.6, the optimisation is repeated for the same system but this time based on spiral-wound modules which are the most widely utilised configuration for reverse osmosis. The computational requirements of the optimisation strategy are assessed in Section 5.7 and in the final section, some conclusions on the importance of using detailed models for the design of membrane systems are presented.

5.2 Solution methodology

In Section 4.3, a methodology for the optimal design of a general membrane separation system was presented. This is now used to generate a suitable representation for a reverse osmosis system. The framework accounts for all the components of reverse osmosis systems (membrane modules, pumps and energy-recovery devices) and enables a full structural optimisation.

5.2.1 Process superstructure

During reverse osmosis, water is driven through the membrane by a pressure difference. To optimise the driving force across the membrane, the feed stream pressure and the permeate pressure are manipulated using high pressure pumps and energy recovery devices.

The superstructure is generated from N^s separation stages using the procedure outlined in Section 4.3.1. The optimiser selects a design from the superstructure by fixing the values for a number of decision variables; these are now considered.

Separation stage decisions

A separation stage for a reverse osmosis system is illustrated in Figure 5.1. The number of modules (N^m), the feed pressure (P_f) and the permeate pressure (P_p) must be determined for each stage. In this work, normalised pressures (D^p) are used, these are linear mappings (Eq 4.5) of the actual pressure, where 0 is atmospheric pressure and 1 is the maximum allowed pressure (P^{max}).

Spiral-wound modules are housed in pressure vessels. Each pressure vessel contains a number of spiral-wound modules connected in series - refer to Section 1.1 for further information. This effectively creates a much longer feed channel. This is easily incorporated into the framework by adding a fourth stage decision variable which describes the number of modules per pressure vessel (N^{pre}). This option does not need to be implemented for hollow-fibre systems where the modules are housed in individual pressure vessels. Of course, if desired, hollow-fibre modules can still be connected sequentially using multiple separation stages.

There are four decision variables per separation stage as shown in Table 5.1. The bounds on each variable are specified in each case except for N^m (the number of modules). It is important that the bounds on the number of modules are set correctly: if the bounds are too small then they might not encompass the optimal solution; too large, and it may take much longer than necessary to find the best solution. For this reason, the bounds on the number of modules are specified separately for each case study (Sections 5.5 and 5.6).

One significant advantage of a genetic algorithm is that multiple solutions are available at the end of the optimisation. To avoid solutions that are too similar being reported the continuous decision variables have been discretised. The discretisation intervals for each variable are also shown in Table 5.1.

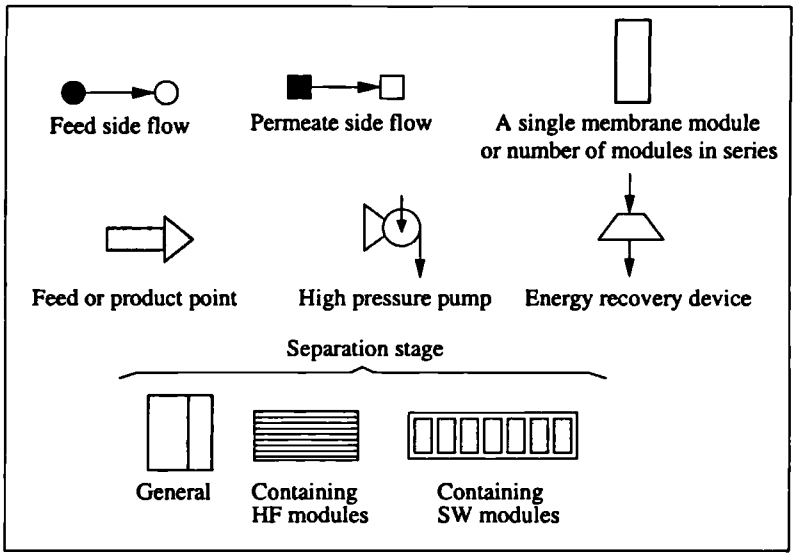

Key to the figures in this chapter

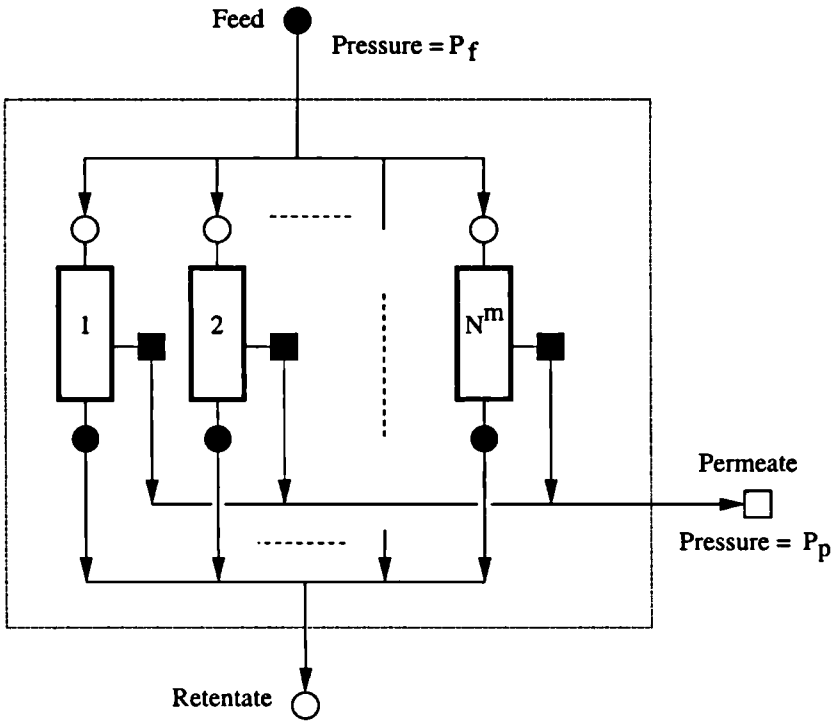

Figure 5.1 *A separation stage for a reverse osmosis process*

Table 5.1 *Stage decision variables for a reverse osmosis system*

Decision variable	Lower bound	Upper bound	Interval
Total number of membrane modules per stage, N^m	n^{min}	n^{max}	1 (integer)
Normalised feed pressure, D_f^p	0	1	0.002
Normalised permeate pressure, D_p^p	0	1	0.002
Number of modules per pressure vessel, N^{pre}	1	10	1 (integer)

The decision variable describing the number of modules per pressure vessel, N^{pre}, is only implemented for spiral-wound systems.

Network decisions

The structural layout of the plant is determined by fixing the values of the network decision variables (see Section 4.3.3). In reverse osmosis, each stage has an upstream input (feed) and output (retentate), as well as a downstream output (permeate). Mixing of the two streams will not be considered in this study, an assumption which greatly reduces the number of network choices (see Table 4.3, Chapter 4) and is reasonable, as it is thermodynamically undesirable to mix already separated streams (El-Halwagi, 1992). Consequently, the permeate streams pass straight to the permeate product point. Therefore, the only network decision variables are the stream distribution set for the feed point and for the retentate outlet of each separation stage. A two stage superstructure is illustrated in Figure 5.2.

The number of network decision variables is dependent on the problem size: $N^s\,(1 + N^s)$ variables need to be specified for a superstructure containing N^s separation stages. The network decision variables for a two stage system are shown in Table 5.2.

5.2.2 Solution strategy

The best plant design will be determined by the solution of the superstructure optimisation problem. The genetic algorithm solution technique described in Section 4.3 will be utilised in this work. To select a design from the superstructure, the genetic algorithm must specify the values of the decision variables. The total number (network + stage) of decision variables is a function of the number of separation stages, N^s. In total, $N^s\,(4 + N^s)$ variables are required for hollow-fibre systems and $N^s\,(5 + N^s)$ are needed for spiral-wound systems.

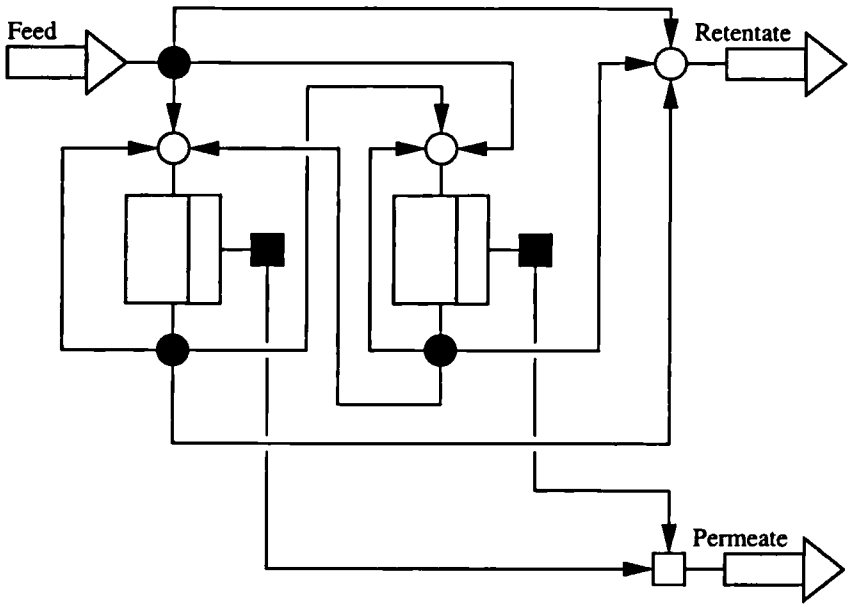

Figure 5.2 *A superstructure for a reverse osmosis process (two stages)*

5.3 Description of the case study

This case study is concerned with the application of reverse osmosis to sea-water desalination. This example has been selected as it is the most widely studied in the literature and thus enables the design strategy developed in this thesis to be evaluated against existing optimal design methods. In this work, system designs based on both hollow-fibre and spiral-wound modules are considered.

Before the design problem is introduced, some important background information relevant to the case study is provided. Following the definition of the design problem, the assumptions used in this work and the membrane characterisation model are discussed. Finally, the optimisation objective function is presented.

5.3.1 Desalination processes

Reverse osmosis offers significant economic and environmental advantages when compared with thermal desalination processes such as multi-stage flash (MSF) evaporation (Voros *et al.*, 1997). Whilst MSF is still the most important desalination process, reverse osmosis is being used to an increasing extent (Mulder, 1996).

Reverse osmosis systems must operate at high pressures in order to overcome the large osmotic pressure of sea-water. Fortunately, a significant amount of the energy used to

Table 5.2 *Network decision variables for a two stage reverse osmosis system*

Decision variable	Lower bound	Upper bound	Interval
Feed to stage 1 inlet, $\sigma_{0,1}$	0	1	0.02
Feed to stage 2 inlet, $\sigma_{0,2}$	0	$1-\sigma_{0,1}$	0.02
Stage 1 to stage 1 inlet, $\sigma_{1,1}$	0	1	0.02
Stage 1 to stage 2 inlet, $\sigma_{1,2}$	0	$1-\sigma_{1,1}$	0.02
Stage 2 to stage 1 inlet, $\sigma_{2,1}$	0	1	0.02
Stage 2 to stage 2 inlet, $\sigma_{2,2}$	0	$1-\sigma_{2,1}$	0.02

The fraction of material to the retentate product point is given from the mass balance (Eq 4.4)

pressurise the feed stream can be recovered - up to 40% of the total energy requirement (Malek *et al.*, 1996). This is usually done using energy recovery devices such as Pelton-wheel impulse turbines or reverse running centrifugal pumps which retrieve mechanical energy from the still highly pressurised retentate stream.

Spiral-wound and hollow-fibre modules are the most common membrane configurations used for the production of drinking water. Of these, the spiral-wound configuration is the most popular, although hollow-fibre configurations are used widely for the desalination of sea-water in the Middle East (Taylor and Jacobs, 1996).

Hollow-fibre modules

The DuPont B9 and B10 modules are the most important types of radial flow hollow-fibre modules (Crowder and Gooding, 1997) and are commonly used for reverse osmosis. They are constructed from polyamide membranes which show much higher salt retention than the older cellulose acetate membranes. In these modules, pressurised feed enters on the shell side with purified water withdrawn from the fibres (see Sections 1.1 and 3.2).

Spiral-wound modules

In general, spiral-wound membranes (Section 1.1) have inherently higher permeabilities than hollow-fibre membranes, so water production costs are relatively low for these modules. Unfortunately, these advantages are somewhat offset by much higher feed side pressure drops. Concentration polarisation is also a more considerable problem.

A large range of spiral-wound membranes are now commercially available - a compre-

Table 5.3 *Sea-water desalination plant requirements (Evangelista, 1985)*

hensive review of which has been provided by Bhattacharyya *et al.* (1992). Over recent years, the most widely studied is the FilmTec spiral-wound module (Dickson *et al.*, 1992; Ben-Boudinar *et al.*, 1992; de Witte, 1997). Like the DuPont modules, these membranes are based on polyamide chemistry, but due to the method of manufacture, the active layer is extremely thin. Hence they are characterised by very high flux rates and excellent salt rejection (Bhattacharyya *et al.*, 1992).

5.3.2 The design problem

This case study is based on the sea-water desalination systems considered originally by Evangelista (1985), and later explored further by El-Halwagi (1992). Evangelista (1985) developed an explicit design methodology for reverse osmosis systems. Using this, he designed a tapered reverse osmosis system to produce 20.8 tonnes/hr of desalinated water from 70 tonnes/hr of sea-water. The design which is based on 131 B10 (6840) hollow-fibre modules is illustrated in Figure 5.3. The production and design constraints for this system are presented in Table 5.3.

El-Halwagi (1992) calculated the annualised cost of this design ($280,503 per year) using the economic criteria given in Table 5.4, and then re-evaluated the design problem. Through the introduction of a formal optimisation technique (the state-space approach) and by introducing energy recovery turbines, a design with a significantly reduced annualised cost was found ($237,990 per year). This design, which is based on 106 B10 modules, is shown in Figure 5.4.

Both designs were developed using an approximate module model (Evangelista, 1985) - this simple design model is presented in Section D.3 (Appendix D). In this work, a thorough study of the same design problem is made using the detailed model. The use of both hollow-fibre and spiral-wound sea-water membrane modules will be considered.

Figure 5.3 *Sea-water desalination design (Evangelista, 1985)*

Figure 5.4 *Sea-water desalination design (El-Halwagi, 1992)*

Table 5.4 *Economic criteria for sea-water desalination plants (El-Halwagi, 1992)*

The annualised costs include replacement costs, labour and maintenance charges (El-Halwagi, 1992)

5.3.3 Assumptions

A number of assumptions have been made in the following work, these are now discussed.

Binary mixture Most published experimental studies use sodium chloride solutions to "approximate" sea-water. Whilst this simplifies both experimental and modelling requirements, it is somewhat unrealistic: a compositional analysis of sea-water shows that it contains a number of additional constituents, including sodium, magnesium, chloride and sulphate ions. Although the detailed model is well suited for describing multicomponent separation (see Chapter 3), due to the limited availability of experimental data, a binary mixture of sodium chloride and water will be assumed in this work.

Membrane degradation Over the life-time of an industrial membrane, a significant decrease in flux is seen, mainly as a result of membrane fouling and scaling. Usually a proportion (often 10-20%) of the modules are replaced each year which results in a variation in membrane age and performance. Reverse osmosis plants are initially over-designed with a guaranteed "purchaser specified" supply rate at the end of 5 years (Malek *et al.*, 1996). Design calculations must focus on meeting product specifications at the end of the five year period. In line with the previous optimisation studies, we will neglect membrane degradation and assume that a representative membrane has been selected.

Physical properties The *Multiflash* physical properties package (Infochem Computer Services Ltd, 1996) as interfaced to g*PROMS* is used to provide fluid viscosities and densities. Osmotic pressure and the diffusivity of salt in water are determined using published empirical correlations (refer to Table D.3, Appendix D).

5.3.4 Membrane characterisation

In addition to the DuPont B10 membranes considered by El-Halwagi (1992) and others, the performance of reverse osmosis systems based on FilmTec FTSW30 spiral-wound membranes will also be assessed in this work. Details of both membranes are given in Section D.1 (Appendix D).

Both types of membrane are based on polyamide chemistry and therefore the same membrane characterisation strategy can be used in each case. For this study, the Kedem-Katchalsky model has been selected (Section 2.2). Although this model suffers from concentration dependent parameters, Soltanieh and Gill (1981) report that the concentration dependence is not as great as that of using solution diffusion based models. The Kedem-Katchalsky model can be written

$$J_W = Q_W c_{W1} \left[(P_1 - P_2) - \sigma \left(\Pi_1 - \Pi_2 \right) \right] \tag{5.1}$$

$$J_s = (1 - \sigma)\, c_{s,LM} \frac{J_W}{c_{W1}} + Q_s \left(c_{s1} - c_{s2} \right) \tag{5.2}$$

To simulate a reverse osmosis system using the detailed model, the membrane flux coefficients must be specified. The three coefficients (Q_W, Q_s, and σ) can be correlated as a function of concentration, pressure, and temperature. A range of different correlations have been suggested in the published literature, and in this study, correlations based on the work of El-Halwagi (1996) and Hawlader *et al.* (1994) will be used. The values of the parameters in the correlations have been estimated by minimising the deviation of simulated results from a set of experimental data. Further information on this parameter estimation is presented in Section D.2 (Appendix D).

5.3.5 Optimisation objective

Economic criteria often determine the optimal plant design. In general terms, the objective is to seek the most profitable solution, or to find the least costly design, that satisfies both design and production constraints. In this case, the objective function is simply to minimise production costs (C) subject to the constraints given earlier in Table 5.3. The objective function is written

$$min \left[C f(\omega_p) g(m_p) \right] \tag{5.3}$$

To ensure that the optimal solution meets the required production quality, it is necessary to penalise solutions that do not satisfy the product constraints. This is done using the penalty functions $f(\omega_p)$ and $g(m_p)$.

$f(\omega_p)$ is given by

$$\text{if } \omega_p \leq \omega_p^{max}$$
$$f(\omega_p) = 1 \tag{5.4}$$

else

$$f(\omega_p) = \left(1 - \frac{\omega_p - \omega_p^{max}}{\omega_p}\right)^{-4} \tag{5.5}$$

Similarly, $g(m_p)$ is written

$$\text{if } m_p \geq m_p^{min}$$
$$g(m_p) = 1 \tag{5.6}$$

else

$$g(m_p) = \left(1 - \frac{m_p^{min} - m_p}{m_p^{min}}\right)^{-4} \tag{5.7}$$

These functions penalise any solution that does not meet the product requirements. This is illustrated in Figures 5.5 and 5.6 which show the effect of permeate purity and flowrate on the values of the penalty functions $f(\omega_p)$ and $g(m_p)$.

5.4 Process simulation

All of the studies on the optimal design of membrane systems that were identified in Chapter 2 are based on approximate and unverified models. To establish technical confidence in the optimisation results, this thesis not only advocates the use of detailed models, but that these models should be verified against experimental data whenever possible. This is now considered for the detailed models (Chapter 3) that will be used to describe the hollow-fibre and spiral-wound modules in this case study. The accuracy of the approximate module models (Section D.3, Appendix D) will also be assessed.

All the calculations reported in this section were performed using the *gPROMS* simulation software (Process Systems Enterprise Ltd, 1999).

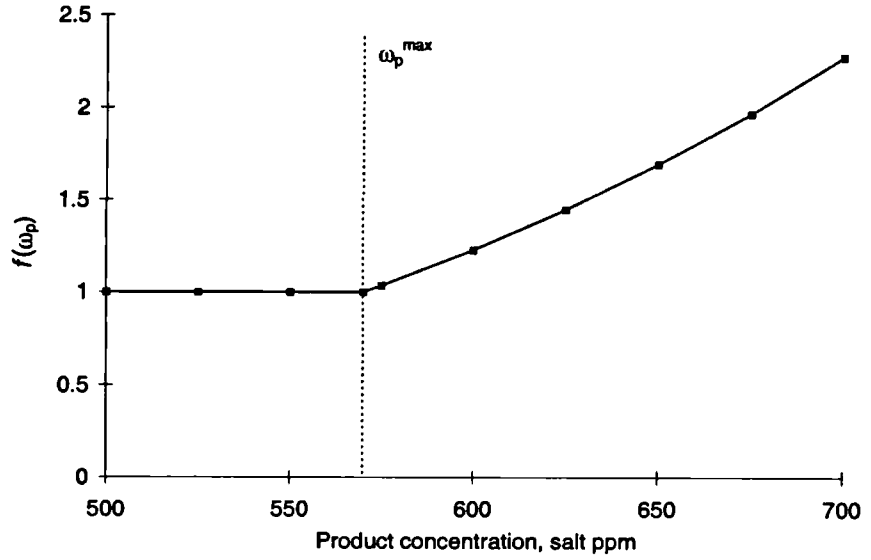

Figure 5.5 *The value of the penalty function, $f(\omega_p)$, for different permeate concentrations*

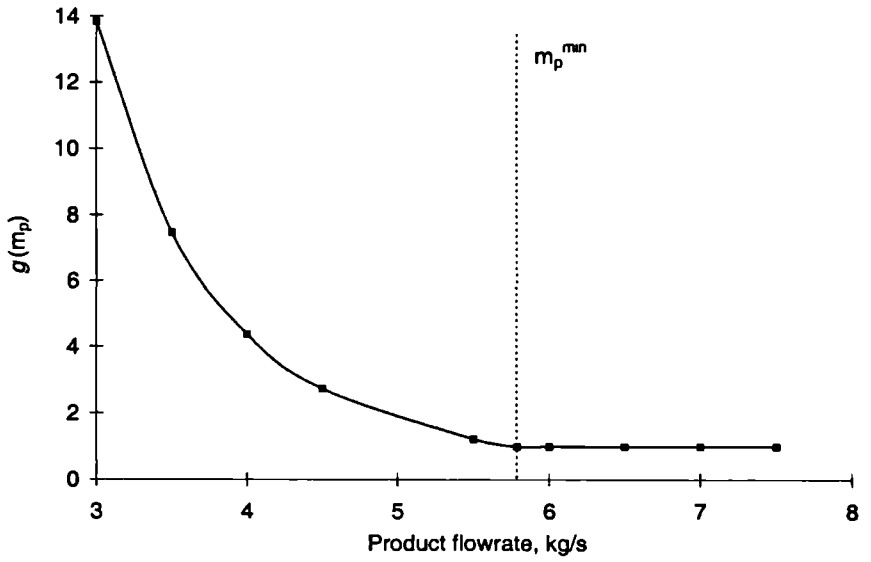

Figure 5.6 *The value of the penalty function, $g(m_p)$, for different permeate flowrates*

5.4.1 Hollow-fibre module

Experimental results for the B10 (6440-T) hollow-fibre module have been presented by Hawlader *et al.* (1994). The accuracy of the detailed model (Chapter 3) and the approximate model (Equations D.6 and D.7, Appendix D) has been assessed against these results.

Detailed model results

In this work, whilst a 2-D flow model will be used to describe radial flow through the fibre bundle, a 1-D plug flow model is used to describe flow in the fibre interior. This is reasonable because the bulk concentration in the permeate channel is similar to that of the material permeating through the membrane - i.e. there is negligible concentration polarisation on the permeate side.

Hawlader *et al.* (1994) presented only limited experimental data for a B10 membrane, giving the product recovery and salt rejection (Eq. D.10, Appendix D) for a range of operating conditions. The accuracy of the detailed model is now assessed by a comparison with this experimental data. The full results are shown in Table D.5 (Appendix D) and are summarised in Table 5.5.

The calculated product recovery shows good agreement with the measured value (typically 4%). The salt rejection also shows good agreement, with errors ranging between 0 and 0.3% for the B10 module. These errors are similar to the uncertainty in the ex-

Table 5.5 *Summarised simulated results calculated using the detailed model*

	B10 HF	**FT30SW**
Feed flowrate, l/hr	1134	760 - 830
Salt concentration, ppm	25000 - 50000	25000 - 40000
Feed pressure, bar	35 - 77	50 - 80
Product recovery	15% - 60%	7% - 13%
Simulation error	≈4% (max 6%)	≈3% (max 8%)
Permeate concentration, ppm	220 - 1300	70 - 400
Simulation error	≈4% (max 12%)	≈5% (max 14%)
Salt rejection	97% - 99%	99 - 99.7
Simulation error	≈0.08% (max 0.3%)	≈0.1% (max 0.1%)

perimental data. However, it should be pointed out that any error in the calculated salt rejection will give a significantly greater error in the permeate concentration. This is reflected in Table 5.5 where a typical deviation of 4% (max 12%) is found between the calculated results and the experimental permeate concentration. The latter is estimated from the salt rejection experimental data reported by Hawlader *et al.* (1994), and so is itself only accurate to within 10% (see Section D.4.1, Appendix D). On the evidence of these results, the detailed model can be said to provide a good description of a B10 hollow-fibre module.

Approximate model results

The calculations are repeated using the approximate hollow-fibre module model (Equations D.6 and D.7, Appendix D) with the same membrane characterisation used by the detailed model. A full comparison with the detailed simulation results is given in Table D.7 (Appendix D) and is summarised in Table 5.6. The approximate model is seen to consistently under-predict both the product recovery and the salt rejection. Whilst the results of the two models show reasonable agreement, the use of an approximate model introduces significantly greater error than the detailed model. Typical deviations from the experimental results for the approximate model are $\approx$7%, compared to $\approx$4% for the detailed model.

5.4.2 Spiral-wound module

This study concentrates on the FT30SW spiral-wound module. Using a simulation model (Section 2.3), Ben-Boudinar *et al.* (1992) found reasonable agreement with the FT30SW experimental results for sea-water desalination. In this work, we will revisit the experimental data using the detailed model developed in this thesis (Chapter 3). The accuracy of the approximate model (Equations D.8 and D.9, Appendix D) will also be assessed for this system.

Detailed model results

The use of the detailed (2-D) model is assessed by a comparison with the extensive experimental data presented by Ben-Boudinar *et al.* (1992). The predicted results are presented in full and compared with the experimental data in Table D.6 (Appendix D). This is summarised in Table 5.5.

Table 5.6 *Assessment of the reverse osmosis simulation results for the approximate module models*

	B10 HF	FT30SW
Deviation from experimental results		
Product recovery	≈4% (max 6%)	≈4% (max 12%)
Permeate concentration, ppm	≈7% (max 16%)	≈6% (max 28%)
Deviation from detailed model results		
Product recovery	≈4% (max 7%)	≈4% (max 16%)
Permeate concentration, ppm	≈7% (max 10%)	≈5% (max 20%)

The product recovery from spiral-wound modules is usually lower than that from hollow-fibre modules (Taylor and Jacobs, 1996). This is seen in the experimental results where the recovery ranges from 7 to 13%, compared with 15 to 60% for the B10 hollow-fibre module. The calculated recovery shows excellent agreement with the measured value, typically 3%. The error in the predicted permeate salt concentration is greater, typically 5%. However, both offer a significant improvement over the work of Ben-Boudinar *et al.* (1992) whose results show errors up to 26%. The improved results in this case can be mainly attributed to the use of a detailed flow model and a more complex membrane characterisation strategy (see Section D.2, Appendix D).

Approximate model results

The calculations for a spiral-wound module are also repeated using an approximate model (Eq. D.8 and D.9, Appendix D). A full comparison with the detailed simulation results is given in Table D.8 (Appendix D) and is summarised in Table 5.6. The approximate model predictions compare badly with both the detailed model results and the experimental data. The most likely explanation for this, is the assumption of a constant mass transfer coefficient (Eq. D.9, Appendix D). This error can easily be avoided using the detailed model.

5.5 Optimal design of hollow-fibre systems

The optimal design of a reverse osmosis system based on the B10 (6840) hollow-fibre modules is now considered. This case study was outlined earlier in Section 5.3 and will later be compared to a similar study based on spiral-wound modules (Section 5.6).

In the first instance, the modules are described using the detailed model which was verified in the previous section. Following this, to assess the validity of using approximate models for the design of membrane systems, the optimisation is repeated using an approximate model.

5.5.1 Solution method

The solution methodology described in Chapter 4 is used to solve the optimisation problem. For this purpose, a process superstructure is generated from N^s separation stages. The genome size is determined by the number of stages. Androulakis and Venkatasubramanian (1991) have shown that it is possible to use variable size genomes with a genetic algorithm. However, for this study, a neater approach is to start with a single separation stage and increase the number of stages if more degrees of freedom are required. As a result, only genomes of the same size will be present for each optimisation.

A significant advantage of the optimisation methodology introduced in Chapter 4 is that multiple solutions are available at the end of the optimisation. Therefore, in this section, as well as recording the best solution found by the genetic algorithm, a database of the top five-hundred solutions is kept.

The optimisation problem is solved using both the detailed model and the approximate model (Section D.3, Appendix D). In both cases, two superstructure sizes are evaluated: a single separation stage system; and a two stage system. The bounds on the number of modules for each separation stage must be specified (see Section 5.2): in this work a separation stage is defined as containing between 20 and 200 parallel modules (i.e. $n^{min} = 20$, $n^{max} = 200$).

5.5.2 Detailed hollow-fibre model results

Figure 5.7 shows the sensitivity of the total annualised cost to the number of membrane modules for the top 150 solutions found by the genetic algorithm (single stage optimisation). The plot demonstrates that the optimisation problem contains a large number

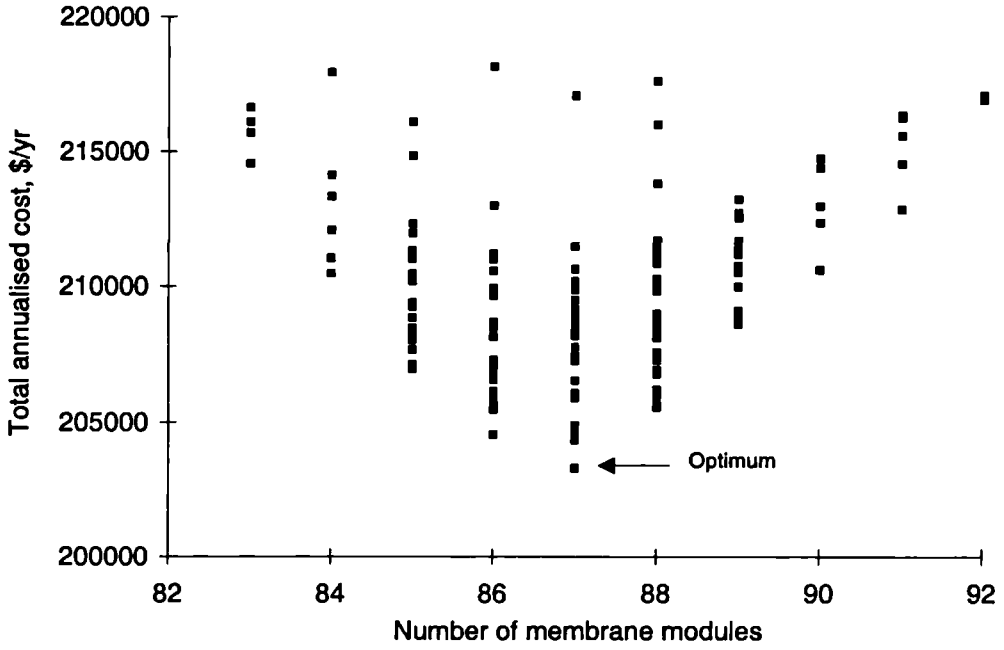

Figure 5.7 *The 150 top solutions plotted as a function of the number of modules*

of near optimum solutions. However, the annualised plant cost is fairly sensitive to the number of membrane modules; using more modules than the optimum number (87) significantly increases the cost of the final design. A study of the solution database suggests that designs that use 84 modules (or less) cannot meet the product flowrate requirement. These solutions are heavily punished by the flowrate penalty function (Eq 5.7) and are also undesirable - note that Figure 5.7 shows the penalised costs.

Four of the designs stored in the solution database have been selected for discussion in this section, these are summarised in Table 5.7. The approximate model is also used to calculate the performance of these designs (Table 5.7) and is seen to under-predict the product flowrate. This concurs with the simulation results presented earlier in Section 5.4.

The best single stage design found by the genetic algorithm has an annualised cost of $203,304 per year. This design is illustrated in Figure 5.8 and is characterised by a feed by-pass: 10% of the feed stream does not actually enter the membrane system. This indicates that it is optimal to operate at 90% of the maximum feed rate. The system contains 87 modules, a pump operating at maximum power and an energy recovery device which is used to recover mechanical energy from the retentate stream. The best design

Table 5.7 *Detailed model optimisation results (hollow-fibre modules)*

	Annualised cost ($/yr)	Calculated production rate	
		Detailed model	Approximate model
One Stage			
Best Design (Fig 5.8)	203,304	5.79 kg/s (567 ppm)	5.63 kg/s (599ppm)
Alternate Design (Fig 5.9)	207,149	5.79 kg/s (531 ppm)	5.64 kg/s (558 ppm)
Two Stages			
Best Design (Fig 5.10)	204,814	5.80 kg/s (561 ppm)	5.65 kg/s (587 ppm)
Alternate Design (Fig 5.11)	207,494	5.79 kg/s (531 ppm)	5.64 kg/s (554ppm)

found by the algorithm without a feed by-pass (Figure 5.9), requires only 85 modules but the increased pumping costs due to the larger flowrate result in a slight increase (1.9%) in the annualised plant cost to $207,149 per year.

To determine the effect of increasing the number of stages, the optimisation is repeated using a superstructure built from two separation stages. The results demonstrate that forcing the optimiser to find a two stage solution actually results in a slightly inferior design - the best design has an annualised cost of $204,814 per year. It contains 87 membrane modules configured in a tapered configuration and, similar, to the one stage design, utilises a feed by-pass. Without a feed by-pass the annualised cost rises to $207,494 per year, which is once again more expensive than its one stage counterpart. These two stage designs are illustrated in Figures 5.10 and 5.11.

The designs without a feed by-pass are only constrained by the required permeate flowrate as the permeate concentration is significantly better than the product specification (570 ppm). The use of a feed by-pass enables the full search space to be explored, solutions that implement this are constrained by both permeate flowrate and concentration. This is reflected in the results shown in Table 5.7. Figure 5.12 shows the sensitivity of the annualised cost to the feed by-pass for the top 150 solutions found by the genetic algorithm. The cost is relatively insensitive to the feed by-pass rate. However, a 10% by-pass is the limiting rate. Beyond this point, the system is unable to meet the product quality constraint and so such solutions are heavily punished by the product quality penalty function (Eq 5.5).

The velocities through the two stage system are larger than for the one stage system due to the reduction in the number of parallel modules. This benefits the system by reducing the effect of concentration polarisation due to an increased mass transfer coefficient (see Section 2.2.4). However, this effect is balanced by the increased pressure drop through

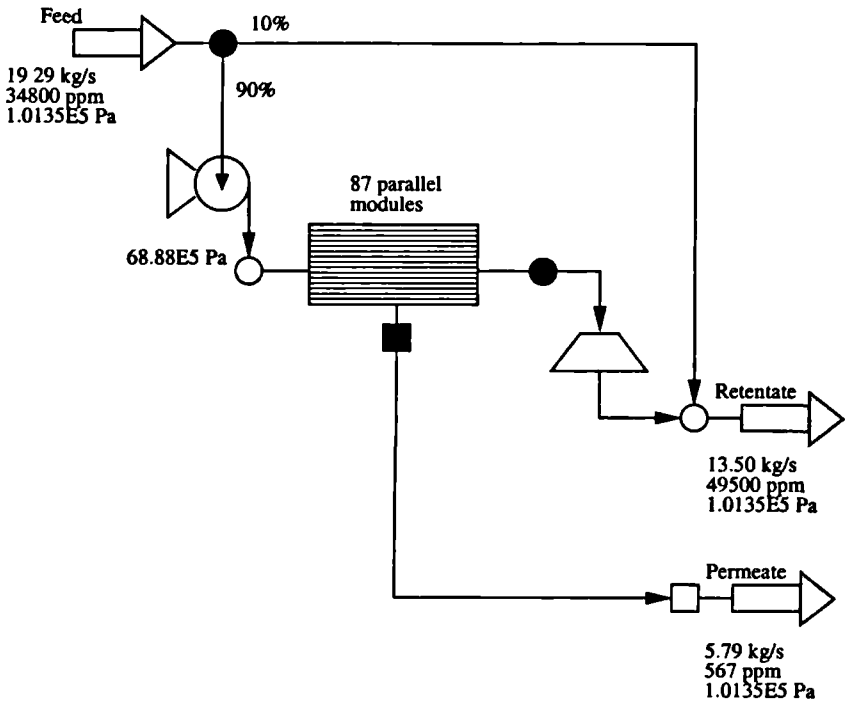

Figure 5.8 *Best one stage design determined using the detailed model: HF modules*

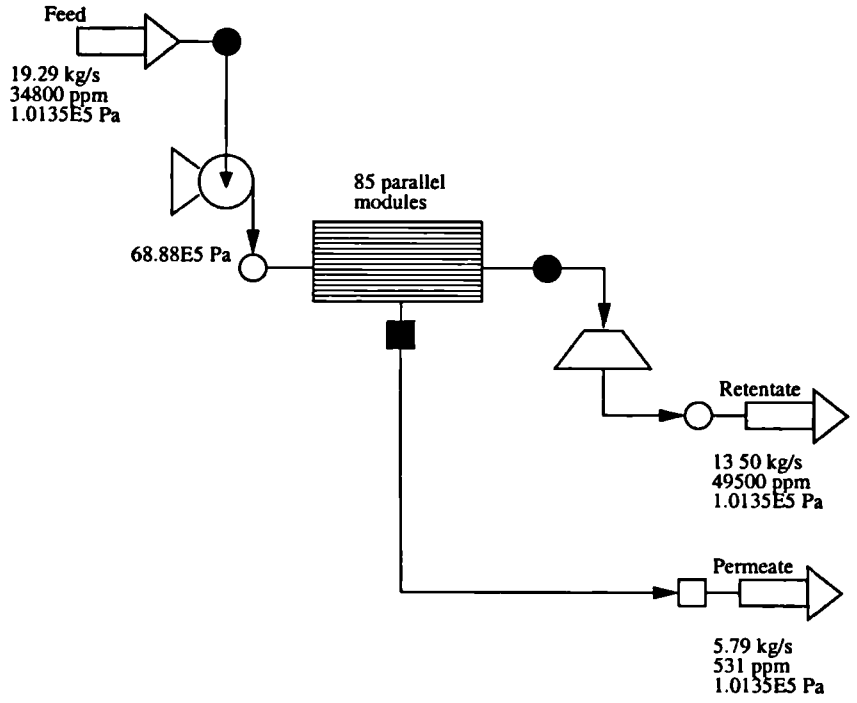

Figure 5.9 *Alternative one stage design determined using the detailed model: HF modules*

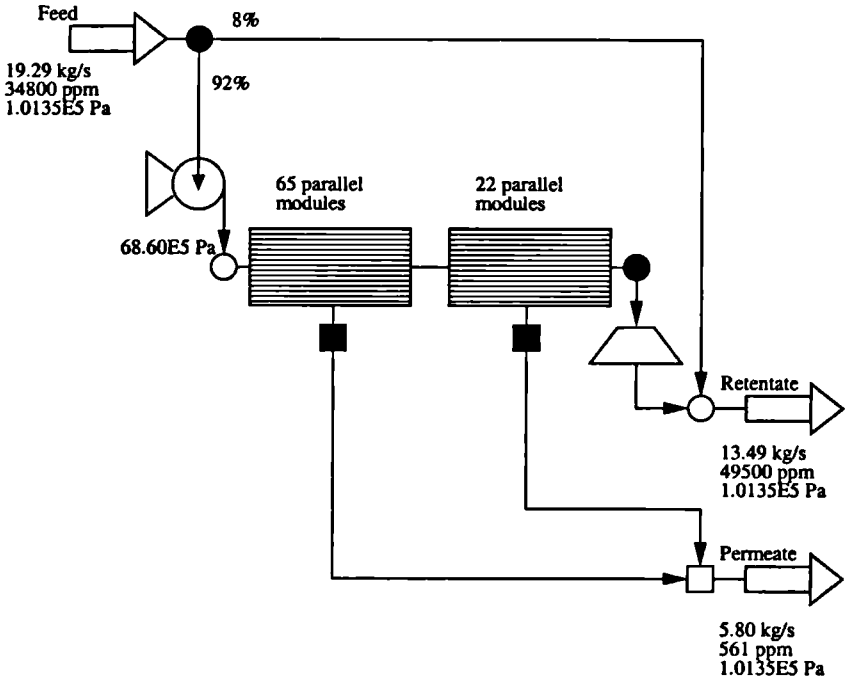

Figure 5.10 *Best two stage design determined using the detailed model: HF modules*

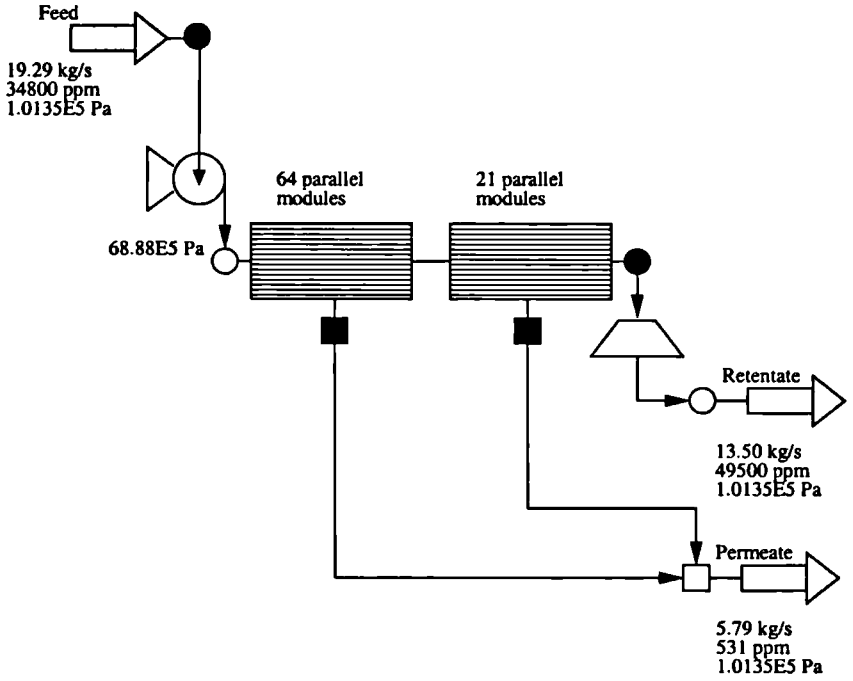

Figure 5.11 *Alternative two stage design determined using the detailed model: HF modules*

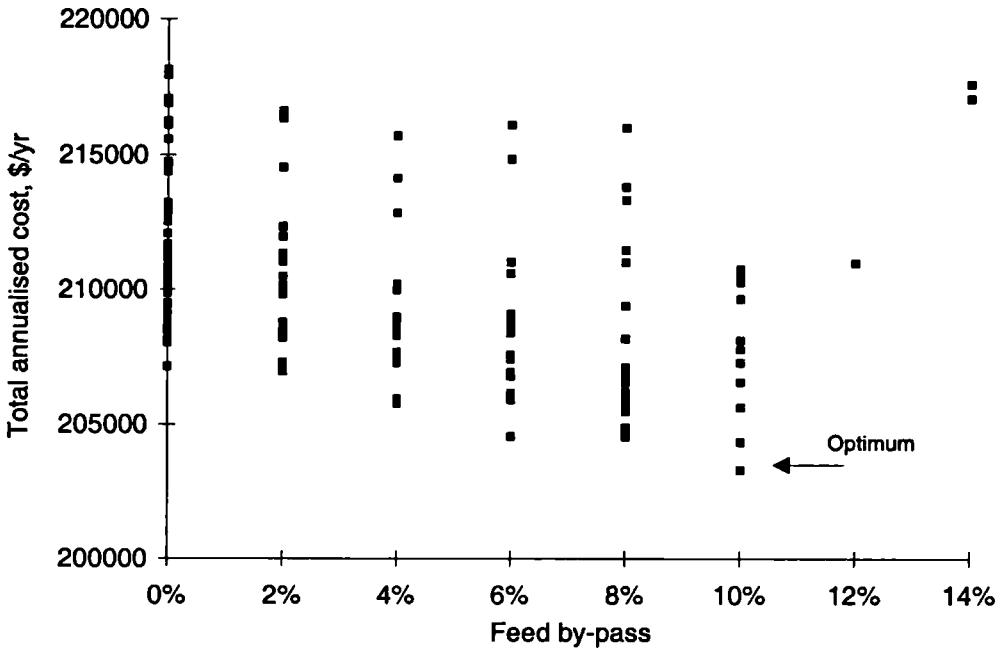

Figure 5.12 *The 150 top solutions plotted as a function of the percentage of feed by-passing the system*

the system. It is the trade-off between these two factors that usually determines the configuration of the membrane modules for a given reverse osmosis system. Clearly, in this case, the lower velocity one stage system is slightly preferable. It must be pointed out that most approximate models (e.g. Evangelista, 1985) do not account for the effect of velocity on either pressure drop or concentration polarisation. This is explored further in the next section, when we tackle the same design problem using the approximate hollow-fibre model.

5.5.3 Approximate hollow-fibre model results

The use of the approximate model described in Section D.3 (Appendix D) for the design of reverse osmosis systems is not straight-forward. A number of additional criteria must be introduced (El-Halwagi, 1992), these are given in Table 5.8. In particular, a minimum flowrate per module is required to limit the effect of concentration polarisation (and hence prevent scaling and fouling) at low flowrates. Similarly, a maximum flowrate is required to prevent excessive pressure drop. As discussed in the previous section, the

Table 5.8 *Approximate hollow-fibre model: additional constraints (Evangelista, 1985)*

detailed model formally accounts for both concentration polarisation and pressure drop and so does not require these constraints.

The additional constraints are introduced to the model and the optimisation is repeated using the approximate module model. The costs and performance of the optimised designs found by the approximate model are summarised in Table 5.9.

The best one stage design (shown in Figure 5.13) found using the approximate model is 4% more expensive than its detailed model counterpart. This increase in costs is due to a greater number of modules (88), and greater pumping and energy recovery costs. The best two stage design (Fig 5.14) is 6% more expensive than its counterpart, it also has 88 modules and has greater pumping costs (it uses two pumps).

The separation stages for the two stage design are connected in parallel rather than in series. The fluid velocity through a series configuration would be much greater and would violate the maximum flow constraint, hence a series configuration is avoided. Instead, a design which is essentially the same as the one stage design, but with two pumps and energy recovery devices, is selected.

Clearly, the designs calculated using the approximate models are structurally different from the detailed model results. The feed by-pass seen in Figures 5.8 and 5.10 is not implemented here. This is most likely because the approximate model predicts much higher salt fluxes than the detailed model and so is already constrained by the product quality (Table 5.9). As a consequence, the introduction of a feed by-pass is avoided.

5.5.4 Summary

The use of an approximate model approach results in a sub-optimal solution for this case study. This was expected from the simulation results (Section 5.4) and is easily avoided using the detailed model. There are also significant structural differences in the designs determined by the detailed and approximate strategies. This is due to the flow constraints required by the approximate model.

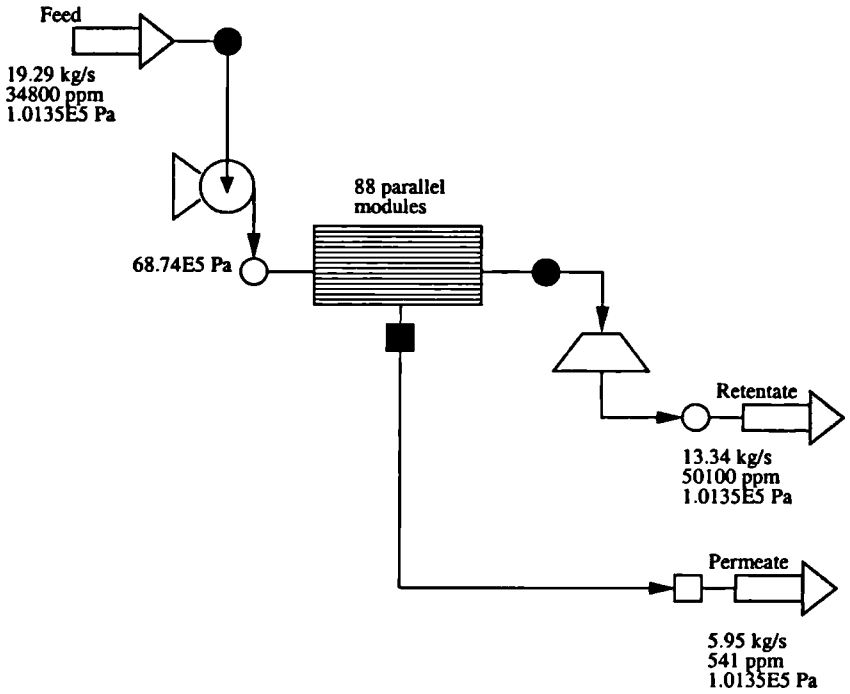

Figure 5.13 *Best one stage design determined using the approximate design model: HF modules*

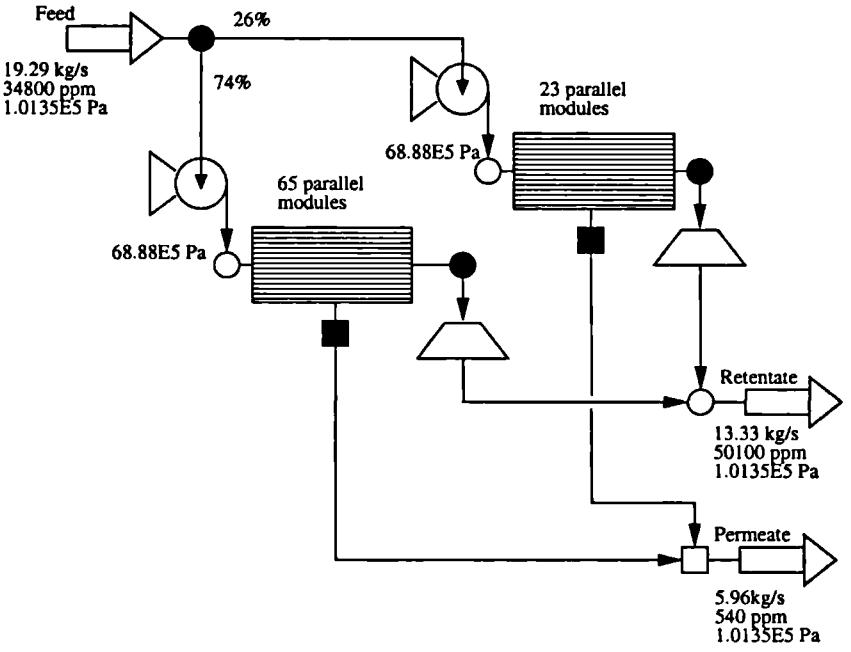

Figure 5.14 *Best two stage design determined using the approximate design model: HF modules*

Table 5.9 *Approximate model optimisation results (hollow-fibre modules)*

	Annualised	Calculated production rate	
	cost ($/yr)	Detailed model	Approximate model
One Stage			
Best Design (Fig 5.13)	211,375	5.95 kg/s (541 ppm)	5.79 kg/s (569 ppm)
Two Stages			
Best Design (Fig 5.14)	217,282	5.96 kg/s (540 ppm)	5.77 kg/s (571 ppm)

The system designs found in this study compare favourably with those proposed in published work. The best design found in this work has a total annualised cost of $203,304 per year which is 15% less expensive than El-Halwagi's design ($237,990 per year) that was based on the approximate module model. Whilst the reduced costs are partly due to the use of a detailed model, they can also be attributed to a more accurate membrane characterisation (verified against experimental data) and a better optimal solution technique (El-Halwagi (1992) failed to find the feed by-pass).

5.6 Optimal design of spiral-wound systems

We now consider the design of a plant to meet the same specifications as in the previous section, but this time based on spiral-wound modules. This study is based on the FT30SW spiral-wound modules.

As in the hollow-fibre study, the modules are described using the detailed model that was verified in Section 5.4. Following this, the optimisation is repeated using the approximate spiral-wound model.

5.6.1 Solution method

The problem is solved in an identical manner to the previous study using the solution methodology described in Chapter 4. However, the following minor changes have been made to the problem definition

1. As discussed in Section 5.2, the additional decision variable describing the pressure vessel length is introduced into the genome. This is implemented using a single model and multiplying the module length by the number of modules in series.

Alternatively, a model for each module could be used, but this would require a much greater computational effort and so is avoided here.

2. A cost for the FT30SW spiral-wound modules must be defined. In this work, a constant annualised cost per module of 483 \$/yr is used. Similar to the costing algorithms suggested by El-Halwagi (1992), this includes membrane replacement, labour and maintenance charges. This cost used here is simply one third of that for the B10 module, roughly in-line with the production rates for the two modules.

3. Spiral-wound modules are often operated at higher pressures than hollow-fibre modules. Therefore, the maximum system pressure (P^{max}) is increased to 80 bar, as simulated earlier in Table 5.5.

Once again, two superstructure sizes are evaluated: a single separation stage system; and a two separation stage system. A database of the top five-hundred solutions is also maintained.

As with the hollow-fibre system, the bounds on the number of modules for each separation stage must be specified (see Section 5.2). The spiral-wound units considered in this work are operated at lower recovery rates than their hollow-fibre counterparts (see Table 5.5), so more modules will be required. Hence, the upper-bound on the number of modules is increased: in this study $n^{min} = 20$ and $n^{max} = 400$.

5.6.2 Detailed spiral-wound model results

Figure 5.15 shows the sensitivity of the annualised cost to the pressure vessel length for the 400 best solutions found by the genetic algorithm. The use of short or long vessels appears to result in inferior solutions. This is because long pressure vessels have higher pressure drops, which limits the driving force for mass transfer across the membrane. On the other-hand, short pressure vessels have lower fluid velocities as more modules are connected in parallel. and as a consequence, concentration polarisation is a bigger problem (see Section 2.2.4).

The costs and performances of three solutions selected from the solution database are shown in Table 5.10. The approximate model is also used to calculate the performance of these designs (Table 5.10) and is seen to over-predict the product flowrate.

The best single stage design found by the genetic algorithm is illustrated in Figure 5.16. This solution has an annualised cost of \$208,066 per year. Like the hollow-fibre system a feed by-pass is utilised: 22% of the feed stream does not actually enter the membrane

Table 5.10 *Detailed model optimisation results (spiral-wound modules)*

	Annualised cost ($/yr)	Calculated production rate	
		Detailed model	Approximate model
One Stage			
Best Design (Fig 5.16)	208,066	5.79 kg/s (193 ppm)	5.96 kg/s (196ppm)
Alternative Design (Fig 5.17)	212,140	5.82kg/s (203 ppm)	6.08 kg/s (196 ppm)
Two Stages			
Best Design (Fig 5.18)	206,336	5.79 kg/s (181 ppm)	5.88 kg/s (184ppm)

system, a much larger fraction than seen in the earlier study. This is possible as the membrane has a much higher salt rejection (Table 5.5). The design contains a total of 266 spiral-wound modules arranged in thirty-eight parallel pressure vessels, each containing seven modules connected in series (the optimal pressure vessel length).

In order to meet product specifications, the best solutions using short pressure vessels require more membrane modules. This is to overcome the increased effect of concentration polarisation due to lower velocities. Figure 5.17 shows an alternative one stage design with shorter pressure vessels (4 modules). This design contains a total of 272 modules (68 pressure vessels) and has an annualised cost of $212,140 per year which is 2% more expensive than the best solution.

The optimisation was repeated using the larger two separation stage superstructure. The best solution found by the genetic algorithm is illustrated in Figure 5.18. Increasing the number of stages enables a small improvement in the annualised plant cost: the best design has an annualised cost of $206,336 per year. This is slightly less expensive (0.8%) than the one stage design. The reduced costs are due to the tapering of the flow structure: the first stage has 51 pressure vessels each containing four spiral-wound modules; and the second has 26 pressure vessels each containing two modules. Therefore, the velocity through the first stage of this design is slower than that through the narrower one-stage solution (38 pressure vessels). Conversely, the velocity through the second stage is much faster. Nevertheless, there is only a small improvement in the plant cost which would probably be outweighed by the increase in capital costs for the smaller pressure vessels as module costs were assumed to be independent of pressure vessel length in this study.

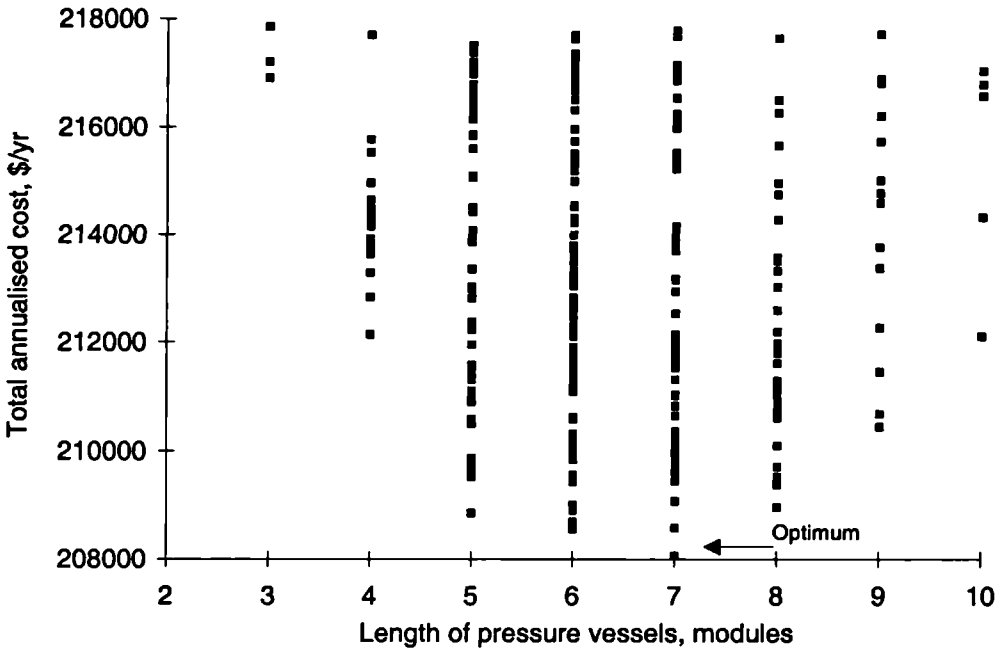

Figure 5.15 *The 400 top solutions plotted as a function of pressure vessel length*

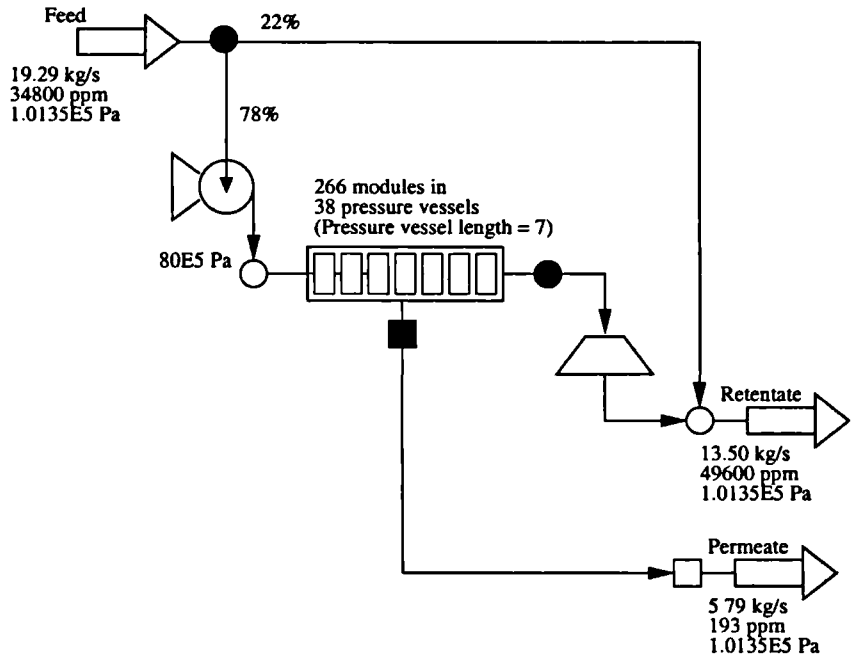

Figure 5.16 *Best one stage design determined using the detailed model: SW modules*

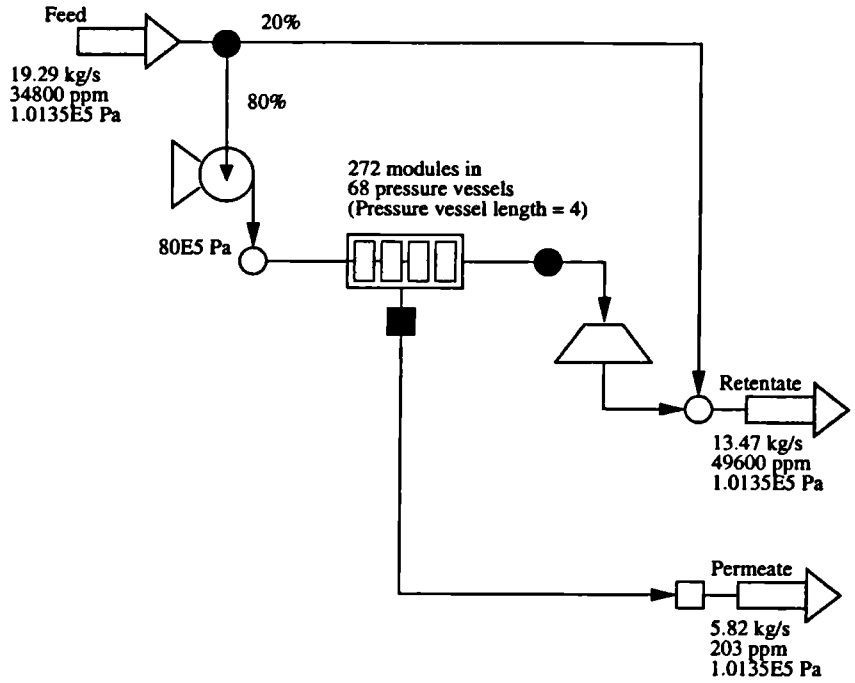

Figure 5.17 *Alternative one stage design determined using the detailed model: SW modules*

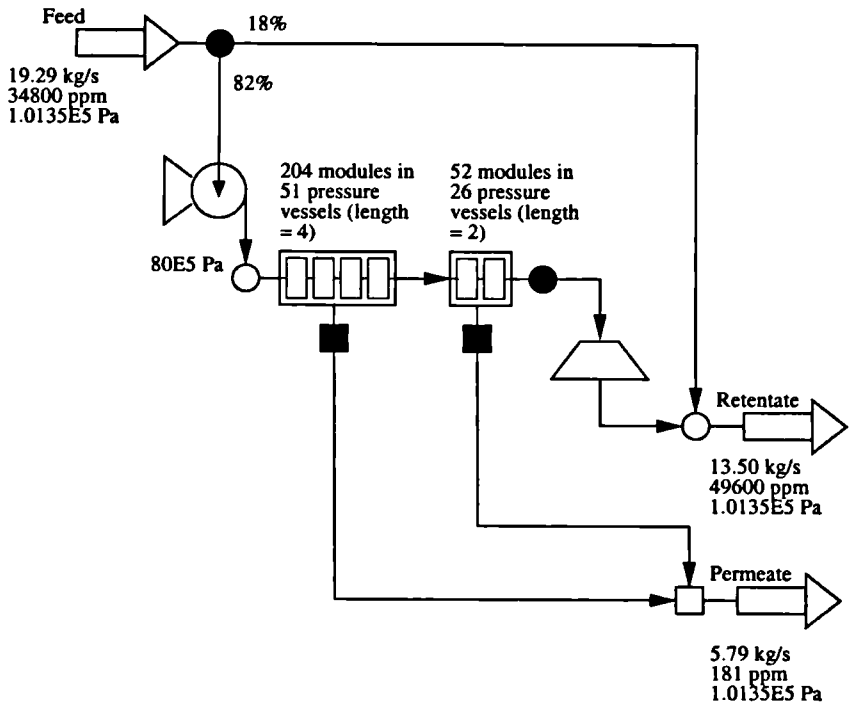

Figure 5.18 *Best two stage design determined using the detailed model: SW modules*

Table 5.11 *Approximate spiral-wound model: additional constraints*

Constraint	Value
Minimum module feed rate, kg/s	0.21
Maximum module feed rate, kg/s	0.23
Nominal pressure drop per module, bar	0.5

5.6.3 Approximate spiral-wound model results

As with the hollow-fibre case study, the use of the approximate model (see Section D.3, Appendix D) requires that a number of additional criteria are introduced: these are given in Table 5.11. These constraints are necessary to limit concentration polarisation and to prevent excessive pressure drop; factors which are formally accounted for by the detailed model. The flowrate constraints and the nominal pressure drop are taken from the operational range of the modules considered in the simulation study (Section 5.4).

The additional constraints are introduced to the model and the optimisation is again repeated using an approximate model (Equations D.8 and D.9, Appendix D). The costs and performance of the best two designs found by the approximate model are summarised in Table 5.12.

The best one stage solution found by the approximate model is shown in Figure 5.19. It has an annualised cost of $203,239 per year and contains a total of 260 spiral-wound modules. These are arranged in 65 pressure vessels each of which contains four modules. This is a substantially shorter and wider system structure than that suggested by the detailed model (Fig 5.16). In fact, the system structure is essentially pre-determined by the flow constraints given earlier in Table 5.11.

In contrast to the results for the hollow-fibre study, the best one-stage design found using the approximate model is less expensive (2%) than its detailed model counterpart. Critically, however, when recalculated using the detailed model it is seen that this design does not meet the required production rate (Table 5.12). This is primarily because the approximate model does not accurately account for the effect of pressure drop and concentration polarisation on module performance.

The best two stage solution, Figure 5.20, is similar to the one stage design. It has a total of 254 spiral-wound modules and again has a wider and shorter structure than that found using the detailed model (Fig 5.18). The annualised cost of the two stage design is $203,439 per year, which is more expensive than the one stage solution. This is not

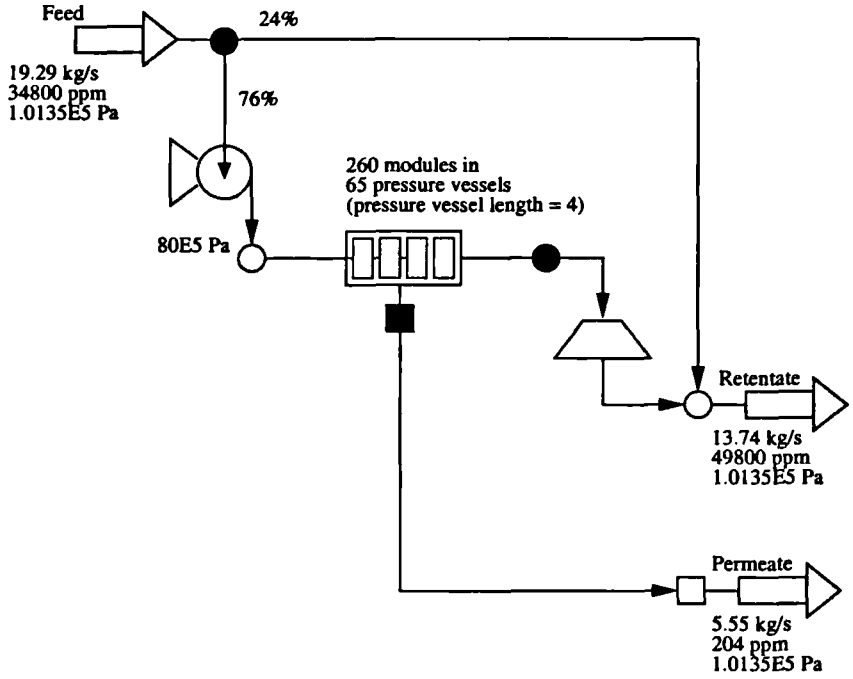

Figure 5.19 *Best one stage design determined using the approximate design model: SW modules*

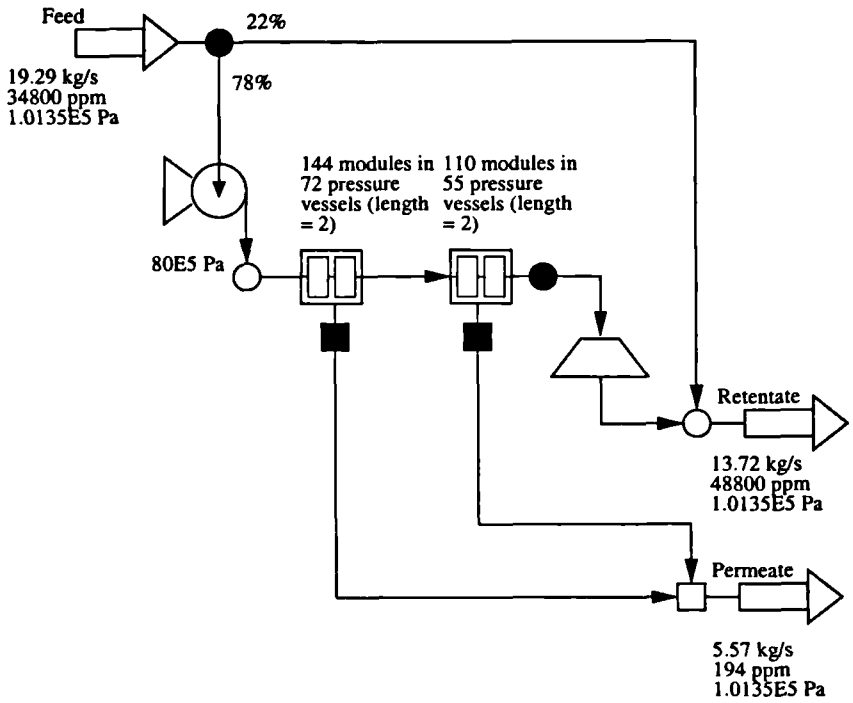

Figure 5.20 *Best two stage design determined using the approximate design model: SW modules*

Table 5.12 *Approximate model optimisation results (spiral-wound modules)*

	Annualised	Calculated production rate	
	cost ($/yr)	Detailed model	Approximate model
One Stage			
Best Design (Fig 5.19)	203,239	5.55 kg/s (204 ppm)	5.80 kg/s (196 ppm)
Two Stages			
Best Design (Fig 5.20)	203,439	5.57 kg/s (194 ppm)	5.79 kg/s (187 ppm)

surprising, as despite the increase in the number of degrees of freedom, the problem is now more heavily constrained due to additional flow restrictions.

5.6.4 Summary

It can be concluded that the approximate design approach evaluated in this study was unable to fully explore the trade-off between concentration polarisation and system pressure drop. Consequently, wider and shorter system structures were imposed than was found to be optimal using the detailed module model. Furthermore, the designs determined using the approximate spiral-wound model are unable to meet the required production rate (m_p^{min}).

In general terms, the modelling and optimisation framework presented in this thesis provides an excellent basis for comparing the relative benefits of hollow-fibre and spiral-wound modules. In this case, the system costs for the two configurations were almost identical. Spiral-wound modules are generally more prevalent for commercial reverse osmosis (Bhattacharyya *et al.*, 1992) which is probably due to more consistent performance (see for example, Butt *et al.*, 1997). However, these results suggest that the design of hollow-fibre units is more straightforward as structural issues are less critical.

5.7 Computational requirements

All of the calculations reported in this chapter were performed on an IBM RISC System/6000 workstation running under the AIX 4.3.2 operating system. The summarised performance of the genetic algorithm in this work is given in Table 5.13.

From Table 5.13 it is seen that the solution time is dependent on the problem size: average simulation times ranged from 1.2 to 3 CPUs in these studies. Actually, most

Table 5.13 *Computational requirements of the genetic algorithm (detailed model)*

Number of separation stages	Simulation time, CPUs	Total number of simulations	Total time, hrs
Hollow-fibre system			
One	1.2	4130	1.4
Two	2.0	9900	5.5
Spiral-wound system			
One	1.5	5750	2.4
Two	3.0	17550	14.7

simulations were executed faster than this, but the occasional infeasible solution[1] increases the average time. Interestingly, these times are not significantly larger than those for the approximate model: whilst the actual execution time was less than 0.1 CPUs, the mean time was again much higher (0.2 - 0.4 CPUs) also due to infeasible solutions.

The number of genome evaluations required to determine the solution of the optimisation problems (Table 5.13) is seen to be relatively low and does not inflate exponentially as the problem size is increased. Therefore, optimisation times ranged from one hour to fifteen hours in this work.

The significant computational effort required for the largest problem sizes can be attributed to two main factors

1. the number of optimisation decision variables, of both integer and binary type
2. the size of the detailed membrane model

It is possible to reduce solution times by using less decision variables and an approximate membrane model. Nevertheless, it is felt that restricting the range of decision variables would reduce the solution space and hide the true potential of membrane separation technology to achieve a given separation. In addition, as has been shown in this chapter, the use of approximate models may lead to inaccurate plant prediction and sub-optimal solutions. Furthermore, as computational power is expected to increase over the next few years, such simplifications are unlikely to be necessary.

[1]Infeasible solutions commonly occur when a separation stage has a large number of modules and a small feed stream. This can result in negative concentrations which are not physically possible and hence a solution cannot be resolved. Infeasible solutions can mostly be avoided by sensibly selecting the bounds on the decision variables - see Section 5.2.

5.8 Conclusions

In this extensive study, the use of detailed models for the optimal design of a reverse osmosis desalination plant has been considered. The results were evaluated through a comparison with those based on approximate module models. The following general conclusions can be drawn

- The use of approximate design models for optimal system design may lead to inferior solutions and incorrect prediction of plant performance: the approximate model design was 4% more expensive for the hollow-fibre system, and did not meet the product specifications for the spiral-wound system.
- The approximate model failed to account for the effect of fluid flowrate on module performance when in fact, pressure drop and concentration polarisation are greatly effected by the fluid velocity. It is these factors that usually control the structural configuration of the membrane system and therefore the approximate models used in this study were unable to fully describe the problem. This effect was most apparent for the spiral-wound system, as pressure drop and concentration polarisation are much greater in this case. Consequently, serious discrepancies were found between the detailed and the approximate model calculations.

In these studies, the design of both hollow-fibre and spiral-wound reverse osmosis systems were considered. The best designs for each case share a number of features: both systems are best operated at maximum pressure, though not all of the feed should be pressurised; and energy recovery devices should be used to recover mechanical energy from the still highly pressurised retentate streams. Structurally, however, the best system designs are quite different. Concentration polarisation is relatively small for hollow-fibre modules, hence a single stage with all the modules connected in parallel can be used with little penalty. In contrast, concentration polarisation is much greater for spiral-wound systems. Consequently, the width of the system is critical. Relatively long systems (6 to 7 modules in depth) were found to provide a good balance between this and pressure drop - which is also a considerable problem for spiral-wound systems.

Only one and two separation stage systems were evaluated in this chapter. Although the computational requirements would have been greater, larger systems could also have been optimised. Indeed, this will be considered in Chapter 6, when a pervaporation case study is evaluated. In this case, however, the use of a two-stage system was actually detrimental to the design of the hollow-fibre system and offered only a marginal improvement for the

spiral-wound system. Therefore, the evaluation of a three stage system would have been of little benefit.

This study has successfully demonstrated the use of the optimisation methodology described in Chapter 4 for the design of a well-established reverse osmosis system. This research is an improvement on previous work in this area for the following two main reasons

- The approach is based on a detailed model that has been verified again experimental data for the modules considered in this study. The model does not make assumptions as to the nature of the separation process and automatically accounts for important effects such as concentration polarisation and pressure drop.
- An optimisation strategy that generates multiple solutions was implemented. This was shown to highlight the important features of the best designs and thus enable a much more through understanding of the design problem than methods that return just a single solution.

In the next chapter, the use of the same optimisation approach is applied to a more complex pervaporation case study. Here, the use of a rigorous model is essential as this process is characterised by large temperature changes and cannot accurately be described by a simple design model. This case study will also be used to evaluate the genetic algorithm solution technique through a comparison with a more conventional gradient-based strategy.

Chapter 6

OPTIMAL DESIGN OF PERVAPORATION SYSTEMS

The optimal process design method outlined in Chapter 4 is demonstrated by application to a pervaporation case study. The use of genetic algorithms for membrane separation system design is also assessed; both in terms of computational requirements and by a comparison with an alternate solution technique. Further details of this work are given in Appendix E.

6.1 Introduction

Many of the liquid mixtures that are encountered in the speciality chemical industries are difficult to separate as they are either close-boiling or azeotropic in nature. Extractive distillation is a common technique for separating such mixtures, however, it is energy intensive and requires the addition of a solvent to change the relative volatilities of the various components. The solvent is often toxic (e.g. benzene) and must subsequently be separated from the mixture. These drawbacks fuel continuous research into new and better separation techniques. The use of pervaporation as an alternative to distillation for difficult separations has been suggested for a number of cases. In particular, the use of pervaporation to separate azeotropic ethanol water mixtures is becoming increasingly important (Fleming and Slater, 1992).

In pervaporation, the membrane forms a semi-permeable barrier between the liquid feed and a low pressure gaseous product. Consequently, the heat of evaporation must be supplied to the permeating material - typically resulting in a feed stream temperature drop. However, in contrast to distillation, only the heat of evaporation for a small fraction of the mixture (the permeating material) must be provided. Thus, the energy requirements of a pervaporation plant are much lower.

The modular nature of membrane systems means that pervaporation is unlikely to compete with distillation for large scale separations as it does not benefit from such great economies of scale. However, pervaporation offers a number of additional advantages (Fleming and Slater, 1992) that make it an attractive option for many separations: lower capital costs for small scale systems, easier retrofitting and debottlenecking (modular design), and often superior separations as it is not constrained by thermodynamic azeotropes.

Pervaporation is inherently complex as large temperature and concentration changes are common inside the membrane modules. Therefore, the accurate simulation and optimisation of pervaporation processes can be computationally expensive. As a result, optimisation studies (e.g. Srinivas and El-Halwagi, 1993) have relied on approximate design models to describe the modules. In fact, all of the literature models described in Section 2.3 rely on the introduction of a number of modelling assumptions. For instance, non-isothermal conditions and constant physical and membrane properties have invariably been assumed. Unfortunately, inaccuracies in modelling the membrane modules will lead to the development of sub-optimal plant designs with the possible over (or under) prediction of plant performance and a lack of generality due to implicit assumptions. The use of approximate models for pervaporation is particularly inappropriate due to the high dependence of permeability on temperature which, if ignored, will cause significant inaccuracies. Therefore, in this chapter, the application of detailed models to the optimal design of pervaporation systems is advocated.

In the following section, a general solution strategy for the optimal design of a pervaporation process is presented. Section 6.3 describes a case study involving the dehydration of azeotropic ethanol. Next, the application of the detailed model to the case study is considered (Section 6.4). The optimal design of the system is then examined using genetic algorithms (Section 6.5). Finally, in Section 6.6, some conclusions are drawn.

6.2 Solution methodology

Whilst design methods for distillation systems are well established, those for pervaporation systems are not. Hence, the use of the simulation and optimisation tools described earlier (see Chapters 3 & 4) may offer significant benefit. The general solution methodology for the optimal design of membrane systems that was described in the previous chapter is demonstrated here for the design of a pervaporation plant.

Table 6.1 *Ancillary equipment for pervaporation processes*

Equipment	Use
Heaters	To provide the heat of evaporation to the liquid stream.
Condenser	1. To condense permeate vapour.
	2. To control downstream permeate vacuum pressure.
Booster compressors	To further reduce downstream vacuum pressure.
Liquid pumps	To pump feed and recycle flows around the system.

In pervaporation, in order to optimise the driving force across the membrane, the feed stream temperature and the permeate pressure are manipulated. Thus, in addition to membrane modules, pervaporation process usually contain ancillary equipment such as heaters and compressors. The individual roles of these items are clarified in Table 6.1.

6.2.1 Process superstructure

In an identical way to the reverse osmosis case study that was investigated in the previous chapter, the generation of the superstructure is now considered for a pervaporation process.

Separation stage decisions

A separation stage for a pervaporation system is illustrated in Figure 6.1. For each stage, the number of modules (N^m), the temperature (T_f), and the permeate pressure (P_p) must be determined.

Normalised temperatures (D^T) are used, these are linear mappings (Eq 4.5) of the actual temperature (T_f), where 0 is the outlet temperature of the previous separation stage (for the first stage the feed temperature is used) and 1 is the maximum process temperature (T^{max}). If no temperature increase is required then a heater is not selected.

The permeate stream pressure is maintained by a condenser. However, the operation of the condenser is fixed and so is not considered as part of the design problem in this study. In some cases, booster compressors are used to further reduce the downstream pressure (e.g. Tsuyumoto *et al.*, 1997): these will also be considered here. Therefore, the pressure of each permeate stream (P_p) is an optimisation decision variable. To enable stages to share a compressor, the permeate pressures will be selected from an *allele* set (this will be of size N^s). The values of the pressures in the allele set (D^P) can of course also be

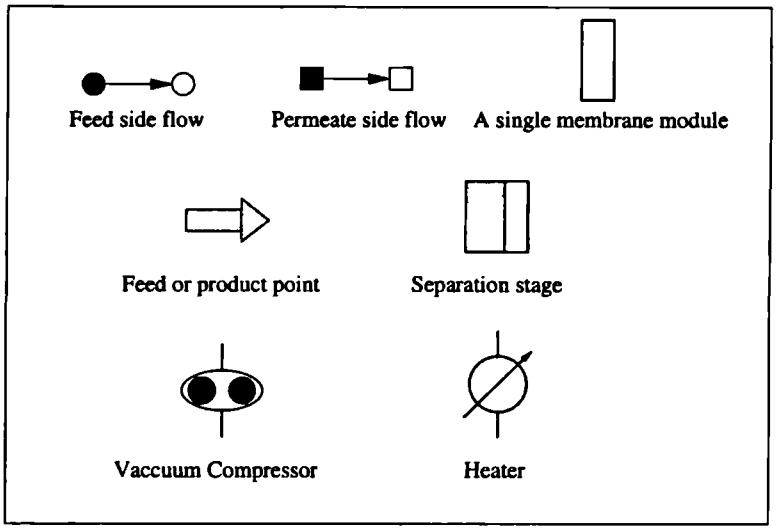

Key to the figures in this chapter

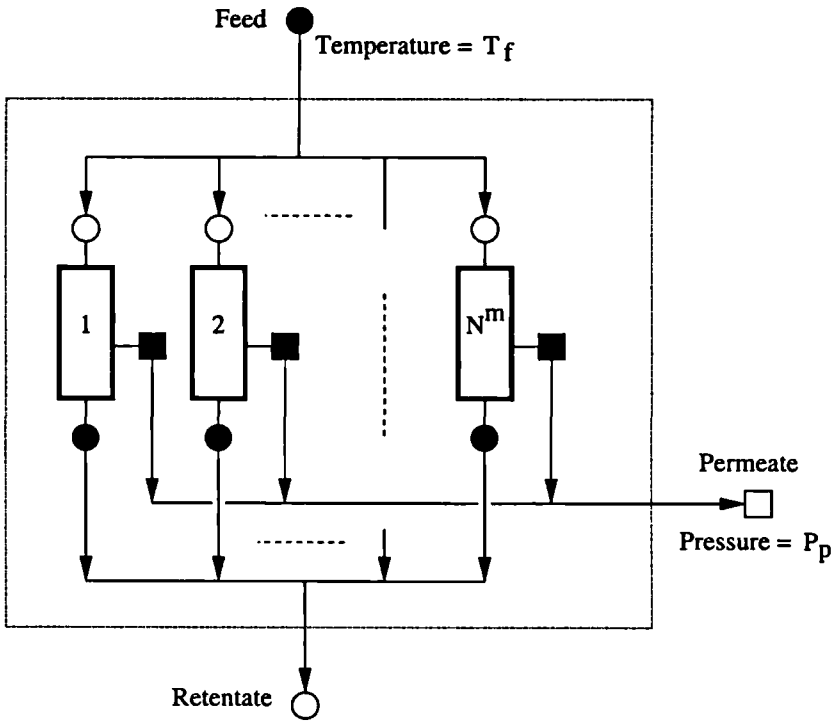

Figure 6.1 *A separation stage for a pervaporation process*

optimised. These pressures have again been normalised using Equation 4.5: where 0 is the minimum attainable pressure (P^{min}) and 1 is the condenser pressure (P^{max}). If the permeate pressure is set at P^{max} then a compressor is not selected.

Network decisions

The structural layout of the plant is determined by fixing the values of the network decision variables (see Section 4.3.3). In pervaporation, each stage has an upstream (liquid) input and an upstream output as well as a downstream (vapour permeate) output. Therefore, the two output streams cannot be mixed. This is a significant advantage as it greatly reduces the number of network choices (see Section 4.3.3). In this study, we will further simplify the system by only allowing separation stages to be connected sequentially - this is reasonable as modules can be connected in parallel inside each stage.

The superstructure consists of N^s separation stages, and is generated by connecting the output from one stage to the input of the next. Consequently, the only network decision variable is the fraction of retentate product that is recycled at each stage. A process superstructure for a two stage system is illustrated in Figure 6.2.

6.2.2 Solution strategy

The best plant design will again be determined by the solution of the superstructure optimisation problem. To select a design from the superstructure, the number of modules, heater temperature, recycle fraction, and the choice of permeate pressures must be specified for each separation stage. The permeate pressures in the allele set must also be determined. This requires a total of five decision variables per stage as indicated in Table 6.2. Like the reverse osmosis case study, the optimisation decision variables have been discretised. The discretisation intervals for each variable are also shown in Table 6.2.

A solution technique based on genetic algorithms was described in Section 4.4 and in this chapter, the application of this method to a pervaporation case study will be assessed.

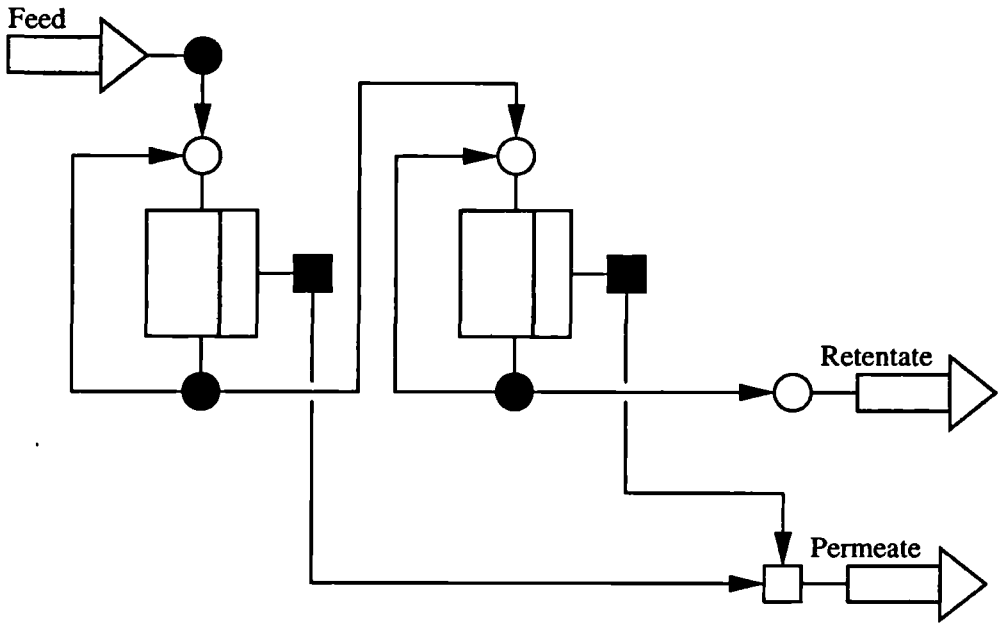

Figure 6.2 *A superstructure for a pervaporation process (two stages)*

Table 6.2 *Decision variables for a pervaporation system*

Decision variable	Lower bound	Upper bound	Interval
The number of membrane modules, N^m	1	n^{max}	1 (integer)
Normalised feed stream temperature, D^T	0	1	0.01
Compressor pressure choice, $D^{P\prime}$	0	N^s	1 (integer)
Normalised compressor pressure(s), D^P	0	1	0.0025
Stage recycle fraction, $\sigma_{a,a}$	0	0.75	0.05

6.3 Description of the case study

The design and performance of a pervaporation pilot plant for the dehydration of azeotropic ethanol/water mixtures has been reported by Tsuyumoto *et al.* (1997). The plant, which is shown in Figure 6.3, is based on nine hollow-fibre modules in seven separation stages, four heaters and two vacuum compressors. Further details of the system are provided in Table E.1 (Appendix E). Models which describe the ancillary equipment have been developed and are given in Section A.4 (Appendix A). In this chapter, the optimal design of this pervaporation process will be determined using genetic algorithms (Chapter 4).

Figure 6.3 *Pervaporation separation process, as proposed by Tsuyumoto et al. (1997)*

This section describes the membrane characterisation method and discusses the assumptions that have been introduced for this case study. The optimisation objective function and design and production constraints are also presented.

6.3.1 Membrane characterisation

The membrane is a polyion complex which preferentially permeates water. Tsuyumoto *et al.* (1997) have characterised the flux of both water and ethanol through the membrane. To enable a fair comparison, the same characterisation will be used in these studies. The flux of water (J_W) is calculated from a solution-diffusion approach where

$$J_W = \frac{D_{W0}K_{cw}}{\delta^m}\left(\gamma_{1W}x_{1W} - \frac{P_2}{P_W^{sat}}x_{2W}\right) + \frac{D_{W0}K_{cw}^2 k_{dw}}{2\delta^m}\left((\gamma_{1W}x_{1W})^2 - \left(\frac{P_2}{P_W^{sat}}x_{2W}\right)^2\right) \tag{6.1}$$

but the ethanol flux (J_E) is given simply

$$J_E = Q_E\omega_E(P_1 - P_2) \tag{6.2}$$

6.3.2 Assumptions

Diffusion coefficients The Reynolds numbers for flow inside the fibre bore are usually low ($Re < 80$) and thus, the rate of dispersion is limited by the molecular diffusivity. Unfortunately, accurate diffusion coefficients for water in 94-99 wt% ethanol are not readily available in the published literature. Therefore, the Wilke equation (Eq. 3.1) will be used to estimate the diffusivity of water in pure ethanol. This is required to account for the effect of concentration polarisation on membrane performance (see Section 3.4.1). Although the effect is not large, it can not be neglected in this case, this is discussed further in Section 6.4.1.

Physical properties The *Multiflash* physical properties package (Infochem Computer Services Ltd, 1996) as interfaced to g*PROMS* is used to provide all physical properties except diffusion coefficients (see above). A variety of thermodynamic models are available within *Multiflash*. In this work, the Soave-Redlich-Kwong equation of state is used for the vapour phase, and the Wilson model is used to calculate liquid phase activity coefficients. The binary interaction parameters used in this work were taken from Gmehling *et al.* (1974-1990). Through a comparison with experimental data, the choice of these values was verified for ethanol/water mixtures by Furlonge (2000).

6.3.3 Optimisation objective and constraints

As with the reverse osmosis case study, economic criteria will be used to determine the optimal plant design. The objective function is therefore to minimise production costs (C) subject to the same constraints used for the Tsuyumoto *et al.* (1997) design (these are given in Table 6.3)

$$min\,[Cf(\omega_r)g(m_r)] \tag{6.3}$$

Two penalty functions are used to penalise solutions that do not satisfy the product constraints. This is done using the same mechanism described earlier in Section 5.3.

In this case, the penalty function $f(\omega_r)$ is written

$$\text{if } \omega_r \geq \omega_r^{min}$$

$$f(\omega_r) = 1 \tag{6.4}$$

else

$$f(\omega_r) = \left(1 - \frac{\omega_r^{min} - \omega_r}{\omega_r^{min} - \omega_f}\right)^{-4} \tag{6.5}$$

and $g(m_r)$ is written

$$\text{if } m_r \geq m_r^{min}$$

$$g(m_r) = 1 \tag{6.6}$$

else

$$g(m_r) = \left(1 - \frac{m_r^{min} - m_r}{m_r^{min}}\right)^{-4} \tag{6.7}$$

Table 6.3 *Production and design constraints for the ethanol dehydration plant (Tsuyumoto et al., 1997)*

6.3.4 Costing

The estimated annualised capital charges for each unit and the utility costs (from Tsuyumoto *et al.*, 1997) are given in Table 6.4. Unfortunately, due to the small scale of the separation system considered in this study (100 kg/hr), accurate capital cost algorithms are unavailable. Therefore, nominal size independent capital costs are used (Table 6.4).

6.3.5 Recycle flows

Theoretically, recycle flows can easily be included as part of the optimisation problem. Previous studies (Tsuyumoto *et al.*, 1997), have shown that recycling some of the outlet flowrate back to the module inlet can improve product quality. However, only a marginal increase in product quality is usually possible and a greater amount of heat must be supplied.

As size-independent capital costing is used for the heater in this study (due to the small scale of the separation system), introducing recycle flows will enable a much higher heat input without increasing equipment costs. The result of a structural optimisation would be an unrealistic plant design with very large recycle flows and a few heaters supplying all the heat. Therefore, recycle flows will be neglected for this optimisation study. It should be noted that this simplification was not required in the reverse osmosis study for which size dependent capital costs were available (Table 5.4).

Table 6.4 *Economic criteria for the ethanol dehydration plant*

Annualised fixed cost of membrane modules, \$/yr	56
Annualised fixed cost of heaters, \$/yr	250
Annualised fixed cost of compressors, \$/yr	150
Steam cost, \$/J	1.316×10^{-3}
Electricity cost, \$/J	2.66×10^{-3}
Mechanical efficiency of compressors	0.75
Operational hours per year	8000

The annualised costs include replacement costs, labour and maintenance charges. The steam and electricity costs are taken from Tsuyumoto *et al.* (1997).

6.4 Process simulation

Before consideration is given to the optimal design of the ethanol dehydration system it is important to determine the accuracy of the detailed model - this is now considered. All the simulations presented in this section were executed using the g*PROMS* simulation software (Process Systems Enterprise Ltd, 1999).

6.4.1 Hollow-fibre module

The ability of the detailed model to simulate the hollow-fibre modules described by Tsuyumoto *et al.* (1997) is now evaluated. The modules are operated conventionally with the feed entering on the fibre-side. The permeate passes first through the membrane and then through a porous support into the shell-side, where it is drawn off under vacuum (Further information on the modules is given in Appendix E). It is important to select the correct flow sub-models (see Section 3.2) to describe conditions on either side of the membrane. This is particularly true for the feed flow through the fibre bore where large concentration and temperature variations are seen.

Two alternate fibre flow models have been developed which can describe the feed flow through the fibre bore (Section 3.2.1). The models are identical except that the 1-D flow model is restricted to systems where concentration polarisation can be neglected. However, the solution of the 2-D flow model generally requires a greater computational effort (see Chapter 3).

Table 6.5 *Ethanol purity calculated using different feed side models (single module)*

Case	Feed conditions		Product concentration (wt% eth.)		
	Flow rate (kg/hr)	Concentration (wt% eth.)	Experimental	Feed side model	
				1-D model	2-D model
1	44.8	94.0	97.2	97.5	97.3
2	248.5	96.8	97.4	97.4	97.4

Feed temperature = $60°C$, Permeate pressure = 400 Pa. Experimental data taken from Tsuyumoto *et al.* (1997)

The use of the detailed model to describe the removal of organics from wastewater by pervaporation was considered earlier in this thesis (see Section 3.4.1). Particular attention was given to the concentration profiles inside the hollow-fibres. It was seen that in addition to axial concentration variations, significant radial concentration variations (*i.e. concentration polarisation*) exist. Therefore, for this system the use of the 1-D model was not recommended.

The ethanol water system is now considered. Simulation results using the 1-D model and the 2-D fibre flow models are compared with the experimental data for two different feed conditions in Table 6.5. In this case, as little information is available on the shell side properties (Tsuyumoto *et al.*, 1997), a 1-D flow model has been used to describe shell side conditions (Section 3.2.1).

The 2-D flow model predicts similar product purities to the 1-D flow model so the effect of concentration polarisation is much lower than in the earlier pervaporation case study (Section 3.4.1). Nevertheless, there is a small effect and the 2-D model is seen to more closely approximate the experimental results and is therefore the most appropriate model. The small error in these results is most likely to be a result of inaccurate membrane characterisation by Equations 6.1 and 6.2.

Srinivas and El-Halwagi (1993) have presented an approximate module model that describes isothermal pervaporation. They used this model to investigate the optimal design of pervaporation systems for the removal of organics from waste-water (see Section 2.4). However, the 2-D model predicts that the liquid temperature will drop from 60°C to 34°C for Case 1. If an isothermal model was used in this study, product purity would be significantly overestimated: 98.4wt% ethanol for Case 1 (this is an error approaching 40%). Thus, isothermal flow models cannot generally be recommended for the design of pervaporation systems and will not be considered in this chapter.

Table 6.6 *Calculated and experimental results for the ethanol dehydration plant*

Simulation	Product concentration wt% ethanol	Product flowrate kg/hr
Experimental (Tsuyumoto *et al.*, 1997)	99.8	94.0
This study	99.7	94.0
Tsuyumoto *et al.* (1997) simulation	99.5	94.3

6.4.2 Ethanol dehydration plant

The performance of the ethanol dehydration pilot plant (Figure 6.3) can also be calculated using the detailed model. The results of the simulation are given in Table 6.6. These show excellent agreement with the experimental data reported by Tsuyumoto *et al.* (1997).

The calculation errors for this study are small and the predicted performance of the plant is seen to be significantly better using the detailed model than that calculated by Tsuyumoto *et al.* (1997). The detailed model predicts the permeate purity to within 0.1wt%, compared to a 0.3wt% simulation error reported by Tsuyumoto *et al.* (1997). Once again, the small error in these results is likely to be a result of inaccurate membrane characterisation by Equations 6.1 and 6.2.

6.5 Optimisation results

The annualised cost of the ethanol dehydration system proposed by Tsuyumoto *et al.* (1997) is calculated as \$6787 per year using the economic data given in Table 6.4. The optimal design strategy presented in Chapter 4 is now used to determine the optimal design of the same system. The design strategy is assessed in terms of computational requirements and then by comparison with a *MINLP* solution technique based on a branch and bound method (see Section 4.2.1).

6.5.1 Number of stages

A separation stage is defined as a number of membrane modules connected in parallel (see Section 4.3). The bounds on the number of modules for each separation stage must be fixed: for this case study a separation stage is specified as containing between 1 and 25 modules (i.e. $n^{min} = 1$, $n^{max} = 25$). The optimisation problem is solved for four superstructure sizes: containing from one to four separation stages. The summarised

results for each case are presented in Table 6.7.

Initially, a superstructure for a single separation stage is generated (i.e. all the modules will be connected in parallel). The solution technique described in Section 4.4 is then used to solve the optimisation problem. The best design (Table 6.7) found by the algorithm has an annualised cost of \$6447 per year, this compares favourably with \$6787 per year for the Tsuyumoto *et al.* (1997) system.

To determine the effect of the number of separation stages, the optimisation is repeated for superstructures built from two, three and four stages (refer to Table 6.7). An improved annualised cost of \$5970 per year is found by increasing the number of separation stages to two. A further slight improvement can be achieved by enabling three separation stages, \$5863 per year. However, forcing the algorithm to choose a design with four stages results in slightly increased costs, \$5873 per year, indicating that the optimum solution is a three stage separation plant. Further details of all the designs are given in Table 6.7.

Despite significant differences in the solutions for each optimisation size (Table 6.7), the calculated profits are all relatively similar. This concurs with the reverse osmosis case study where a large number of structurally different solutions with similar costs were found, and is common to most superstructure optimisation problems. As highlighted in the previous study, a significant advantage afforded by genetic algorithms is that multiple solutions are available at the end of the optimisation.

6.5.2 Design comparison

The new design based on three stages is illustrated in Figure 6.4. The main emphasis of the design is to keep the temperature high throughout the process by adding heat in the initial stages, where most of it is otherwise lost. The higher initial temperatures mean that less membrane area is necessary for the first two stages and that lower compressor duties are required than in the Tsuyumoto *et al.* (1997) design (Figure 6.3). Furthermore, additional heaters are not required at the end of the process.

Summarised cost comparisons are given in Figure 6.5. This shows that capital, membrane and utility costs are all lower for the optimised design with a total saving of 13.5%. The new design contains less modules and heaters leading to the reduction in capital costs. Operating costs are lower due to a similar total heat input but lower compressor duties. In fact, it is interesting to note that whatever costing algorithm is used, this design would provide a cost saving over the base design.

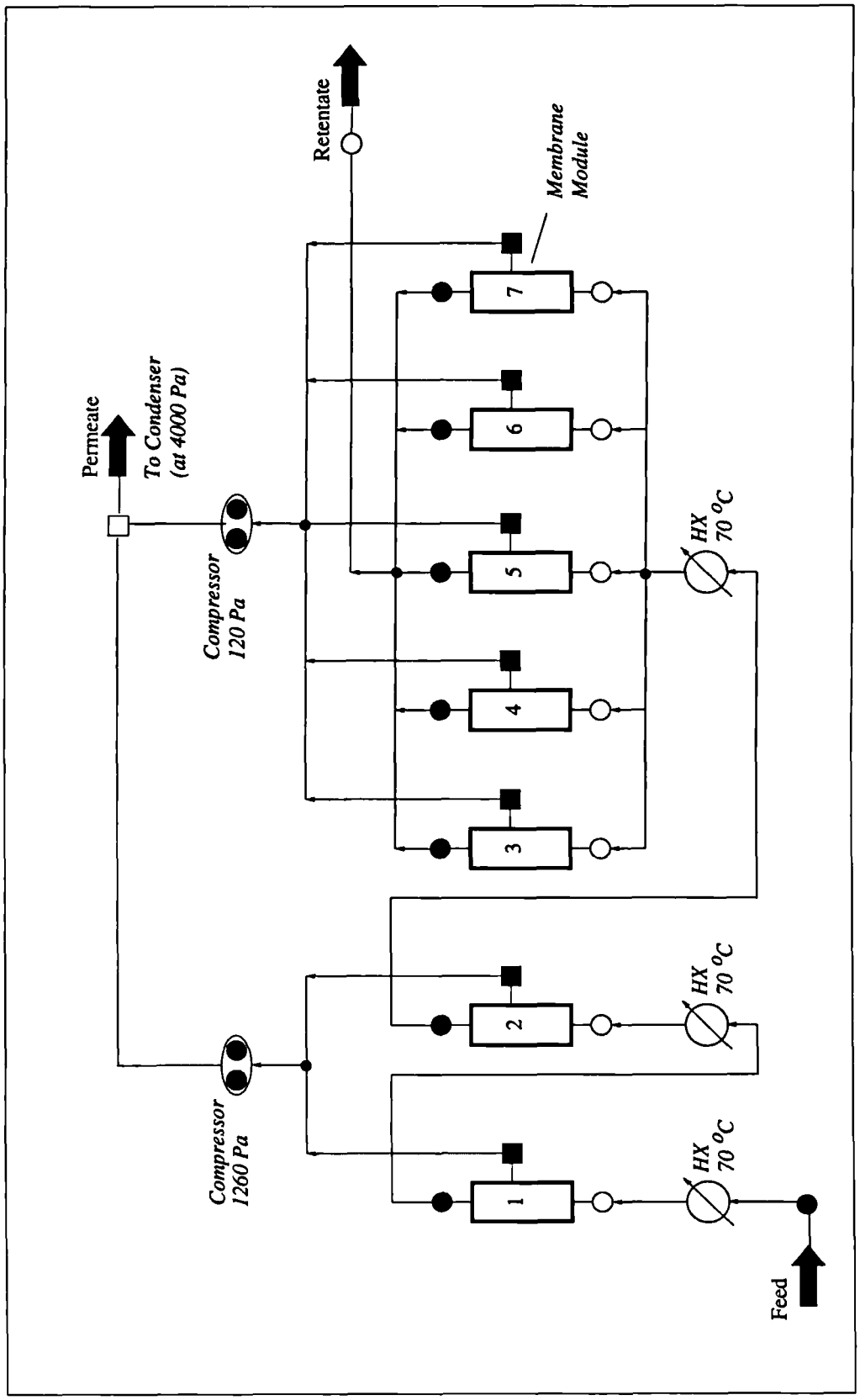

Figure 6.4 *Optimal plant design identified using the genetic algorithm*

Table 6.7 *Optimal pervaporation plant designs for different numbers of separation stages*

		Number of separation stages			
		One	**Two**	**Three**	**Four**
Stage 1	Number of modules	16	2	1	1
	Heater, ^oC	70	70	70	70
	Permeate pressure, Pa	60	630	1260	1300
Stage 2	Number of modules	-	6	1	1
	Heater, ^oC	-	70	70	70
	Permeate pressure, Pa	-	60	1260	1300
Stage 3	Number of modules	-	-	5	1
	Heater, ^oC	-	-	70	none
	Permeate pressure, Pa	-	-	120	90
Stage 4	Number of modules	-	-	-	3
	Heater, ^oC	-	-	-	70
	Permeate pressure, Pa	-	-	-	90
Number of compressors		1	2	2	2
Annualised cost, \$/yr		6447	5970	**5863**	5873

A disadvantage of the new design is its lack of flexibility - there is little scope to increase the purity of the product if required later, without additional capital investment. This is because the heaters are already operating at the maximum process temperature. To overcome this problem it is relatively straightforward to initially over-design the plant by setting tighter product specifications than required. However, that is beyond the scope of this work.

6.5.3 Computational requirements

All of the calculations reported in this chapter were performed on an IBM RISC System/6000 workstation running under the AIX 4.3.2 operating system.

The optimisation results are summarised in Table 6.8. This demonstrates that the fraction of candidate solutions evaluated by the genetic algorithm is tiny - for the three stage case, less than 5000 evaluations were required out of more than 3.5×10^{16} possibilities. Yet the genetic algorithm works remarkably well: the optimal solution is seen to offer a significant improvement over the actual plant design.

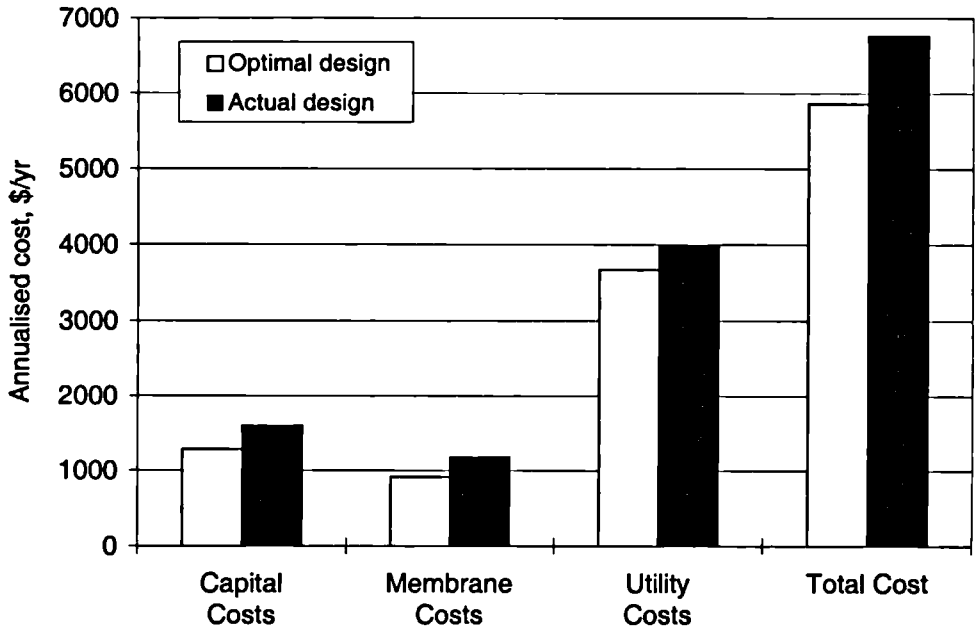

Figure 6.5 *Cost comparison between the optimal and Tsuyumoto et al. (1997) designs*

Typical g*PROMS* simulation (genome evaluation) times ranged from 2 CPUs for a single stage to 10 CPUs for a four stage plant. The number of genome evaluations required to determine the solution (Table 6.8) is seen to be relatively low and does not inflate exponentially as the genome size is increased. Therefore, optimisation times range from one hour for the small one stage problem, to just under forty hours for the largest problem. These times are comparable to those seen for the reverse osmosis case study (Chapter 5) and are despite the larger problem sizes considered here. The main reason for this is that the pervaporation superstructure requires fewer decision variables than its reverse osmosis counterpart. Consequently, less simulations were needed - this is seen by a comparison of Tables 6.8 and 5.13.

Like the previous case study, this study requires a significant computational effort. However, whilst it would again be possible to reduce solution times by using less decision variables, the use of an approximate design model cannot be justified in this case due to the highly non-isothermal system (see Section 6.4). Furthermore, it is felt that restricting the range of decision variables could hide the true potential of pervaporation for liquid mixture separation by reducing the solution space.

Table 6.8 *Summarised optimisation results for the pervaporation case study*

Number of stages	Best solution $/yr	Total number of simulations	Total time, hrs
One	6447	1200	0.7
Two	5970	3100	4.2
Three	**5863**	5000	9.6
Four	5873	13500	36.8
Tsuyumoto *et al.* (1997) design	6787		

6.5.4 Solution using an *NLP* solver

In Section 4.2, a number of methods for the solution of *MINLP* optimisation problems were identified. In order that the performance of the genetic algorithm can be assessed, the optimisation has been repeated using a *MINLP* solution technique based on a branch and bound method (refer to Section 4.2 for further details). Further details of this optimisation are presented in Appendix E.

With this method, approximately 40 *NLP* sub-problems were solved using the g*OPT* solver which is incorporated in the g*PROMS* software (Process Systems Enterprise Ltd, 1999). Each *NLP* optimisation took approximately 20 minutes, however, a guarantee of global optimality is not possible so each optimisation was repeated from two or three different initial conditions. Consequently, over 100 *NLP* optimisations were performed, taking a total of 35 hours of computational time.

The solution found using this method ($5927 p.a.), is similar (although, not quite as good) to the best design found by the genetic algorithm - in a comparable computation time. However, it should be noted that the designs cannot be compared directly as a simpler module model was used in the *MINLP* case. Nevertheless, the study was able to highlight two short-comings of this solution technique.

- Only a single best solution was found: a significant advantage of genetic algorithms is that multiple solutions are available following the optimisation.
- It is difficult to automate the manual branch and bound technique, due to the subjective need to repeat each optimisation until the global optimum is found. This is usually necessary in order to prevent the search space being *pruned* prematurely and the best solutions being cut off. This problem is inherent to all current *NLP* solvers where a guarantee of global optimality is not possible.

Whilst potentially faster solution strategies based on *NLP* solvers exist (e.g. outer approximation methods - Section 4.2), these suffer from the same disadvantages that were highlighted above: namely that only a single best solution is reported, convergence to local optima and, because of this, implementation is difficult. In contrast, genetic algorithms are not subject to such concerns and find equally good, if not better solutions, without significantly increasing computational expense.

6.6 Conclusions

In this chapter, the optimisation strategy proposed in Chapter 4 for the design of membrane systems has been implemented. A pervaporation system to concentrate 100 kg/hr of 94wt% ethanol to a purity in excess of 99.7wt% ethanol has been designed. Reduced operating and capital charges of 13.5% are seen in comparison to the actual plant (Tsuyumoto *et al.*, 1997). These substantially lower costs are a result of smaller equipment duties and a modified configuration with two less modules and one less heater.

Unlike previous optimisation studies (see Section 2.4), this design was produced using accurate membrane unit models that have been assessed against experimental data for a range of different conditions (see Section 6.4). The unit models do not make assumptions as to the nature of the process and fully account for interacting decisions. The use of accurate models not only ensures that any proposed designs will meet product specifications but that similar designs, such as those seen in Table 6.7, can be compared fairly. The use of a rigorous model is essential for this case study as this process is characterised by large temperature changes which cannot accurately be described by a simple design model.

It has also been shown that genetic algorithms are an excellent basis for an effective and powerful tool for the optimal design of membrane systems. The computational requirements of the method were relatively large but necessary, if all the degrees of freedom in the design are to be explored. The method compared favourably when contrasted to more conventional *MINLP* optimisation solution methods.

Chapter 7

CONCLUSIONS AND DIRECTIONS FOR FUTURE RESEARCH

This chapter summarises the work that has been presented in this thesis. In Section 7.1, the contributions of this research to the modelling and simulation of membrane systems are considered. Next, conclusions on the use of mathematical models for the optimal design of such systems are presented (Section 7.2). Finally in Section 7.3, some possible directions for future research are suggested.

7.1 Detailed modelling of membrane separation systems

This research is primarily concerned with the use of mathematical models for the design of membrane systems. It is argued in this thesis that optimal and reliable designs can only be generated using rigorous mathematical models that accurately describe whole membrane systems and their building blocks - membrane modules. However, as highlighted in the literature review (Chapter 2), the use of detailed models for membrane separation system simulation and design has hardly been considered. Existing work has focussed on specific separations and a general modelling approach has not been attempted.

In response, the first major contribution of this work is the development of a general modelling framework for hollow-fibre and spiral-wound membrane modules (Chapter 3). This proposes that the flow patterns either side of the membrane can be described by independent flow sub-models. These are linked by a coupling sub-model that describes the rate of transport of material through the membrane itself.

The rigorous sub-models presented in Appendix A disregard many common assumptions and so describe the separation of a *general* mixture. The generality of the approach has been demonstrated in this thesis through consideration of a number of important membrane processes: pervaporation, gas separation and reverse osmosis. However, the models can easily be applied to other systems, though some adjustment may be required for certain cases. For example: in ultrafiltration and microfiltration systems, fouling is of much greater importance and would need to be taken into account; similarly the effect of temperature polarisation (see Mulder, 1996) should be incorporated into the model equations for membrane distillation.

The models presented in Appendix A were developed for spiral-wound and hollow-fibre modules, but again the extension to different membrane configurations would be straightforward. The fibre flow sub-model which describes flow inside hollow-fibres (Section A.2) is equally applicable at the much larger internal diameters found in tubular membranes. The channel flow model (Section A.3) can likewise be adapted to describe the flat flow channels seen in plate-and-frame modules.

Mathematical models are used at many stages in the evolution of process plants. Model applications range from unit design, parameter estimation and process synthesis, to process simulation and model based control. In the literature review it was indicated that, generally, the level of model complexity has depended on the final application. For simulation studies, more detailed models are usually used whereas approximate models have been developed to enable quick design calculations. In this thesis we argue that a single model can be used throughout. This avoids the necessity to develop and test new models for each application and ensures consistent predictions. This has been demonstrated in this work where the same model is used for process simulation and optimisation, and for parameter estimation.

7.2 Optimal design of membrane separation systems

A significant contribution of this work is the development of a new methodology for the optimal design of membrane systems (Chapter 4). In this approach, genetic algorithms are used to solve a superstructure optimisation problem. This enables the structural and equipment requirements of the separation system to be considered simultaneously. The methodology has been applied to two different case studies: a reverse osmosis separation (Chapter 5) concerned with the desalination of sea-water, and a pervaporation example (Chapter 6) that investigates the use of membranes for ethanol dehydration. Several

general conclusions can be drawn from these studies

1. *Detailed versus approximate models*

   The use of detailed models for the design of reverse osmosis systems was investigated in Chapter 5. The results were compared with those from an identical study based on approximate models. The use of an approximate approach was seen to lead to sub-optimal solutions for the first example investigated, and a design which critically failed to meet product specifications for the second. The approximate models were also unable to fully account for the effect of fluid flowrate on module performance. Furthermore, in many cases, suitable approximate models are unavailable due to complex modelling issues, such as non-isothermal flow. This point was highlighted in Chapter 6 when a pervaporation example was evaluated. For these reasons, the use of detailed models for the design of membrane systems is advocated.

2. *The importance of model verification*

   In the two case studies considered in this research, an assessment of the model accuracy was made by a comparison with experimental data. Consequently, technical confidence in the designs developed in this study is high. In contrast, many of the literature studies concerned with the design of membrane systems rely on unverified approximate models, this makes the proposed designs and the conclusions drawn highly questionable. Therefore, wherever possible, model verification should be undertaken.

3. *Multiple solutions provide greater insight*

   An important feature of the design strategy proposed in this work is that multiple solutions are available following the optimisation. This was explored in Chapter 5, where the production of multiple solutions enabled an assessment of the sensitivity of the design to important decision variables (such as the number of membrane modules). This feature is also of significant benefit in situations where important design decisions cannot be incorporated into the objective function. Examples of this may range from ease of cleaning and maintenance, to plant layout issues. In such cases, the availability of multiple solutions enables the engineer to interpret the optimisation results and to make an informed decision based on a database of good designs.

7.3 Future research

The limitations of the research presented in this thesis and related directions for future work are now discussed.

7.3.1 Primary recommendations

Extending this research

The scope of this research has been confined to pervaporation, gas separation, and reverse osmosis. Nevertheless, as discussed in Section 7.1, the general modelling framework proposed in Chapter 3 can be applied to other separations. Similarly, the optimisation approach introduced in Chapter 4 considers a general membrane separation and so can also be used to investigate a wider range of systems. Of these processes, ultrafiltration and microfiltration have the greatest industrial significance (Ho and Sirkar, 1992) and provide a straightforward but highly influential area for future research. However, the methodology would need to be adjusted to incorporate the effects of fouling and membrane degradation (see below). Emerging technologies such as vapour permeation and membrane distillation are currently of great academic interest (Mulder, 1996) and may also benefit from economic assessment studies.

In this thesis, our studies have been restricted to the steady-state simulation and optimisation of continuous membrane processes. However, an important area for future research is an investigation into the dynamics of membrane processes. Accurate dynamic simulation of membrane modules is critical for the design of control systems and the description of batch processes. This is easily facilitated by the detailed model presented in this thesis as it does not assume steady-state conditions.

Membrane degradation

The effects of membrane degradation and fouling on module performance have not been incorporated directly into the design methodology outlined in this work. However, such effects can be significant, for example in reverse osmosis, a 50% decrease in flux is not uncommon over the lifetime of an industrial membrane (e.g. Butt *et al.*, 1997).

A more rigorous approach requires the description of the variation in membrane properties with time. The extension of the methodology presented here to dynamic optimisation is both complex and interesting and is perhaps the most useful area for future research.

However, the following issues would demand particular attention

- The accurate description of fouling and membrane degradation rates, and of their subsequent effect on membrane performance.
- The variation in membrane properties throughout the system.
- Maintenance scheduling.
- The large computational requirements of dynamic simulation and optimisation.

There has been very little previous research in this area, however, reference should be made to the work of Zhu *et al.* (1997) who investigate the optimal design of a reverse osmosis system using an approximate module model. They consider maintenance scheduling and the variation of water permeability with time.

7.3.2 Additional recommendations

Hybrid separation systems

In this research, the membrane system was treated in isolation from the rest of the process plant. In reality, the interaction with other equipment will have a significant impact on the design of the separation system. This is particularly true for hybrid separation systems which are of increasing interest. A commonly suggested example of this is a combined pervaporation and distillation system for ethanol dehydration (Fleming and Slater, 1992). Clearly, treating the problem as a whole enables a much better solution than if the distillation and membrane systems are considered independently.

Degrees of freedom

In the design studies presented in this thesis, a wide range of degrees of freedom were explored. This was seen to be essential if all possible process configurations are to be assessed. Nevertheless, the incorporation of module characteristics into the optimisation problem was not considered in this work (i.e. a fixed module design was assumed). Thus, the optimisation of the module configuration as part of the design problem provides an interesting opportunity for further research.

New solution techniques

This thesis has demonstrated the use of genetic algorithms for the optimal design of membrane systems. However, it must be noted that this solution technique cannot guarantee that the best design embedded in the superstructure will be found. Although, from a practical point of view, if the solutions generated are better than those that could obtained using heuristic techniques, then considerable progress has been made.

Whilst there is currently a considerable research effort developing rigorous methods for the global optimisation of superstructure optimisation problems (Adjiman *et al.*, 1997), these are still some-way from being suitable for the large problem sizes considered in this study. Determination of the global optimum is important as it identifies the best possible solution, against which other designs can be assessed. However, methods that return multiple solutions, such as genetic algorithms, are of significantly greater benefit to the design engineer who is usually required to make a decision based on both quantitative and qualitative criteria. Therefore, a combination of the two methods may provide the best balance and would be worthy of future attention.

REFERENCES

[1] Adjiman C.S., Androulakis I.P. and Floudas C.A. Global optimization of *MINLP* problems in process synthesis and design. *Computers and Chemical Engineering*, S21:445–450, 1997.

[2] Al-Bastaki N.M. and Abbas A. Modeling an industrial reverse osmosis unit. *Desalination*, 126:33–39, 1999.

[3] Al-Mutaz I.S., Soliman M.A. and Al-Zahrani A.E.S. Modeling and simulation of hollow fine fiber modules with radial dispersion - a parametric sensitivity study. *Desalination*, 110:239–250, 1997.

[4] Al-Ahmad M. and Aleem F.A. Scale formation and fouling problems effect on the performance of MSF and RO desalination plants in Saudi Arabia. *Desalination*, 93:287–310, 1993.

[5] Androulakis I.P. and Venkatasubramanian V. A genetic algorithm framework for process design and optimization. *Computers and Chemical Engineering*, 15:217–228, 1991.

[6] Bacchin P., Aimar P. and Sanchez V. Model for colloidal fouling of membranes. *AIChE Journal*, 41:368–376, 1995.

[7] Bandini S., Saavedra A. and Sarti G.C. Vacuum membrane distillation: Experiments and modeling. *AIChE Journal*, 43:398–408, 1997.

[8] Beigler L.T., Grossmann I.E. and Westerberg A.W. *Systematic Methods of Chemical Process Design.* Prentice Hall, New Jersey, 1997.

[9] Ben-Boudinar M., Hanbury W.T. and Avlonitis S. Numerical simulation and optimization of spiral wound modules. *Desalination*, 86:273–290, 1992.

[10] Bhattacharyya D., Williams M.E., Ray R.J. and McCray S.B. Reverse osmosis: Design. In Ho, W.S.W. and Sirkar K.K., editors, *Membrane Handbook*, chapter, 23. Van Nostrand Reinhold, 1992.

[11] Bird R.B., Stewart W.E. and Lightfoot E.N. *Transport Phenomena.* John Wiley, New York, 1960.

[12] Brouckaert C.J. and Buckley C.A. Simulation of tubular reverse osmosis. *Water SA*, 18(3):215–224, 1992.

[13] Butt F.H., Rahman F. and Baduruthamal U. Hollow fine fiber vs. spiral-wound RO desalination membranes, part 1: Pilot plant evaluation. *Desalination*, 109:67–82, 1997.

[14] Chern R.T., Koros W.J. and Fedkiw P.S. Simulation of a hollow-fiber gas separator: the effects of process and design variables. *Industrial and Engineering Chemistry Process Design and Development*, 24:1015–1022, 1985.

[15] Chiolle A., Gianotti G., Granomdo M. and Parrini G. *Desalination*, 24:3, 1978.

[16] Coker D.T., Freeman B.D. and Fleming G.K. Modeling multicomponent gas separation using hollow-fibre membrane contactors. *AIChE Journal*, 44:1289–1302, 1998.

[17] Cote P. and Lipski C. Mass transfer limitations in pervaporation for water and wastewater treatment,. *IN R.Baksih (Ed) Proceedings of the Third International Conference on Pervaporation Processes in the Chemical Industries*, 1988.

[18] Crowder M.L. and Gooding C.H. Spiral-wound, hollow-fiber membrane modules: A new approach to higher mass transfer efficiency. *Journal of Membrane Science*, 137:17–29, 1997.

[19] Cussler E.L. *Diffusion.* Cambridge University Press, 2nd edition, 1997.

[20] Dandavati M.S., Doshi M.R. and Gill W.N. Hollow fiber reverse osmosis: Experiments and analysis of radial flow systems. *Chemical Engineering Science*, 30:877 886, 1975.

[21] Deen W.M. Hindered transport of large molecules in liquid filled pores. *AIChE Journal*, 33:1409–1425, 1987.

[22] Dickson J.M., Spencer J. and Costa M.L. Dilute single and mixed solute systems in spiral wound reverse osmosis module: Part 1, theoretical model development. *Desalination*, 89:63 88, 1992.

[23] Duran M.A. and Grossmann I.E. An outer-approximation algorithm for a class of mixed-integer non-linear programs. *Mathematical Programming*, 36:307–339, 1986.

[24] El-Halwagi M.M. Synthesis of reverse osmosis networks for waste reduction. *AIChE Journal*, 38:1185–1198, 1992.

[25] El-Halwagi A.M., Manousiouthakis V. and El-Halwagi M.M. Analysis and simulation of hollow-fiber reverse osmosis modules. *Separation Science and Technology*, 31:2505–2529, 1996.

[26] Evangelista F. A short cut method for the design of reverse osmosis desalination plants. *Industrial and Engineering Chemical Process Design and Development*, 24:211–223, 1985.

[27] Evangelista F. Improved graphical analytical method for the design of reverse osmosis plants. *Industrial and Engineering Chemical Process Design and Development*, 25:366, 1986.

[28] Evangelista F. and Jonsson G. Optimal design and performance of spiral-wound modules II: analytical method. *Chemical Engineering Communications*, 72:83–94, 1988.

[29] Farnand B.A., Talbot F.D.F., Matsuura T. and Sourirajan S. Reverse osmosis separations of some organic and inorganic solutes in ethanol solutions with cellulose acetate membranes. *Industrial and Engineering Chemistry Research*, 26:1080–1087, 1987.

[30] Fleming H.L. and Slater C.S. Pervaporation. In Ho, W.S.W. and Sirkar K.K., editors, *Membrane Handbook*, chapter 7. Van Nostrand Reinhold, 1992.

[31] Fraga E.S. and Senos Matias T.R. Synthesis and optimization of a nonideal distillation system using a parallel genetic algorithm. *Computers and Chemical Engineering*, 20:S79 S84, 1996.

[32] Furlonge H.I. *Optimal operation of unconventional batch distillation columns.* PhD thesis, University of London, 2000.

[33] Garrard A. and Fraga E.S. Mass exchange network synthesis using genetic algorithms. *Computers and Chemical Engineering*, 22:1837–1850, 1998.

[34] Geoffrion, A. M. Generalized benders decomposition. *Journal of Optimization Theory and Applications*, 10:237 260, 1972.

[35] Gmehling J., Onken U. and Arlt W. *Vapour-liquid equilibrium data collection, Chemistry data series.* Dechema, Frankfurt/Maine, 1974-1990.

[36] Greenlaw F.W., Prince W.D., Shelden R.A. and Thompson E.V. Dependence of diffusive permeation rates on upstream and downstream pressures. 1: Single component permeant. *Journal of Membrane Science*, 2:141–151, 1977.

[37] Grossmann I.E. and Kravanja Z. Mixed integer nonlinear programming techniques for process systems engineering. *Computers and Chemical Engineering*, 19:S189–S204, 1995.

[38] Grossmann I.E. and Daichendt M.M. New trends in optimization-based approaches to process synthesis. *Computers and Chemical Engineering*, 20:665–683, 1996.

[39] Happel J. Viscous flow relative to an array of cylinders. *AIChE Journal*, 5:174–177, 1959.

[40] Hawlader M.N.A., Ho J.C. and Malek A. An experimental and analytical study of permasep-B10 separation characteristics. *Journal of Membrane Science*, 87:1–21, 1994.

[41] Heintz A. and Stephan W. Generalized solution-diffusion model of the pervaporation process through composite membranes parts 1 and 2. *Journal of Membrane Science*, 89:143–169, 1994.

[42] Hickey P.J. and Gooding C.H. Modeling spiral-wound membrane modules for the pervaporative removal of volatile organic compounds from water. *Journal of Membrane Science*, 88:47–68, 1994.

[43] Ho W.S.W. and Sirkar K., editors. *Membrane Handbook.* Van Nostrand Reinhold, New York, first edition, 1992.

[44] Holland J.H. *Adaptation in Natural and Artificial Systems.* University of Michigan Press, Michigan, 1975.

[45] Infochem Computer Services Ltd, London. *Mulitflash Physical Properties Software*, 1996.

[46] Ito A., Watanabe K. and Feng Y. Swollen-dry-layer model for the pervaporation of ethanol-water solution through hydrophilic membranes. *Separation Science and Technology*, 30:3045–3060, 1995.

[47] Ito A., Feng Y. and Sasaki H. Temperature drop of feed liquid during pervaporation. *Journal of Membrane Science*, 133:95–102, 1997.

[48] Ji W. Hilaly A., Sikdar S. and Hwang S. Optimization of multicomponent pervaporation for removal of volatile organic components from water. *Journal of Membrane Science*, 97:109–125, 1994.

[49] Kabadi V.N., Doshi M.R. and Gill W.N. Radial flow hollow-fiber reverse osmosis: Experiments and theory. *Chemical Engineering Communications*, 30:339–365, 1979.

[50] Kaldis S.P., Kapantaidakis G.C., Papadopoulos T.I. and Sakellaropoulos G.P. Simulation of binary gas separation in hollow-fiber asymmetric membranes by orthogonal collocation. *Journal of Membrane Science*, 142:43–59, 1998.

[51] Kerkhof P.J.A.M. Modified Maxwell-Stefan model for transport through inert membranes: The binary friction model. *Chemical Engineering Journal*, 64:319–342, 1996.

[52] Koros W.J. Model for sorption of mixed gases in glassy polymers. *Journal of Polymer Science*, 18:981–992, 1980.

[53] Krovvidi K.R., Kovalli A.S., Venury S. and Khan A.A. Approximate solutions for gas permeators separating binary mixtures. *Journal of Membrane Science*, 66:103–118, 1992.

[54] Kulkarni S.S., Funk E.W. and Li N.N. Ultrafiltration. In Ho W.S.W. and Sirkar K.K., editors, *Membrane Handbook*, chapter 26-30. Van Nostrand Reinhold, 1992.

[55] Lawson K.W. and Lloyd D.R. Membrane distillation. 1: Module design and performance evaluation using vacuum membrane distillation. *Journal of Membrane Science*, 120:111–121, 1996.

[56] Lemanski J. and Lipscomb G.G. Effect of fiber variation in the performance of countercurrent hollow-fiber gas separation modules. *Journal of Membrane Science*, 167:241–252, 2000.

[57] Lewin D.R., Wang H. and Shalev O. A generalized method for HEN synthesis using stochastic optimization - 1. General framework and MER optimal synthesis. *Computers and Chemical Engineering*, 22:1503–1513, 1998.

[58] Lightfoot E.N. *Transport in Living Systems*. Wiley, 1974.

[59] Malek A., Hawlader M.N.A. and Ho J.C. A lumped transport parameter approach in predicting B10 RO permeator performance. *Desalination*, 99:19, 1994.

[60] Malek A., Hawlader M.N.A. and Ho J.C. Design and economics of RO sea water desalination. *Desalination*, 105:245–261, 1996.

[61] Manousiouthakis V. and Bagajewicz M. Synthesis of distillation networks featuring minimum utility use. *AIChE Meeting, Chicago, Nov.11-16*, 1990.

[62] Manousiouthakis V., Bagajewicz M. and Pham R. Total annualized cost minimization for heat/mass exchange networks. *AIChE Meeting, Chicago (Nov.11-16, 1990*, 1990.

[63] Mason E.A. and Lonsdale H.K. Statistical mechanical theory of membrane transport. *Journal of Membrane Science*, 51:1–81, 1990.

[64] Matsuura T. and Sourirajan S. Reverse osmosis transport through capillary pores under the influence of surface forces. *Industrial and Engineering Chemistry*, 20:273, 1981.

[65] van der Meer W.G.J., Riemersma M. and van Dijk J.C. Only two membrane modules per pressure vessel? Hydraulic optimization of spiral-wound membrane filtration plants. *Desalination*, 119:57–74, 1998.

[66] Mehta G.D., Morse T.F., Mason E.A. and Daneshpajooh MH. Generalised Nernst-Plank and Stefan-Maxwell equations for membrane transport. *Journal of Chemical Physics*, 64:3917, 1976.

[67] Mitchell M. *An Introduction to Genetic Algorithms.* MIT Press, 1996.

[68] Molina C., Steinchen A., Charbit G. and Charbit F. Model for pervaporation: Application to ethanolic solutions of aroma. *Journal of Membrane Science*, 132:119 129, 1997.

[69] Mulder M.H.V., Franken A.C.M. and Smolders C.A. On the mechanism of separation of ethanol-water mixtures by pervaporation. 2: Experimental concentration profiles. *Journal of Membrane Science*, 23:41–59, 1985.

[70] Mulder M.H.V. *Basic Principles of Membrane Technology.* Kluwer Academic Publishers, The Netherlands, 2nd edition, 1996.

[71] Muldowney G. P. and Punzi V. L. Comparison of solute rejection models in reverse osmosis membranes for the system water-sodium chloride-cellulose acetate. *Industrial and Engineering Chemistry Research*, 27:2342, 1988.

[72] Narinsky A.G. Applicability conditions of idealized flow models for gas separations by asymmetric membrane. *Journal of Membrane Science*, 55:333–347, 1991.

[73] Oh M. *Modelling and simulation of combined lumped and distributed processes.* PhD thesis, University of London, 1995.

[74] Ohya H. and Taniguchi Y. Analysis of reverse osmosis characteristics of Roga-400 spiral-wound modules. *Desalination*, 16:359–373, 1975.

[75] Ohya H. *Desalination*, 21:257, 1977.

[76] Okada T. and Matsuura T. A new transport model for pervaporation. *Journal of Membrane Science*, 59:133–150, 1991.

[77] Pan C.Y. Gas separation by permeators with high-flux asymmetric membranes. *AIChE Journal*, 29, 1983.

[78] Pan C.Y. Gas separation by high flux, asymmetric hollow fibre membrane. *AIChE Journal*, 32, 1986.

[79] Pantelides C.C. Dynamic behaviour of process systems (lecture notes). Centre for Process Systems Engineering, Imperial College of Science, Technology and Medicine, London, 1998.

[80] Pettersen T. and Lien K.M. A new robust design model for gas separating membrane modules based on analogy with counter-current heat exchangers. *Computers in Chemical Engineering*, 18:427–439, 1994.

[81] Process Systems Enterprise Ltd, London. *gPROMS Advanced User's Guide*, 1999.

[82] Psaume R., Aptel P., Aurelle Y., Mora J.C. and Bersillon J.I. Pervaporation: Importance of concentration polarisation in the extraction of trace organic from water. *Journal of Membrane Science*, 36:373–384, 1988.

[83] Qi R. and Henson M.A. Approximate modeling of spiral-wound gas permeators. *Journal of Membrane Science*, 121:11–24, 1996.

[84] Qi R. and Henson M.A. Modelling of spiral-wound permeators for multicomponent gas separations. *Industrial and Engineering Chemistry Research*, 36:2320–2331, 1997.

[85] Qi R. and Henson M.A. Optimal design of spiral-wound membrane networks for gas separations. *Journal of Membrane Science*, 148:71–89, 1998.

[86] Qi R. and Henson M.A. Membrane system design for multicomponent gas mixtures via mixed-integer nonlinear programming. *Computers and Chemical Engineering*, 24:2719 2737, 2000.

[87] Rangarajan R., Majid M.A., Matsuura T. and Sourirajan S. Permeation of pure gases under pressure through asymmetric porous membranes membrane characterisation and prediction of performance. *Industrial and Engineering Chemistry Design and Development*, 23:79, 1984.

[88] Rautenbach R. and Albrecht R. The separation potential of pervaporation (parts 1 and 2). *Journal of Membrane Science*, 25:1–55, 1985.

[89] Rautenbach R. and Albrecht R. *Membrane Processes.* John Wiley & Sons, Chichester, 1989.

[90] Rautenbach R. and Dahm W. Design and optimization of spiral-wound and hollow-fiber RO-modules. *Desalination*, 65:259–275, 1987.

[91] Rautenbach R., Herion C., Franke M., Asfour A.F., Bemquerer-Costa A. and Bo E. Investigation of mass transport in asymmetric pervaporation membranes. *Journal of Membrane Science*, 36:445–462, 1988.

[92] Rice R.G. and Duoung D.D. Applied Mathematics for Chemical Engineers. John Wiley, New York, 1995.

[93] Schaetzel P., Favre E., Nguyen Q.T. and Neel J. Mass transfer analysis of pervaporation through an ion exchange membrane. *Desalination*, 90:259–276, 1993.

[94] Schock. G. and Miquel A. Mass-transfer and pressure loss in spiral-wound modules. *Desalination*, 64:339–352, 1987.

[95] Schofield R.W., Fane A.G. and Fell C.J.D. Gas and vapour transport through microporous membranes. *Journal of Membrane Science*, 53:159, 1990.

[96] Sekino M. Precise analytical model of hollow-fiber reverse osmosis modules. *Journal of Membrane Science*, 85:241–252, 1993.

[97] Singh V., Rhinehart R.R., Narayan R.S. and Tock R.W. Transport analysis of hollow-fiber gas separation membranes. *Industrial and Engineering Chemistry Research*, 34:4472–4478, 1995.

[98] Sirkar K.K., Dong P.T. and Rao G.H. Approximate design equations for reverse osmosis desalination by spiral-wound modules. *Chemical Engineering Science*, 21:517–527, 1982.

[99] Sirkar K.K. Membrane separation technologies: Current developments. *Chemical Engineering Communications*, 157:145–184, 1996.

[100] Smith E.M.B. *On the Optimal Design of Continuous Processes.* PhD thesis, London:Imperial College, 1996.

[101] Soltanieh M. and Gill W.N. Review of reverse-osmosis membranes and transport models. *Chemical Engineering Communications*, 12:279–363, 1981.

[102] Soltanieh M. and Gill W.N. Analysis and design of hollow-fiber reverse-osmosis systems. *Chemical Engineering Communications*, 18:311–330, 1982.

[103] Soltanieh M. and Gill W.N. An experimental-study of the complete-mixing model for radial flow hollow-fiber reverse-osmosis systems. *Desalination*, 49:57–88, 1984.

[104] Soltanieh M. and Zaare-Asl T. Modified solution-diffusion model for separation of ethanol-water azeotropic mixtures in pervaporation. *Chemical Engineering Communications*, 152-153:406–412, 1996.

[105] Sourirajan S. and Matsuura T. Science of reverse osmosis - an essential tool for the chemical engineer. *Chemical Engineer (London)*, pages 359–368, 1982.

[106] Srinivas B.K. and El-Halwagi M.M. Optimal design of pervaporation systems for waste reduction. *Computers and Chemical Engineering*, 17:957–970, 1993.

[107] Sullivan R.R. and Hertel K.L. The flow through porous media. *Journal of Applied Physics*, 11:761, 1940.

[108] Taylor J.S. and Jacobs E.P. Reverse osmosis and nanofiltration. In *Water Treatment, Membrane Processes*, chapter 9. McGraw Hill, 1996.

[109] Tessendorf S., Gani R. and Michelsen M.L. Aspects of modelling and operation of membrane-based separation processes for gaseous mixtures. *Computers and Chemical Engineering*, 20. suppl:S653–S658, 1996.

[110] Tessendorf S., Gani R. and Michelsen M.L. Modeling, simulation and optimization of membrane-based gas separation systems. *Chemical Engineering Science*, 54:943 955, 1999.

[111] Tsuyumoto M., Teramoto A. and Meares P. Dehydration of ethanol on a pilot plant scale, using a new type of hollow-fibre membrane. *Journal of Membrane Science*, 133:83–94, 1997.

[112] Tyagi R.K., Fouda A.E. and Matsuura T. Concentration polarisation occurring inside the membrane during steady state pervaporation. *Chemical Engineering Communications*, 134:157–170, 1995.

[113] Van Guawbergen D. and Baeyens J. Macroscopic fluid flow conditions in spiral-wound membrane elements. *Desalination*, 110:287–299, 1997.

[114] Van Guawbergen D. and Baeyens J. Assessment of the design parameters for wastewater treatment by reverse osmosis. *Water Science and Technology*, 40:269–276, 1999.

[115] Van Guawbergen D. and Baeyens J. Macroscopic fluid flow conditions in spiral-wound membrane elements: packed bed approach. *Water Science and Technology*, 41:85–91, 2000.

[116] Voros N.G., Maroulis Z.B. and Marinos-Kouris D. Short-cut structural design of reverse osmosis desalination plants. *Journal of Membrane Science*, 127:47–68, 1997.

[117] Wesselingh J.A. and Krishna R. *Mass Transfer*. Ellis Horwood, New York, 1990.

[118] Winograd Y., Solan A. and Toren M. Mass transfer resistance in narrow channels in the presence of turbulence promoters. *Desalination*, 13:171–186, 1973.

[119] de Witte J. New development in nanofiltration and reverse osmosis membrane manufacturing. *Desalination*, 113:153–156, 1997.

[120] Yuan S.W. and Finkelstein A.B. Laminar pipe flow with injection and suction through a porous wall. *Transactions of the American Society of Mechanical Engineers*, 78:719–724, 1956.

[121] Zhu M., El-Halwagi M.M. and Al-Ahmed M. Optimal design and scheduling of flexible reverse osmosis networks. *Journal of Membrane Science*, 129:161–174, 1997.

[122] Zolandz R.R and Fleming G.K. Gas permeation. In Ho W.S.W. and Sirkar K.K., editors, *Membrane Handbook*, chapter 2. Van Nostrand Reinhold, 1992.

[123] Zydney A.L. Stagnant film model for concentration polarization in membrane systems. *Journal of Membrane Science*, 130:275–281, 1997.

NOMENCLATURE

A	Membrane area	m^2
a	Unit outlet number	-
a_i	Activity of component i	-
B^o	Dusty gas model coefficient (Eq. 2.16)	m^2
b	Unit inlet number	-
b'	Constant	$(m/s)^{0.5}$
C^{Total}	Total production cost	$\$/yr$
C^{fixed}	Fixed unit cost	\$/yr
C^{op}	Operating cost	\$/yr
C^{elec}	Electricity cost	\$/J
C^{steam}	Steam cost	\$/J
C_p	Heat capacity	$J/molK$
c	Molar concentration	mol/m^3
c^m	Molar concentration in membrane	mol/m^3
D	Dispersion coefficient	m^2/s
D^m	Molecular diffusion coefficient	m^2/s
D^D	Dusty gas model diffusion coefficient (Eq. 2.16)	m^2/s
D^F	Friction model diffusion coefficient (Eq. 2.17)	m^2/s
D^S	Normalised state decision variable (Eq. 4.5)	-
D^T	Normalised temperature	-
D^P	Normalised pressure	-
$D^{P\prime}$	Pressure selector variable	-
E	Mass balance error (Eq. C.1)	-
e	Energy flux	W/m^2
F	Molar flux	mol/m^2s
f_v	Frictional force	Pa/m
g	Non-ideality constant in Eq. 2.5	Pa/m
H	Enthalpy	J/mol
H^J	Enthalpy of penetrant	J/mol
H^V	Heat of evaporation	J/mol

h	Half channel height (spiral-wound module)	m
J	Molar flux of through membrane	mol/m^2s
K_{cw}	Sorption coefficient	mol/m^3
K_F	Frictional parameter	m^2
K_M	Mass transfer coefficient parameter	m
k	Mass transfer coefficient	m/s
k'	Representative mass transfer coefficient (Eq. D.8)	m/s
k_{ov}	Overall mass transfer coefficient (Eq. 3.6)	m/s
k^c	Thermal conductivity	W/mK
k_{dw}	Numerical constant (Eq. 6.2)	m^3/mol
L	Module length	m
l	Characteristic length	m
M_i	Molecular mass of component i	kg/mol
m	Molar or mass feed rate	$mol/s, kg/s, kg/hr$
m^{out}	Molar flow at outlet	mol/s
m_a^{out}	Total mass flowrate of material leaving unit a	kg/s
$m_{a,b}^{in}$	Mass of material entering unit b from unit a	kg/s
N^c	Number of components	-
N^f	Number of feed points	-
N^i	Number of inlets	-
N^m	Number of modules	-
N^p	Number of product points	-
N^{pre}	Number of modules per pressure vessel	-
N^s	Number of separation stages	-
n_d	Number of discretisation points	-
n_e	Number of discretisation elements	-
n^{max}	Maximum number of membrane modules per separation stage	-
n^{min}	Minimum number of membrane modules per separation stage	-
o	Order of approximation	-
P	Pressure	Pa
ΔP^S	Estimated pressure drop in sealed length	Pa
p	Distance along spiral (increasing in direction of permeate flow)	m
Q_i	Permeability	various

q	Heat flux through the membrane	W/m^2
q'	Heater duty	W
R	Fibre inner radius	m
R'	Ideal gas constant	$J/molK$
R^f	Feed pipe radius	m
R^o	Fibre outer radius	m
R^p	Pore radius	m
R^s	Fibre bundle radius	m
r	Radial distance from centre (fibre)	m
r^j	Salt rejection of membrane	–
S	Fluid state (temperature or pressure)	Kor Pa
s	Radial distance from centre (module shell)	m
T	Temperature	K
t	Time	s
U	Internal energy	J/mol
V	Volume	m^3/mol
v	Velocity	m/s
W	Membrane width	m
W^f	Feed channel width	m
W^G	Extra width of feed channel = $W^f - W$	m
w	Work	W
x_i	Mole fraction of component i	-
y	Binary variable	–
y^h	Heater binary variable	–
y^p	Compressor binary variable	–
z	Axial distance along module (increasing in main direction of flow)	m
z^m	Distance through membrane	m

Greek symbols

α	Separation factor	–
$\alpha*$	Ideal separation factor	–
α^K	Separation factor for Knudsen diffusion	–
α_n	Constant	–
α_i^D	Selectivity coefficient used in Eq. 2.16	–
β	Geometric parameter equal to the ratio of membrane surface area to volume	m^{-1}
β_n	Constant	–

γ	Activity coefficients	-
γ'	Geometric parameter, (Eq. D.6)	-
δ^m	Membrane thickness	m
δ	Boundary layer thickness	m
η	Efficiency	-
κ	Permeability constant (Eq. 2.15)	m^3/mol
λ	Mean free molecular path	m
μ	Viscosity	$Pa \cdot s$
ν	Volumetric flowrate	m^3/s
Π	Osmotic pressure	Pa
ρ	Molar density	mol/m^3
ρ^m	Mass density	kg/m^3
σ	Coupling parameter in Kedem-Katchalsky model	-
$\sigma_{a,b}$	Stream split fraction from unit a outlet to unit b inlet	-
ϕ	Volume fraction	J/mol
ψ	Chemical potential	J/mol
Ω	Reciprocal of permeability (resistance)	various
ω	Weight fraction	-
ω_p	Weight fraction of key component in permeate	-
ω_r	Weight fraction of key component in retentate	-
∇	Gradient operator (across membrane)	m^{-1}
$\nabla_{T,P}$	Gradient operator (across membrane), constant temperature and pressure	m^{-1}

Subscripts

0	Standard conditions
1	Feed side
2	Permeate side
b	Bulk
E	Ethanol
f	Feed
i	Component i
j	Component j
L	Liquid
lm	Log mean
m	at the membrane interface
n	Any number

o	Outlet
p	Permeate product
r	Retentate product
S	Stage
s	Salt
T	Isothermal
V	Vapour
v	Volumetric basis
W	Water
Σ	Total

Superscripts

*	Ideal value
0	Standard conditions
in	Value at system or unit inlet
liq	Pure liquid value
max	Maximum value
min	Minimum value
out	Value at system or unit outlet
p	Spiral component
r	Radial (fibre) component
ref	Reference value
s	Radial (shell) component
sat	Saturated value
z	Axial component

Appendix A

MATHEMATICAL MODELS

A set of mathematical models that describe flow through hollow-fibre and spiral-wound membrane modules were introduced in Chapter 3. This section gives a more detailed description of these models. Ancillary equipment models are also described in this appendix.

A.1 Introduction

In Chapter 3, a modelling approach for hollow-fibre and spiral-wound modules was presented. The behaviour of a membrane module is described using three sub-models; two which describe the flow on either side of the membrane and a third model which characterises the separative properties of the membrane and any porous support material. The model equations are now presented.

The two flow sub-models chosen to describe flow through a given membrane module are completely independent except for the coupling terms describing the molar flux (J_i) and energy flux (q) through the membrane. These are given by the membrane characterisation model. For each flow model, it is also necessary to specify the feed rate (m_i), the feed temperature (T_f) and the outlet pressure (P_o).

First the models developed for hollow-fibre modules are presented (Section A.2). Next, spiral-wound modules are considered (Section A.3). In the final section (A.4), ancillary equipment models used for the optimisation case studies (Chapter 5 and 6) are presented.

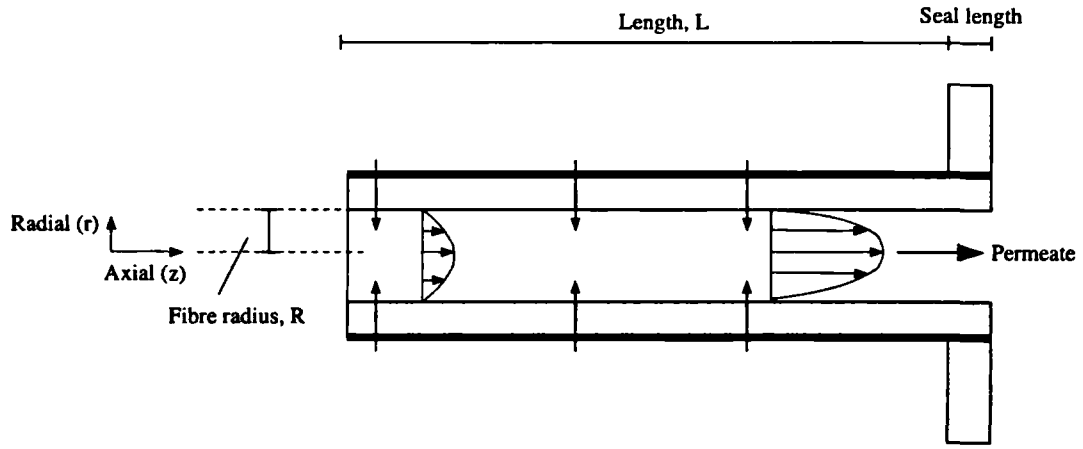

Figure A.1 *Illustration of a single hollow-fibre with material injection at the fibre walls*

A.2 Hollow-fibre module

The mathematical models used to describe hollow-fibre modules are given in Sections A.2.1 and A.2.2. The main features and assumptions of these models were summarised in Section 3.2.1.

A.2.1 Fibre flow sub-model

This model describes liquid or gas flow through a hollow-fibre at a radial position s in the module shell. A two-dimensional model and a simpler one-dimensional version have been developed. These are both now considered. A fibre with material injection at the walls is illustrated in Figure A.1.

Two-dimensional model

This model is developed from a two-dimensional mass balance and one dimensional momentum and energy balances $\forall z \in (0, L), \forall r \in (0, R)$

Axial and radial molar balance on component i

$$\frac{\partial c_i}{\partial t} = -\frac{\partial F_i^z}{\partial z} - \left(\frac{1}{r}\right)\frac{\partial \left(rF_i^r\right)}{\partial r} \tag{A.1}$$

Axial momentum balance

$$\frac{\partial \left(\rho^m v^z\right)}{\partial t} = -\frac{\partial P}{\partial z} - \frac{\partial \left(\rho^m v^{z2}\right)}{\partial z} - \left(\frac{1}{r}\right)\frac{\partial \left(r\rho^m v^r v^z\right)}{\partial r} + \left(\frac{\mu}{r}\right)\frac{\partial}{\partial r}\left(r\frac{\partial v^z}{\partial r}\right) + \mu\frac{\partial^2 v^r}{\partial z^2} \tag{A.2}$$

Axial energy balance

$$\frac{\partial(\rho U)}{\partial t} = -\frac{\partial e^z}{\partial z} + \beta q \tag{A.3}$$

Definitions

The axial (F^z) and radial (F^r) molar fluxes are defined

$$F_i^z = c_i v^z - D_i^m \frac{\partial c_i}{\partial z} \tag{A.4}$$

$$F_i^r = c_i v^r - D_i^m \frac{\partial c_i}{\partial r} \tag{A.5}$$

and the density, ρ, is calculated

$$\rho = \sum_{i=1}^{N^c} c_i \tag{A.6}$$

e^z is the energy flux which is given by

$$e^z = \rho \bar{v}^z H - k^c \frac{\partial T}{\partial z} \tag{A.7}$$

Axial boundary conditions

$$v^z|_{z=0} = 2\bar{v}^z \left(1 - \left(\frac{r}{R}\right)^2\right) \tag{A.8}$$

$$v^r|_{z=0,z=L} = 0 \tag{A.9}$$

$$\left.\frac{\partial P}{\partial z}\right|_{z=0} = 0 \tag{A.10}$$

$$\left.\frac{\partial v^z c_i}{\partial z}\right|_{z=L} = 0 \tag{A.11}$$

$$\left.\frac{\partial T}{\partial z}\right|_{z=L} = 0 \tag{A.12}$$

Radial boundary conditions

At the centre of the fibre (radial symmetry)

$$\left.\frac{\partial(v^z c_i)}{\partial r}\right|_{r=0} = 0 \tag{A.13}$$

$$v_r|_{r=0} = 0 \tag{A.14}$$

At the fibre wall (no slip)

$$F_i^r|_{r=R} = -J_i \tag{A.15}$$

$$v^z|_{r=R} = 0 \tag{A.16}$$

$$\left.\frac{\partial v^r}{\partial r}\right|_{r=R} = 0 \tag{A.17}$$

Component concentration at membrane surface

$$c_{i,m} = c_i|_{r=R} \tag{A.18}$$

Degrees of freedom

$$m_i = \pi R^2 \left(c_i \bar{v^z}\right)|_{z=0} \tag{A.19}$$

$$T_f = T|_{z=0} \tag{A.20}$$

$$P_o = P|_{z=L} - \Delta P^s \tag{A.21}$$

One-dimensional model

The model is identical to the 2-D model except that radial variations in concentration and velocity are neglected (i.e. plug flow is assumed). Consequently, this model is developed from one-dimensional mass, momentum and energy balances $\forall z \in (0, L)$.

Axial molar balance on component i

$$\frac{\partial c_i}{\partial t} = -\frac{\partial F_i^z}{\partial z} + \beta J_i \tag{A.22}$$

Axial momentum balance

$$\frac{\partial \left(\rho^m v^z\right)}{\partial t} = -\frac{\partial P}{\partial z} - \frac{\partial \rho^m v^{z2}}{\partial z} - f_v \tag{A.23}$$

Axial energy balance

$$\frac{\partial \left(\rho U\right)}{\partial t} = -\frac{\partial e^z}{\partial z} + \beta q \tag{A.24}$$

Definitions

The axial, F^z, molar flux is defined

$$F_i^z = c_i v^z - D_i^m \frac{\partial c_i}{\partial z} \tag{A.25}$$

and the density, ρ, is calculated

$$\rho = \sum_{i=1}^{N^c} c_i \tag{A.26}$$

f_v represents the frictional losses at the pipe wall. From the Hagen-Poiseuille (Bird *et al.*, 1960) equation for laminar flow we get

$$f_v = 8\mu v^z / R^2 \tag{A.27}$$

e^z is the energy flux which is given by

$$e^z = \rho v^z H - k^c \frac{\partial T}{\partial z} \tag{A.28}$$

Boundary conditions

$$\left.\frac{\partial v^z c_i}{\partial z}\right|_{z=L} = 0 \tag{A.29}$$

$$\left.\frac{\partial P}{\partial z}\right|_{z=0} = 0 \tag{A.30}$$

$$\left.\frac{\partial T}{\partial z}\right|_{z=L} = 0 \tag{A.31}$$

Component concentration at membrane surface (plug flow)

$$c_{i,m} = c_i \tag{A.32}$$

Degrees of freedom

$$m_i = \pi R^2 \left(c_i v^z\right)|_{z=0} \tag{A.33}$$

$$T_f = T|_{z=0} \tag{A.34}$$

$$P_o = P|_{z=L} - \Delta P^s \tag{A.35}$$

A.2.2 Shell flow sub-model

This model describes the flow pattern through the porous fibre bundle in the module shell. A two-dimensional model and a simpler one-dimensional model have been developed and are both now considered. The two-dimensional model is used to describe radial flow hollow-fibre modules (but could equally be used for parallel flow modules with some adjustment of the boundary conditions). A radial flow hollow-fibre module is illustrated in Figure A.2. The alternate one-dimensional model is also described, this should only be used for parallel flow modules for which radial variations can be neglected (see Section 3.2.1).

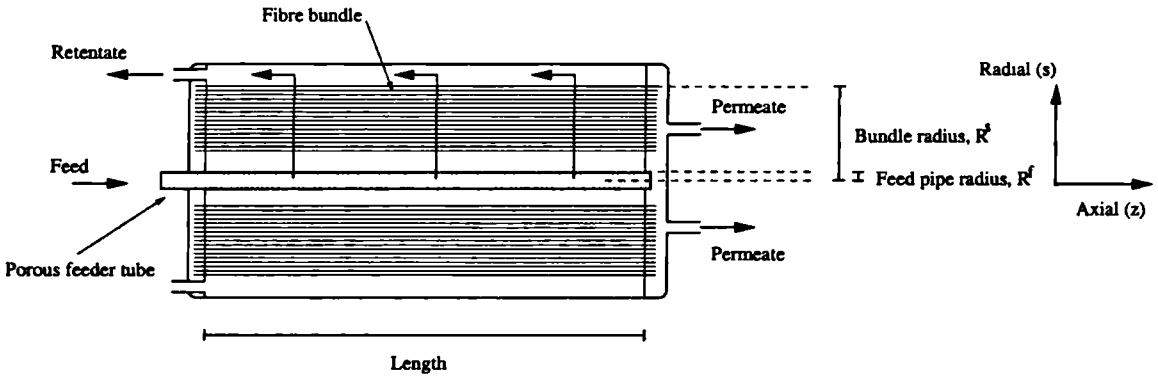

Figure A.2 *Illustration of a radial flow hollow-fibre module*

Two-dimensional model (radial flow module)

The fibre bundle is treated as a continuous radially symmetric porous medium and the model is developed from two-dimensional mass, momentum and energy balances $\forall z \in (0, L), \forall s \in (R^f, R^s)$.

Axial and radial molar balance on component i

$$\frac{\partial c_i}{\partial t} = -\frac{\partial F_i^z}{\partial z} - \left(\frac{1}{s}\right)\frac{\partial \left(sF_i^s\right)}{\partial s} + \beta J_i \tag{A.36}$$

Momentum balance (axial)

$$\frac{\partial \left(\rho^m v^z\right)}{\partial t} = -\frac{\partial \left(\rho^m v^{z2}\right)}{\partial z} - \left(\frac{1}{s}\right)\frac{\partial \left(s\rho^m v^z v^s\right)}{\partial s} - \frac{\partial P}{\partial z} - f_v^z \tag{A.37}$$

Momentum balance (radial)

$$\frac{\partial \left(\rho^m v^s\right)}{\partial t} = -\frac{\partial \left(\rho^m v^s v^z\right)}{\partial z} - \left(\frac{1}{s}\right)\frac{\partial \left(s\rho^m v^{s2}\right)}{\partial s} - \frac{\partial P}{\partial s} - f_v^s \tag{A.38}$$

Energy balance

$$\frac{\partial \left(\rho U\right)}{\partial t} = -\frac{\partial e^z}{\partial z} - \frac{1}{s}\frac{\partial s e^s}{\partial s} + \beta q \tag{A.39}$$

Definitions

The axial (F^z) and radial (F^s) molar fluxes are defined

$$F_i^z = c_i v^z - D_i \frac{\partial c_i}{\partial z} \tag{A.40}$$

$$F_i^s = c_i v^s - D_i \frac{\partial c_i}{\partial s} \tag{A.41}$$

and the density, ρ, is calculated

$$\rho = \sum_{i=1}^{N^c} c_i \tag{A.42}$$

f_v^z and f_v^s represent the frictional pressure losses due to the flow through the porous fibre bundle, these are calculated

$$f_v^z = \frac{\mu}{K_F^z} v^z \tag{A.43}$$

$$f_v^s = \frac{\mu}{K_F^s} v^s \tag{A.44}$$

e^z and e^s are given by

$$e^z = \rho v^z H - k^c \frac{\partial T}{\partial z} \tag{A.45}$$

$$e^s = \rho v^s H - k^c \frac{\partial T}{\partial s} \tag{A.46}$$

Axial boundary conditions

$$v^z|_{z=0,z=L} = 0 \tag{A.47}$$

$$\left.\frac{\partial v^s c_i}{\partial z}\right|_{z=0,z=L} = 0 \tag{A.48}$$

Radial boundary conditions

$$v^z|_{s=R^f,s=R^s} = 0 \tag{A.49}$$

$$\left.\frac{\partial P}{\partial s}\right|_{s=R^f} = 0 \tag{A.50}$$

$$\left.\frac{\partial v^s c_i}{\partial s}\right|_{s=R^s} = 0 \tag{A.51}$$

$$\left.\frac{\partial T}{\partial s}\right|_{s=R^s} = 0 \tag{A.52}$$

Component concentration at membrane surface (stagnant film model)

$$c_{i,m} = \frac{\rho J_i}{J_\Sigma} + \left(c_i - \frac{\rho J_i}{J_\Sigma}\right) exp\left(\frac{-J_\Sigma}{\rho k}\right) \tag{A.53}$$

Degrees of freedom

$$m_i = R^f L\,(c_i v^s)|_{s=R^f} \tag{A.54}$$

$$T_f = T|_{s=R^f} \tag{A.55}$$

$$P_o = P|_{s=R^s} \tag{A.56}$$

One-dimensional model (parallel flow module)

This model is very similar to the 1-D fibre flow model in that all radial variations are neglected (i.e. plug flow parallel to the hollow fibres is assumed). It is developed from one-dimensional mass, momentum and energy balances $\forall z \in (0, L)$.

Axial molar balance on component i

$$\frac{\partial c_i}{\partial t} = -\frac{\partial F_i^z}{\partial z} + \beta J_i \tag{A.57}$$

Axial momentum balance

$$\frac{\partial (\rho^m v^z)}{\partial t} = -\frac{\partial \rho^m v^{z2}}{\partial z} - \frac{\partial P}{\partial z} - f_v^z \tag{A.58}$$

Axial energy balance

$$\frac{\partial (\rho U)}{\partial t} = -\frac{\partial e^z}{\partial z} + \beta q \tag{A.59}$$

Definitions

The axial, F^z, molar flux is defined

$$F_i^z = c_i v^z - D_i \frac{\partial c_i}{\partial z} \tag{A.60}$$

and the density, ρ, is calculated

$$\rho = \sum_{i=1}^{N^c} c_i \tag{A.61}$$

The frictional pressure losses due to the flow through the porous fibre bundle are accounted for using the friction factor f_v^z which is calculated from

$$f_v^z = \frac{\mu}{K_F} v^z \tag{A.62}$$

e^z is the energy flux, which in this case is given by

$$e^z = \rho \bar{v}^z H - k^c \frac{\partial T}{\partial z} \tag{A.63}$$

Boundary conditions

$$\left.\frac{\partial v^z c_i}{\partial z}\right|_{z=L} = 0 \tag{A.64}$$

$$\left.\frac{\partial P}{\partial z}\right|_{z=0} = 0 \tag{A.65}$$

$$\left.\frac{\partial T}{\partial z}\right|_{z=L} = 0 \tag{A.66}$$

Component concentration at membrane surface (stagnant film model)

$$c_{i,m} = \frac{\rho J_i}{J_\Sigma} + \left(c_i - \frac{\rho J_i}{J_\Sigma}\right) exp\left(\frac{-J_\Sigma}{\rho k}\right) \tag{A.67}$$

Degrees of freedom

$$m_i = \pi \left(R^S\right)^2 (c_i v^z)|_{z=0} \tag{A.68}$$

$$T_f = T|_{z=0} \tag{A.69}$$

$$P_o = P|_{z=L} \tag{A.70}$$

A.2.3 Membrane characterisation sub-model

The complete model is formed by linking a fibre flow and shell flow sub-model. This is done using an appropriate local transport model (see Section 2.2). This describes the rate of transport of material (and energy) between the feed (1) and permeate (2) phases either side of the membrane. This will generally be of the form

$$J(s,z) = f\left(c_{1,i,m}(s,z), c_{2,i,m}(s,z), P_1(s,z), P_2(s,z), T_1(s,z), T_2(s,z)\right) \tag{A.71}$$

For non-isothermal processes, it is important that the net rate of energy flux, q, is determined. This is calculated

$$q = H^j J \tag{A.72}$$

A.3 Spiral-wound module

The mathematical models used to describe flow in the feed and permeate channels of a spiral-wound module are presented in this section. The features and assumptions of this model were summarised in Section 3.2.2. A spiral-wound module is illustrated in Figure A.3.

A.3.1 Feed channel flow sub-model

Once again, a two-dimensional model and a simpler one-dimensional model have been developed and these are now considered. Both models describe flow through a porous channel with a height of $2h$. The two membranes on either side of the channel are assumed to be identical (Assumption 5, Section 3.2.2).

Two-dimensional model

This model can describe flow in the feed and permeate channels (see Section A.3.2). It is developed from two-dimensional mass, momentum and energy balances over the axial and spiral domains $\forall z \in (0, L), \forall p \in (0, W^F)$

Molar balance on component i

$$\frac{\partial c_i}{\partial t} = -\frac{\partial F_i^z}{\partial z} - \frac{\partial F_i^p}{\partial p} + \frac{1}{h} J_i \tag{A.73}$$

Momentum balance (z-direction)

$$\frac{\partial \left(\rho^m v^z\right)}{\partial t} = -\frac{\partial \left(\rho^m v^{z2}\right)}{\partial z} - \frac{\partial \left(\rho^m v^z v^p\right)}{\partial p} - \frac{\partial P}{\partial z} - f_v^z \tag{A.74}$$

Momentum balance (p-direction)

$$\frac{\partial \left(\rho^m v^p\right)}{\partial t} = -\frac{\partial \left(\rho^m v^{p2}\right)}{\partial p} - \frac{\partial \left(\rho^m v^p v^z\right)}{\partial z} - \frac{\partial P}{\partial p} - f_v^p \tag{A.75}$$

Energy balance

$$\frac{\partial \left(\rho U\right)}{\partial t} = -\frac{\partial e^z}{\partial z} - \frac{\partial e^p}{\partial p} + \frac{1}{h} q \tag{A.76}$$

Definitions

The molar fluxes in the axial and spiral directions are defined

$$F_i^z = c_i v^z - D_i \frac{\partial c_i}{\partial z} \tag{A.77}$$

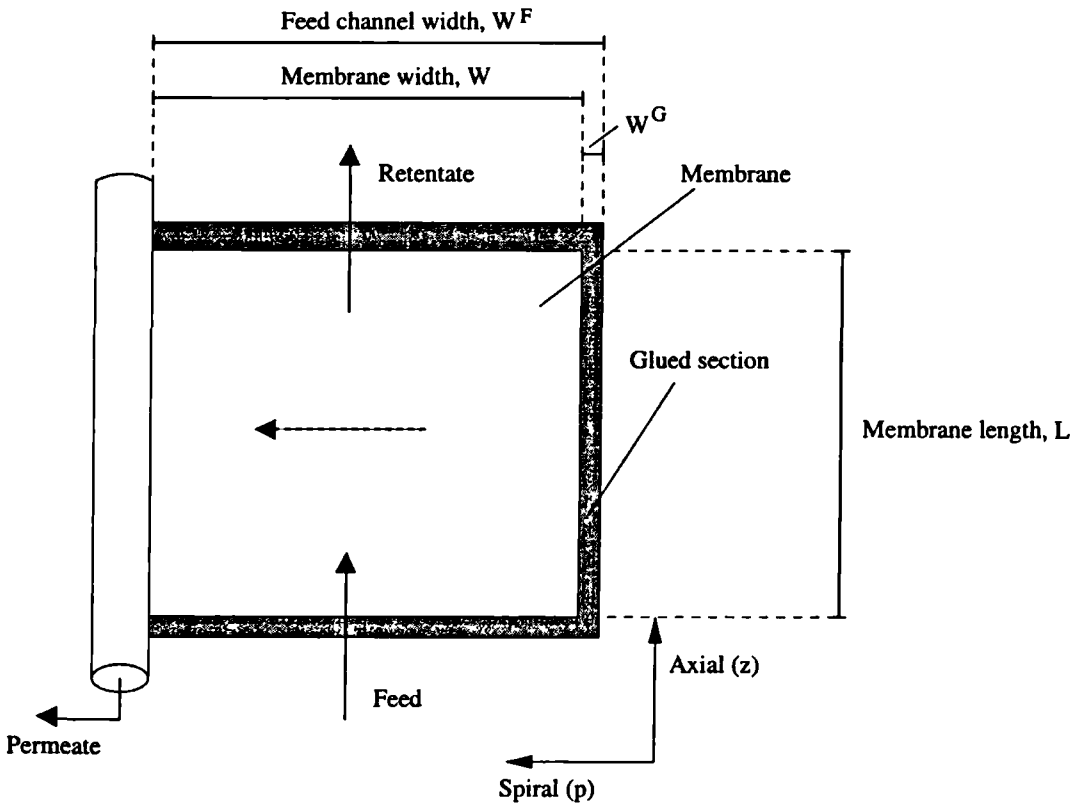

Figure A.3 *Illustration of a spiral-wound module*

$$F_i^p = c_i v^p - D_i \frac{\partial c_i}{\partial p} \tag{A.78}$$

and the density, ρ, is calculated

$$\rho = \sum_{i=1}^{N^c} c_i \tag{A.79}$$

f_v^z and f_v^p represent the frictional losses in the flow through the porous spacer medium and are calculated

$$f_v^z = \frac{\mu}{K_F} v^z \tag{A.80}$$

$$f_v^p = \frac{\mu}{K_F} v^p \tag{A.81}$$

e^z and e^p are the energy fluxes in the z and p directions and are given by

$$e^z = \rho v^z h - k^c \frac{\partial T}{\partial z} \tag{A.82}$$

$$e^p = \rho v^p h - k^c \frac{\partial T}{\partial p} \tag{A.83}$$

Axial boundary conditions

$$v^p|_{z=0,z=L} = 0 \tag{A.84}$$

$$\left.\frac{\partial P}{\partial z}\right|_{z=0} = 0 \tag{A.85}$$

$$\left.\frac{\partial v^z c_i}{\partial z}\right|_{z=L} = 0 \tag{A.86}$$

$$\left.\frac{\partial T}{\partial z}\right|_{z=L} = 0 \tag{A.87}$$

Wall boundary conditions

$$v^p|_{p=0,p=W^F} = 0 \tag{A.88}$$

$$\left.\frac{\partial v^z c_i}{\partial p}\right|_{p=0,p=W^F} = 0 \tag{A.89}$$

Component concentration at membrane surface (stagnant film model)

$$c_{i,m} = \frac{\rho J_i}{J_\Sigma} + \left(c_i - \frac{\rho J_i}{J_\Sigma}\right) exp\left(\frac{-J_\Sigma}{\rho k}\right) \tag{A.90}$$

Degrees of freedom

$$m_i = 2hW^F \left(c_i v^z\right)|_{z=0} \tag{A.91}$$

$$T_f = T|_{z=0} \tag{A.92}$$

$$P_o = P|_{z=L} - \Delta P^s \tag{A.93}$$

One-dimensional model

This model only describes feed flow. It neglects variations in the spiral direction and so assumes perfect mixing in the permeate channel. The model is developed from one-dimensional mass, momentum and energy balances $\forall z \in (0, L)$.

Molar balance on component i

$$\frac{\partial c_i}{\partial t} = -\frac{\partial F_i^z}{\partial z} + \frac{1}{h} J_i \tag{A.94}$$

Momentum balance

$$\frac{\partial \left(\rho^m v^z\right)}{\partial t} = -\frac{\partial \left(\rho^m v^{z2}\right)}{\partial z} - \frac{\partial P}{\partial z} - f_v^z \tag{A.95}$$

Energy balance

$$\frac{\partial \left(\rho U\right)}{\partial t} = -\frac{\partial e^z}{\partial z} + \frac{1}{h} q \qquad \forall z \in (0, L) \tag{A.96}$$

Definitions

The molar flux in the axial direction is given by

$$F_i^z = c_i v^z - D_i \frac{\partial c_i}{\partial z} \tag{A.97}$$

and the density, ρ, is calculated

$$\rho = \sum_{i=1}^{N^c} c_i \tag{A.98}$$

f_v^z represents the frictional losses

$$f_v^z = \frac{\mu}{K_F} v^z \tag{A.99}$$

The energy flux, e^z, is written

$$e^z = \rho v^z h - k^c \frac{\partial T}{\partial z} \tag{A.100}$$

Boundary conditions (z-direction)

$$\left.\frac{\partial v^z c_i}{\partial z}\right|_{z=L} = 0 \tag{A.101}$$

$$\left.\frac{\partial P}{\partial z}\right|_{z=0} = 0 \tag{A.102}$$

$$\left.\frac{\partial T}{\partial z}\right|_{z=L} = 0 \tag{A.103}$$

Component concentration at membrane surface (stagnant film model)

$$c_{i,m} = \frac{\rho J_i}{J_\Sigma} + \left(c_i - \frac{\rho J_i}{J_\Sigma}\right) exp\left(\frac{-J_\Sigma}{\rho k}\right) \tag{A.104}$$

Degrees of freedom

$$m_i = 2hW^F \left(c_i v^z\right)\big|_{z=0} \tag{A.105}$$

$$T_f = T|_{z=0} \tag{A.106}$$

$$P_o = P|_{z=L} - \Delta P^s \tag{A.107}$$

A.3.2 Permeate channel flow sub-model

Mathematical models that describe flow through the permeate channels of spiral-wound modules are now considered.

Two-dimensional model

This model is identical to the feed channel model except that the domains are switched over (i.e. where z appeared in the previous model it is replaced with p, and vice-versa). The mass balance equations hold $\forall z \in (0, L), \forall p \in (W^G, W^F)$.

One-dimensional model

This model assumed perfect mixing in the permeate channel (see Section A.3.1). Hence, there is just an overall molar balance which is written simply

$$x_i m^{out} = W \int_0^L J_i dz \tag{A.108}$$

and hence

$$c_i = c_{i,m} = x_i \rho \tag{A.109}$$

and the pressure in the permeate channel is the outlet pressure

$$P_o = P \tag{A.110}$$

A.3.3 Membrane characterisation sub-model

The model is formed by linking the two instances of the channel flow model. This is again done using an appropriate local transport model (see Section 2.2) which describes the rate of transport of material (and energy) between the feed (1) and permeate (2) phases on either side of the membrane. For a spiral-wound module, the local transport model will generally be of the form

$$J(z,p) = f\left(c_{1,i,m}(z,p), c_{2,i,m}(z,p), P_1(z,p), P_2(z,p), T_1(z,p), T_2(z,p)\right) \tag{A.111}$$

The rate of energy flux, q, is given by

$$q = H^J J \tag{A.112}$$

A.4 Ancillary equipment models

This section presents the additional models used in the optimal design case studies (Chapters 5 and 6). The full separation process is modelled by connecting, in the correct configuration, several unit models by information streams. These correspond to actual stream flows on the real plant. The main unit model is that of the membrane module (Sections A.2. and A.3). However, additional unit models are also required to describe the ancillary equipment operation. Models for pumps, energy recovery devices, heaters and compressors are now presented. Essentially, these models determine the energy and utility requirements of the membrane system.

Liquid Pump

Here $P^{out} > P^{in}$ and the power requirement is written

$$-w = \frac{\nu}{\eta}\left(P^{out} - P^{in}\right) \tag{A.113}$$

the operating cost is

$$C^{op} = -wC^{elec} \tag{A.114}$$

Energy recovery device (e.g. reverse running centrifugal pump)

Here $P^{in} > P^{out}$ and the power required (generated) is written

$$w = \nu\eta\left(P^{in} - P^{out}\right) \tag{A.115}$$

and the operating cost (profit) is

$$C^{op} = -wC^{elec} \tag{A.116}$$

Heater

The heat duty is defined

$$q' = m\left(H^{in} - H^{out}\right) \tag{A.117}$$

and the operating cost is

$$C^{op} = q'C^{steam} \tag{A.118}$$

Compressor

The compressor work is calculated assuming isothermal compression

$$-w = \frac{\nu}{\eta} P^{in} ln\left(\frac{P^{out}}{P^{in}}\right) \tag{A.119}$$

and again the operating cost is

$$C^{op} = -wC^{elec} \tag{A.120}$$

Appendix B

MIXING AND DISPERSION WITHIN MEMBRANE MODULES

In Chapter 3 it was stated that the detailed model accounts for both viscous and dispersive flow mechanisms. The purpose of this appendix is to assess the importance of describing dispersion when modelling fluid flow in hollow-fibre and spiral-wound modules. The study is based on a simple reverse osmosis example.

B.1 Introduction

As a fluid flows through a membrane module, a concentration profile usually develops. However, due to the effect of slippage and turbulent eddies, a degree of back mixing may help promote a uniform concentration. The effect of this mixing on the macroscopic fluid flow conditions within membrane modules, has only been considered in a few papers (e.g. Van Gauwbergen and Baeyens, 1997, 1999 and 2000; Al-Mutaz *et al.* 1997). Whilst most membrane flow models neglect the effect of mixing, the detailed model is able to take this into account using the dispersion coefficient (D) - see Equations A.40, A.41, A.77, A.78.

The rate of mixing is often measured using the dimensionless Peclet number

$$Pe = \frac{vl}{D} \tag{B.1}$$

where v is the fluid velocity and l is the characteristic length.

Table B.1 *Mixing in membrane modules - standard test conditions*

Module	B10 module	FT30SW module
Feed flow	1134 l/hr	784 l/hr
Feed concentration (NaCl)	50000ppm	25000ppm
Feed temperature	28^oC	20^oC
Feed pressure	70 bar	50 bar

A large Peclet number indicates that little mixing will take place, whereas the system approaches perfect mixing at very low Peclet numbers. For low Reynolds numbers, such as those inside hollow-fibres, the dispersion coefficient (and thus the Peclet number) is controlled by the molecular diffusion rate and its effect is very low. As flow becomes more turbulent (at high Reynolds numbers) dispersion becomes a function of the flow (Cussler, 1997) and increases in importance.

We will now consider how the detailed model (Chapter 3) accounts for dispersion by using a **reverse osmosis** example.

B.2 Description of the system

Both hollow-fibre and spiral-wound reverse osmosis modules can be used for sea-water desalination purposes. In this study, the DuPont B10 radial flow hollow-fibre module and the FilmTec FT30SW spiral-wound module are considered. These will be used to investigate the effect of the dispersion coefficient on module performance for the standard test conditions given in Table B.1. Further information on these modules can be found by reference to Appendix D.

B.3 Mixing rates in hollow-fibre modules

Some authors (Soltanieh and Gill, 1982; Hawlader *et al.* 1994) have suggested that the rate of mixing in the shell side of radial flow hollow-fibre modules is sufficient to assume that the concentration is homogeneous (the complete mixing model - refer to Section 2.3). This assumption can be analysed using the two dimensional flow model.

The effect of different dispersion coefficient values on product purity is shown in Table B.2 and the effect on the radial concentration profile is illustrated by Figure B.1. The results

Table B.2 *Effect of the dispersion coefficient on the product concentration from a hollow-fibre module*

D	Pe_f	**Product concentration**
m^2/s	-	ppm
1×10^{-9}	1.64×10^{5}	110.3
1×10^{-7}	1.64×10^{3}	110.4
1×10^{-6}	1.64×10^{2}	111.4
1×10^{-5}	1.64×10^{1}	119.3
1×10^{-4}	1.64×10^{-1}	135.6
1×10^{-3}	1.64×10^{-2}	141.3

demonstrate that the dispersion coefficient has little effect on the product purity and the concentration profile at values less than $10^{-5}m^2/s$. It can be seen from Figure B.1 that in order to approximate complete mixing, the dispersion coefficient must be greater than $10^{-3}m^2/s$. However, in a radial flow hollow-fibre module the Reynolds numbers through the fibre bundle are low (≈ 0.1), and at this point dispersive effects are usually limited by the molecular diffusivity (Cussler, 1997). Typically molecular diffusivity (e.g. for NaCl) is of the order of $10^{-9}m^2/s$. Consequently, we can expect the mixing rate in hollow-fibre modules to be small, so therefore a complete mixing model is not recommended.

B.4 Mixing rates in spiral-wound modules

Van Gauwbergen and Baeyens (1997, 1999 and 2000) have investigated the fluid flow conditions within spiral-wound modules. Their results demonstrate that, to adequately describe flow through spiral-wound modules, dispersive effects should be considered. In their experiments the Peclet number ranged from approximately 0.025 to 0.055, and no obvious dependence on Reynolds number was observed.

The effect of the dispersion coefficient on product purity is calculated using the detailed model. The results are shown in Table B.3 and in Figure B.2. As the dispersion coefficient increases (and thus the Peclet number is reduced), the effect of mixing increases, approaching complete mixing at very low Peclet numbers (< 0.001).

The value of the dispersion coefficient is clearly important to the fluid flow conditions in spiral-wound modules. The difficulty in predicting an accurate value has been shown by Van Gauwbergen and Baeyens (1997, 1999 and 2000). Based on their work, a realistic

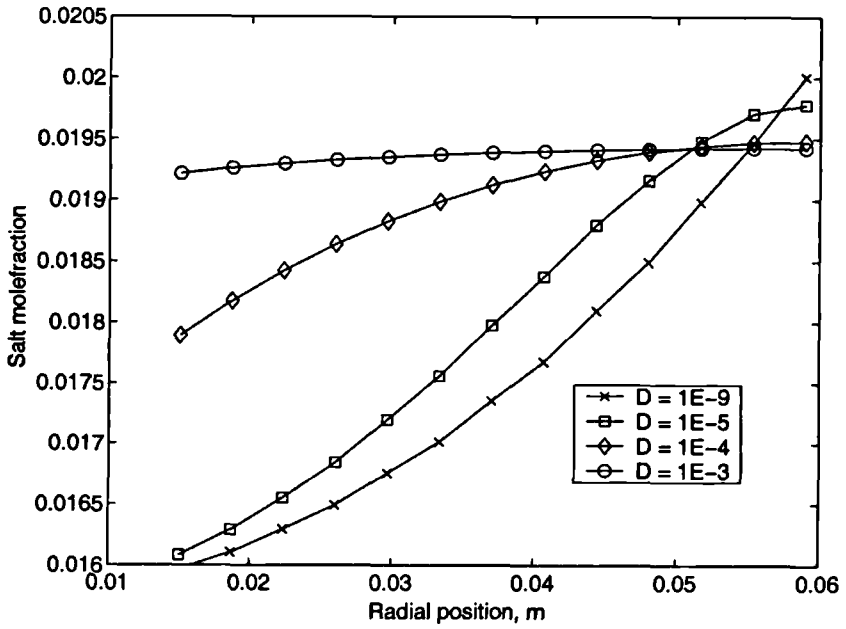

Figure B.1 *The effect of the dispersion coefficient on the radial concentration profile in a hollow-fibre module*

Peclet number of 0.025 will be used to estimate the dispersion coefficient for this type of module (Eq. B.1).

B.5 Summary

The detailed model has been used to investigate the effect of dispersion within reverse osmosis membrane modules. In hollow-fibre modules the effect of mixing is seen to be negligible and the use of complete mixing models is not recommended. However, there is some effect of mixing within spiral-wound modules as Reynolds numbers are much higher. For a greater understanding of the effect of dispersion on the flow patterns within membrane modules, more experimental studies are required. In this appendix, the detailed model has been shown to be an excellent tool for analysing the results of such studies.

Based on these experiences, the dispersion coefficient in hollow-fibre modules (inside and outside the fibres) will be assumed to be equal to the molecular diffusivity. Whereas for spiral-wound modules, a constant Peclet number equal to 0.025 will be used to calculate the dispersion coefficient.

Table B.3 *Effect of the dispersion coefficient on the product concentration from a spiral-wound module*

D	Pe_f	**Product concentration**
m^2/s	-	ppm
1×10^{-9}	1.64×10^{5}	95.09
1×10^{-5}	1.64×10^{1}	95.09
1×10^{-3}	1.64×10^{-1}	95.09
1×10^{-2}	1.64×10^{-2}	95.54
1×10^{-1}	1.64×10^{-3}	99.06
1×10^{0}	1.64×10^{-4}	101.6

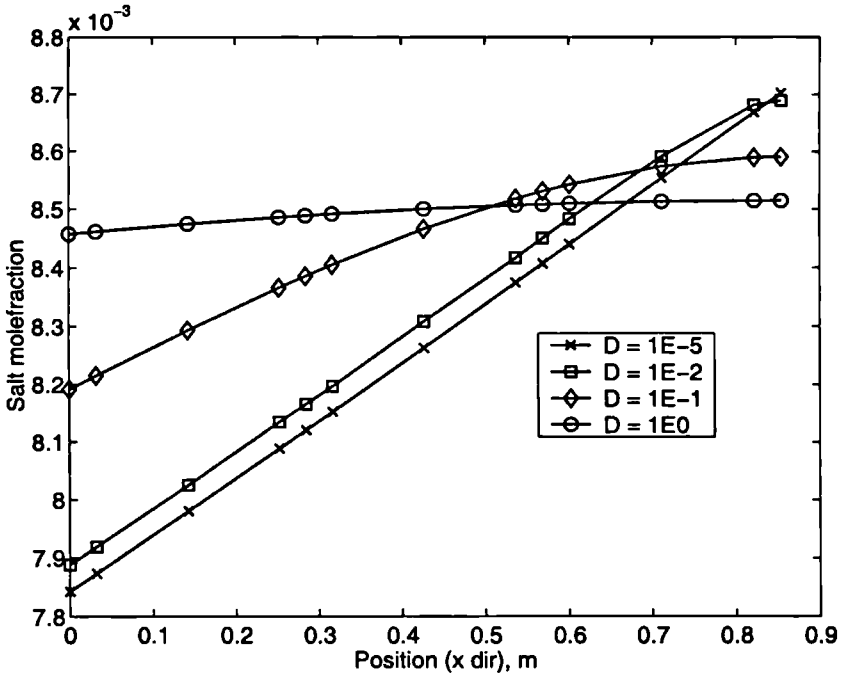

Figure B.2 *The effect of the dispersion coefficient on the concentration profile inside the feed channel of a spiral-wound module*

Appendix C

CHOICE OF SPATIAL DISCRETISATION TECHNIQUE

The purpose of this appendix is to further investigate the choice of spatial discretisation technique as indicated in Section 3.3. Using a simple reverse osmosis example, finite difference and orthogonal collocation on finite element methods are compared.

C.1 Case study

A reverse osmosis separation based on the (2-D) fibre flow model is used to illustrate the effect of the choice of discretisation strategy. In this study, sea-water (35,000ppm) is fed at a rate of 4.5×10^5 mol/s through a 305 μm i.d. hollow-fibre. Constant flux rates of $0.015 mol/ms$ and $1 \times 10^{-5} mol/ms$ for water and salt respectively are used in the calculations which are carried out using the g*PROMS* simulation software (Process Systems Enterprise Ltd, 1999).

The accuracy of the discretisation method will be evaluated by determining the error (E) in the steady-state mass balance. This is calculated from the following equation

$$E = \left(1 - \frac{J_\Sigma A}{m^{out} - m^{in}}\right) \times 100\% \tag{C.1}$$

For the type of system studied in this thesis, the model size is proportional to the number of discretisation points, n_d, which is calculated *for each domain* (axial or radial), thus

Finite difference

$$n_d = n_e + 1 \tag{C.2}$$

Orthogonal collocation

$$n_d = on_e + 1 \tag{C.3}$$

where o is the order of the approximation and n_e is the number of elements.

C.2 Comparing discretisation methods

In these comparisons, second order backward finite difference (BFD) and fourth order orthogonal collocation on finite elements (OCFE) methods were used to discretise the axial domain inside the fibres. For both methods the number of axial elements is adjusted in order to assess their effect on the accuracy of the mass balance. (A fourth order OCFE method over two elements is used for the radial domain.) A centred finite difference (CFD) approach was not considered in this case as it was unable to solve the model equations. This was anticipated as such methods are not suitable for solving strongly convective problems (Process Systems Enterprise Ltd, 1999).

Summarised simulation results are presented in Table C.1. This shows the effect of the discretisation strategy on the mass balance error for the axial domain. For the OCFE method, there is a negligible discrepancy in the mass balance even when only using a single finite element. By comparison, the use of a BFD approach results in a significant

Table C.1 *Comparison of discretisation strategies (axial domain)*

Discretisation method	Number of elements	Discretisation points	Error (%) E
OCFEM^4	2	9	5.24×10^{-5}
OCFEM^4	1	5	5.24×10^{-5}
BFDM^2	50	51	0.41
BFDM^2	30	31	0.68
BFDM^2	13	14	1.56
BFDM^2	6	7	3.32

4: fourth order; 2: second order

error. This is primarily a result of the one-sided approximation of the exit boundary condition (Eq. A.11). In effect, this means that the mass balance is neglected for the final discretisation element. Increasing the number of elements reduces the importance of this approximation and the size of the error (Table C.1). However, this also increases the model size and, consequently, the computational requirements. Thus, the use of one-sided finite difference methods cannot be recommended for this system.

C.3 Conclusions

It is seen that orthogonal collocation on finite elements (OCFE) is the most efficient discretisation approach for the example investigated in this appendix. This is primarily because of the one-sided approximation of the exit boundary condition (Eq A.11). This boundary condition is actually used in all the flow models developed in this research (Sections A.2.1, A.2.2, A.3.1, Appendix A). Consequently, it can be concluded that orthogonal collocation generally provides the best discretisation approach for this problem type.

In most cases, when using OCFE, a single finite element provides sufficient accuracy (as seen in Table C.1). For certain systems more elements will be required due to steep concentration gradients. However, it is relatively easy to determine the number of elements required for a certain case study by increasing the number of elements until no effect on model accuracy is detected.

Appendix D

SEA-WATER DESALINATION

Further information is presented for the reverse osmosis case study that is investigated in Chapter 5. Following a description of the membrane modules used in these studies, the parameter estimation that has been carried out is described. Then, two approximate design models that have been proposed for these modules are presented. Extensive simulation results for the detailed and approximate models are presented at the end of this appendix.

D.1 Membrane modules

Two different sea-water membranes are considered in these studies: the DuPont B10 (6440-T and 6840) radial flow hollow-fibre membrane and the FilmTec FT30SW spiral-wound membrane. For illustrations of these modules refer to Figures 3.3 and 3.5. Tables D.1 and D.2 show the properties of the two modules.

Table D.1 *B10 hollow-fibre module details (Hawlader et al., 1994; Evangelista, 1985)*

Image has been removed for copyright reasons

Table D.2 *FT30SW spiral-wound module details (Ben-Boudinar et al., 1992)*

The hollow-fibre module contains a substantially larger membrane area than the spiral-wound unit. However, spiral-wound membranes are intrinsically more water permeable than their hollow-fibre counterparts (Bhattacharyya *et al.*, 1992) and so, in many cases operate at comparable production rates.

D.2 Parameter estimation

In this section, parameter values for the B10 hollow-fibre and the FT30SW spiral-wound membrane are calculated.

D.2.1 Introduction

To simulate a reverse osmosis system using the detailed model, values of a number of parameters must be known. In addition to membrane characterisation parameters a number of values are required, such as diffusivities and mass transfer coefficients. Some of these values are available from the published literature (Table D.3). The remaining parameters must be estimated. This can be done by minimising the deviation of simulated results from sets of experimental data by adjusting the parameter values.

Table D.3 *Parameter values for the sea-water desalination case study*

Parameter	Value	Reference
Properties of salt water solutions		
Osmotic pressure, Pa	$\Pi = gR'Tc_s$	Eq 2.5, Chapter 2
Salt diffusivity in water, m^2/s	$D_s \times 10^9 = 0.72598$ $+0.023087\,(T - 273.15)$ $+0.00027657\,(T - 273.15)^2$	Ben-Boudinar *et al.* (1992)
B10 hollow-fibre module		
Mass transfer coefficient, m/s	$k = 0.048\frac{D_s}{2R'}Re^{0.6}Sc^{\frac{1}{3}}$	Sekino (1993)
K_F, m^2	36×10^{-13}	Estimated from experimental pressure drop data
FT30SW spiral-wound module		
Mass transfer coefficient, m/s	$k = K_M D_s^{\frac{2}{3}} \mu^{\frac{-1}{6}} v^{\frac{1}{2}}$	Dickson *et al.* (1992)
K_F, m^2	1.009×10^7 (feed channel)	Ben-Boudinar *et al.* (1992)
	7.41×10^4 (permeate channel)	

D.2.2 Membrane characterisation parameters

For this case study, the Kedem-Katchalsky model is used to characterise the membranes

$$J_W = Q_W c_{W1} \left[(P_1 - P_2) - \sigma\,(\Pi_1 - \Pi_2)\right] \tag{D.1}$$

$$J_s = (1 - \sigma)\, c_{s,LM} \frac{J_w}{c_{w1}} + Q_s\,(c_{s1} - c_{s2}) \tag{D.2}$$

The three coefficients in this model (Q_W, Q_s, and σ) can be correlated as a function of concentration, pressure, and temperature. Several authors have suggested a range of different correlations, and in this study, correlations based on the work of El-Halwagi *et al.* (1996) and Hawlader *et al.* (1994) will be used.

Water permeability, m/sPa:

$$Q_W = Q_{W0} e^{-m_1 \Delta P} e^{-\alpha_1 C_s} \beta_1^{(T - T_{ref})} \tag{D.3}$$

Salt permeability, m/s:

$$Q_s = Q_{s0} \left(\frac{C_s}{C_{ref}}\right)^{\alpha_2} \left(\frac{P_f}{Q_{ref}}\right)^{m_2} e^{\beta_2 (T - T_{ref})} \tag{D.4}$$

Flux coupling coefficient:

$$\sigma = 1 - \sigma_0 e^{\beta_3 (T - T_{ref})} \tag{D.5}$$

For both membranes, the correct values of the parameters must be estimated. This can be done automatically within the g*PROMS* simulation environment (Process Systems Enterprise Ltd, 1999) using the g*EST* tool, which minimises the deviation of the simulated results from the experimental data by adjusting the parameter values.

D.2.3 Hollow-fibre membrane

Unfortunately, there is a lack of detail in the results for the B10 module reported by Hawlader *et al.* (1994). Therefore, a simplified model will be used to characterise this membrane: the coupling term (σ) will be neglected, as will the effect of pressure and concentration on water flux. The temperature dependence of the fluxes has not been included, instead the coefficients suggested by Hawlader *et al.* (1994) will be used.

In total, then, there are just three unknown parameters (Q_{W0}, Q_{s0}, and α_2). The value of these parameters can be estimated from the experimental data for pure water and salt solution permeation that has been presented in the open literature (Hawlader *et al.*, 1994).

The pure water permeation data is used to determine the value of Q_{W0}. The values of the two remaining parameters are determined using the salt experimental data. The relatively strong effect of salt concentration on the salt flux parameter, Q_s is most likely an effect of neglecting the coupling term, σ. The coefficient values are given in Table D.4.

D.2.4 Spiral-wound membrane

As with the hollow-fibre modules, the values of the coefficients are determined by minimising the deviation of the simulation results from experimental data. In addition the mass transfer coefficient parameter, K_m, will be estimated. This gives a total 12 parameters, and as more extensive data is available (see Table D.6), these can all be estimated.

Using experimental data at 20 ^oC, all of the parameters, except the three temperature dependence parameters ($\beta_1, \beta_2, \beta_3$), were estimated. These are estimated using the 35 ^oC experimental data. All of the coefficient values are given in Table D.4.

Table D.4 *Reverse osmosis membrane characterisation parameter values for the sea water desalination case studies*

Parameter	B10 module	FT30SW module
Q_{W0}, $ms^{-1}Pa^{-1}$	1.44×10^{-13}	4.94×10^{-12}
m_1, Pa^{-1}	0	3.66×10^{-8}
α_1, m^3mol^{-1}	0	2.61×10^{-4}
β_1,	1.03	1.03
Q_{s0}, ms^{-1}	1.62×10^{-9}	1.95×10^{-8}
α_2,	0.627	0.234
β_2, $^oC^{-1}$	0.05	0.051
σ_0, ms^{-1}	0	$6.22\times^{-5}$
β_3, $^oC^{-1}$	0	-1.05×10^{-2}
K_M, m	-	11.1

D.2.5 Assessment

The values of the three flux coefficients (Q_W, Q_S and σ) only vary slightly with pressure and concentration over the operating range considered in these studies. This is indicated by the low values of α_1, α_2 and m_1 in both cases. This suggests that the Kedem-Katchalsky model provides a good characterisation for both membranes. This is also shown by the accuracy of the simulations results presented later in Tables D.5 and D.6. Nevertheless, it should be stressed that the parameter values reported here are confined to the modules and systems (salt-water) investigated in this study.

For both module types, the accuracy of the detailed model has been verified using experimental data different to that than used for parameter fitting. These results are presented in Section D.4.

D.3 Approximate module models

In Chapter 5, the results of the optimal design study using the detailed model (Chapter 3) are contrasted with designs developed using the approximate module models described by Evangelista (1985). These models have been used in a number of previous design studies (e.g. Evangelista, 1985 and 1986; El-Halwagi, 1992; Voros *et al.*, 1997). The equations for these models are now presented.

Hollow-fibre membranes

$$\bar{J}_w = Q_W \bar{c_{w1}} \left(\Delta P - \Pi_f\right) \gamma' \tag{D.6}$$

$$\bar{J}_s = Q_S \bar{c_{s1}} \tag{D.7}$$

γ' is a geometric parameter which is constant for a given hollow fibre module (0.88 for the B10 modules used in these studies).

Spiral-wound membranes

$$\bar{J}_w = Q_W \bar{c_{w1}} \left(\Delta P - \Pi_f \left(1 + \frac{\bar{J}_w}{\bar{c_{w1}} k'}\right)\right) \tag{D.8}$$

$$\bar{J}_s = Q_S \bar{c_{s1}} \left(1 + \frac{\bar{J}_w}{\bar{c_{w1}} k'}\right) \tag{D.9}$$

k' is a representative mass transfer coefficient for the spiral wound membrane.

D.4 Desalination simulation results

This section presents simulation results calculated using the detailed model for the hollow-fibre and spiral-wound modules discussed in this appendix. The calculations have been repeated using the approximate module models described in the previous section, and these results are also given. The detailed model and approximate model results have both been summarised earlier in this thesis (Section 5.4).

D.4.1 Detailed model results

Both reverse osmosis modules have been simulated using the detailed model. The results are now compared with experimental data (Hawlader *et al.*, 1994; Ben-Boudinar *et al.*, 1992) for each system. The simulated and experimental results for the B10 module are given in Table D.5; and in Table D.6 the results for the FT30SW module are presented.

Hollow-fibre module

Hawlader *et al.* (1994) presented rather limited experimental data for a B10 membrane, reporting the product recovery and salt rejection (r^j) for a range of operating conditions.

The salt rejection can be calculated from the ratio of permeate to feed concentration using the following equation

$$r^j = 1 - \frac{c_p}{c_f} \tag{D.10}$$

From this equation it can be seen that any error in the calculated salt rejection will give a significantly greater error in the permeate concentration. Furthermore, the experimental data reported by Hawlader *et al.* (1994) is only accurate to within ±0.2% (as the results were presented graphically). For typical conditions this translates to an uncertainty in the experimental permeate concentration of about 10%.

The calculated product recovery for the B10 module shows good agreement with the measured value (typically 4%). The salt rejection also shows good agreement, with errors ranging between 0 and 0.3% for the B10 module. These errors are similar to the uncertainty in the experimental data.

Spiral-wound module

The use of the detailed (2-D) model is assessed by a comparison with the extensive experimental data presented by Ben-Boudinar *et al.* (1992). They report experimentally measured product recovery and permeate concentration data for the FT30SW module over a wide range of operating conditions. The calculated recovery again shows excellent agreement with the measured value, typically 3%, though the error in the predicted permeate salt concentration is larger, typically 5% (max 14%). However, both offer a significant improvement over the work of Ben-Boudinar *et al.* (1992) whose simulation results show errors up to 26%.

D.4.2 Approximate model results

The performance of both modules was also calculated for the same operating conditions using the approximate module models (Equations D.6 - D.9). Table D.7 shows results for the B10 module, and Table D.8 the results for the FT30SW module.

In both cases, the approximate model predictions compare badly with those for the detailed model. The approximate model results deviate from those for the detailed model by up to 10% for the hollow-fibre module, and for the spiral-wound module by up to 20%. Similar errors are seen when they are compared with the experimental data (see Table 5.6).

Image has been removed for copyright reasons

Table D.5 *B10 hollow-fibre membrane module: comparing simulation results with experimental data (Hawlader et al., 1994)*

Table D.6 *FT30SW spiral-wound module: comparing simulation results with experimental data (Ben-Boudinar et al., 1992)*

Table D.6 *(continued)*

Feed				Product recovery			Salt concentration		
Flowrate *l/hr*	Concentration *ppm*	Temperature *°C*	Pressure *bar*	Experimental	Calculated	Error	Experimental *ppm*	Calculated *ppm*	Error
Simulation results									
795	25	25	50	9.2%	8.9%	3.0%	98	108	-10.4%
804	25	25	55	10.2%	10.0%	2.3%	95	99	-3.7%
813	25	25	60	11.2%	11.0%	1.8%	89	91	-2.6%
832	25	25	70	13.3%	12.8%	3.7%	82	81	1.1%
848	25	25	80	14.8%	14.4%	2.8%	72	74	-3.5%
807	25	30	50	10.5%	10.0%	4.4%	118	124	-5.1%
816	25	30	55	11.6%	11.3%	2.7%	108	113	-4.9%
828	25	30	60	12.9%	12.4%	3.9%	100	105	-5.1%
770	35	25	50	6.3%	6.3%	-1.2%	248	221	11.0%
780	35	25	55	7.5%	7.4%	1.1%	207	193	7.0%
788	35	25	60	8.4%	8.4%	-0.3%	179	173	3.4%
804	35	25	70	10.2%	10.2%	0.1%	141	147	-4.5%
818	35	25	80	11.8%	11.8%	-0.4%	129	131	-1.9%
776	35	30	50	7.0%	7.2%	-3.2%	279	252	9.6%
788	35	30	55	8.5%	8.3%	1.3%	238	221	7.3%
796	35	30	60	9.3%	9.5%	-2.0%	220	199	9.7%
814	35	30	70	11.4%	11.5%	-1.2%	178	170	4.6%
831	35	30	80	13.1%	13.3%	-1.0%	158	152	3.7%
760	40	25	50	5.0%	5.1%	-2.4%	332	313	5.6%
769	40	25	55	6.1%	6.2%	-0.9%	277	265	4.3%
778	40	25	60	7.2%	7.2%	0.3%	232	233	-0.4%
793	40	25	70	9.0%	9.0%	-0.5%	182	193	-5.9%
805	40	25	80	10.4%	10.6%	-2.4%	150	169	-12.6%
763	40	30	50	5.4%	5.8%	-7.6%	372	358	3.9%
775	40	30	55	6.9%	7.0%	-1.5%	330	303	8.2%
783	40	30	60	7.8%	8.1%	-4.1%	276	267	3.3%
802	40	30	70	10.0%	10.1%	-1.8%	220	222	-0.8%
820	40	30	80	12.0%	11.9%	1.1%	189	195	-3.1%

Table D.7 *B10 hollow-fibre membrane module: comparison of the approximate model results and the detailed model results*

Feed				Product recovery			Salt rejection		
Flowrate *l/hr*	Concentration *ppm*	Temperature *°C*	Pressure *bar*	Approximate	Detailed	Error	Approximate	Detailed	Error
1134	0	28	35.5	28.2%	28.5%	-1.3%			
1134	0	28	49.5	39.6%	40.2%	-1.4%			
1134	0	28	63.1	50.7%	51.5%	-1.5%			
1134	0	28	69.9	56.3%	57.2%	-1.5%			
1134	45000	28	56.16	26.0%	26.7%	-2.8%	98.7%	98.8%	-0.1%
1134	40000	28	56.16	15.3%	16.4%	-6.7%	97.0%	97.3%	-0.3%
1134	30000	28	56.16	32.2%	33.2%	-3.1%	98.7%	98.8%	-0.1%
1134	25000	28	56.16	35.6%	36.7%	-3.0%	98.9%	99.0%	-0.1%
1134	50000	28	63.05	27.2%	28.2%	-3.8%	98.2%	98.3%	-0.1%
1134	40000	28	63.05	13.5%	14.5%	-7.0%	96.9%	97.2%	-0.3%
1134	30000	28	63.05	16.5%	17.4%	-5.0%	97.6%	97.8%	-0.2%
1134	25000	28	63.05	22.7%	23.5%	-3.2%	98.4%	98.5%	-0.1%
1134	50000	28	69.95	21.2%	22.1%	-4.0%	98.0%	98.1%	-0.1%
1134	40000	28	69.95	27.5%	28.4%	-3.1%	98.6%	98.7%	-0.1%
1134	30000	28	69.95	30.8%	31.7%	-2.8%	98.9%	98.9%	-0.1%
1134	25000	28	69.95	19.8%	20.9%	-5.0%	97.6%	97.8%	-0.2%
1134	45000	28	76.84	25.8%	26.8%	-3.6%	98.3%	98.4%	-0.1%
1134	35000	28	76.84	33.4%	34.6%	-3.4%	98.6%	98.7%	-0.1%
1134	25000	28	76.84	40.2%	41.5%	-3.2%	99.0%	99.1%	-0.1%

Table D.8 *FT30SW spiral-wound module: comparison of the approximate model results and the detailed model results*

Feed				Product recovery			Salt concentration		
Flowrate *l/hr*	Concentration *ppm*	Temperature *°C*	Pressure *bar*	Approximate	Detailed	Error	Approximate *ppm*	Detailed *ppm*	Error
784	25000	20	50	8.0%	7.9%	1.4%	92	95	-3.1%
791	25000	20	55	9.1%	8.8%	2.4%	82	86	-4.3%
799	25000	20	60	10.1%	9.7%	3.2%	75	80	-5.2%
815	25000	20	70	11.9%	11.4%	4.4%	66	70	-6.6%
830	25000	20	80	13.5%	12.8%	5.2%	60	64	-7.6%
818	25000	35	50	10.6%	11.3%	-6.3%	155	143	8.7%
831	25000	35	55	12.0%	12.6%	-4.9%	141	131	7.5%
765	35000	20	50	5.5%	5.6%	-0.7%	193	194	-0.4%
774	35000	20	55	6.6%	6.5%	1.2%	165	169	-2.4%
781	35000	20	60	7.6%	7.4%	2.6%	145	151	-3.8%
795	35000	20	70	9.4%	9.0%	4.4%	121	128	-5.8%
805	35000	20	80	11.1%	10.5%	5.7%	106	114	-7.1%
781	35000	35	50	7.1%	8.1%	-12.0%	331	289	14.5%
792	35000	35	55	8.6%	9.5%	-9.1%	283	254	11.3%
804	35000	35	60	9.9%	10.7%	-7.0%	250	229	9.3%
756	40000	20	50	4.4%	4.5%	-2.2%	280	276	1.4%
764	40000	20	55	5.5%	5.5%	0.5%	229	233	-1.4%
785	40000	20	70	8.3%	8.0%	4.6%	159	168	-5.6%
799	40000	20	80	9.9%	9.4%	6.0%	136	147	-7.0%
770	40000	35	50	5.5%	6.6%	-16.0%	489	409	19.7%
780	40000	35	55	7.0%	7.9%	-11.8%	398	348	14.4%
791	40000	35	60	8.3%	9.2%	-8.9%	342	307	11.3%
811	40000	35	70	10.8%	11.4%	-5.3%	276	256	7.8%
832	40000	35	80	12.9%	13.3%	-3.1%	240	226	6.1%

Table D.8 *(continued)*

Feed				Product recovery			Salt concentration		
Flowrate	Concentration	Temperature	Pressure	Approximate	Detailed	Error	Approximate	Detailed	Error
l/hr	*ppm*	*°C*	*bar*				*ppm*	*ppm*	
795	25000	25	50	8.8%	8.9%	-1.0%	109	108	0.5%
804	25000	25	55	10.0%	10.0%	0.1%	98	99	-0.7%
813	25000	25	60	11.1%	11.0%	1.0%	90	91	-1.5%
832	25000	25	70	13.1%	12.8%	2.3%	79	81	-2.8%
848	25000	25	80	14.9%	14.4%	3.2%	72	74	-3.7%
807	25000	30	50	9.7%	10.0%	-3.6%	130	124	4.5%
816	25000	30	55	11.0%	11.3%	-2.3%	117	113	3.3%
828	25000	30	60	12.2%	12.4%	-1.3%	108	105	2.4%
770	35000	25	50	6.1%	6.3%	-4.4%	230	221	4.1%
780	35000	25	55	7.2%	7.4%	-2.1%	196	193	1.8%
788	35000	25	60	8.4%	8.4%	-0.5%	173	173	0.2%
804	35000	25	70	10.4%	10.2%	1.7%	145	147	-1.9%
818	35000	25	80	12.2%	11.8%	3.1%	127	131	-3.2%
776	35000	30	50	6.6%	7.2%	-8.1%	275	252	9.1%
788	35000	30	55	7.9%	8.3%	-5.6%	235	221	6.4%
796	35000	30	60	9.1%	9.5%	-3.7%	208	199	4.6%
814	35000	30	70	11.4%	11.5%	-1.2%	174	170	2.4%
831	35000	30	80	13.3%	13.3%	0.4%	154	152	1.1%
760	40000	25	50	4.8%	5.1%	-6.7%	335	313	6.9%
769	40000	25	55	6.0%	6.2%	-3.5%	274	265	3.4%
778	40000	25	60	7.1%	7.2%	-1.3%	236	233	1.2%
793	40000	25	70	9.1%	9.0%	1.4%	190	193	-1.4%
805	40000	25	80	11.0%	10.6%	3.2%	164	169	-3.0%
763	40000	30	50	5.2%	5.8%	-11.3%	404	358	12.9%
775	40000	30	55	6.5%	7.0%	-7.6%	329	303	8.7%
783	40000	30	60	7.7%	8.1%	-5.1%	283	267	6.0%
802	40000	30	70	10.0%	10.1%	-1.9%	229	222	3.0%
820	40000	30	80	11.9%	11.9%	0.1%	198	195	1.4%

Appendix E

ETHANOL DEHYDRATION

Further information on the pervaporation case study that was investigated in Chapter 6 is presented here. The hollow-fibre membrane modules used in the study are described and the membrane characterisation parameters are presented. In Chapter 6, the optimisation problem was solved using genetic algorithms, and for comparison, the optimisation is repeated here using a MINLP solution technique based on a branch and bound method.

E.1 Membrane modules

The modules are operated with the feed entering on the fibre-side. The permeate passes first through the membrane and then through a porous support into the shell-side as illustrated in Figure E.1. The permeate is drawn off under vacuum through three outlets on the shell-side. The fibre bundle is highly porous (75%) so that pressure build-up in

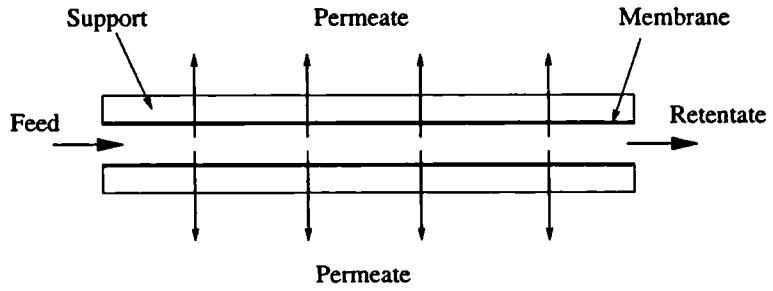

Figure E.1 *A single hollow-fibre*

Table E.1 *Module details for ethanol/water separation (Tsuyumoto et al., 1997)*

the permeate stream is minimised: hence, K_F is estimated from the superficial area for flow as $2.2 \times 10^{-4} m^2$. Module details are given in Table E.1.

E.2 Membrane characterisation

For this study, the local transport model developed by Tsuyumoto *et al.* (1997) is used to characterise the membrane. Hence, the flux of water (J_W) is calculated from

$$J_W = \frac{D_{W0}K_{cw}}{\delta^m}\left(\gamma_{1W}x_{1W} - \frac{P_2}{P_W^{sat}}x_{2W}\right) + \frac{D_{W0}K_{cw}^2 k_{dw}}{2\delta^m}\left((\gamma_{1W}x_{1W})^2 - \left(\frac{P_2}{P_W^{sat}}x_{2W}\right)^2\right) \tag{E.1}$$

and the ethanol flux (J_E) is given

$$J_E = Q_E\omega_E(P_1 - P_2) \tag{E.2}$$

The model parameters are also given by Tsuyumoto *et al.* (1997)

$$D_{wo}K_{cw} = 8.086 \times 10^6 exp^{\left(\frac{-11500}{T}\right)} mol/ms \tag{E.3}$$

$$\frac{D_{wo}K_{cw}^2 k_{dw}}{2} = 3.441 \times 10^{-3} exp^{\left(\frac{-3390}{T}\right)} mol/ms \tag{E.4}$$

$$Q_E = 1.72 \times 10^{-10} mol/m^2 sPa \tag{E.5}$$

E.3 Optimisation using a *MINLP* solution technique

In Chapter 6, the optimal design of the ethanol dehydration case study was determined using a solution technique based on genetic algorithms. To assess the performance of this solution method, the optimisation has also been carried out using a *MINLP* solution technique, results of which are presented in this section.

To minimise computational expense this work, was carried out using a simpler 1-D model. Using this model, the retentate product (ω_r) purity is calculated as 99.5 wt% ethanol for the Tsuyumoto *et al.* (1997) design. So, to enable a fair comparison, the product quality specification has been reduced from 99.7 to 99.5 wt% ethanol. Furthermore, the costs found in this study do not compare directly with those presented in Chapter 6 as the calculated volume of permeate product is lower in this case. In every other way, this problem is identical to that defined in Section 6.3.

E.3.1 Solution of *MINLP* optimisation problems

The superstructure optimisation problem requires the solution of equations containing both linear and non-linear functions as well as discrete and continuous variables - it is therefore a *MINLP* problem. Three *MINLP* solution methods were discussed in Section 4.2.1: enumeration, branch and bound, and generalised Benders Decomposition/Outer-Approximation methods.

In this case, an enumeration approach is not viable due to the large number of integer variables. Although generalised Benders Decomposition/Outer-Approximation methods are usually more efficient, the branch and bound method is selected due to its ease of application and higher transparency. In this work, the branch and bound is carried out manually and the g*OPT* solver which is incorporated in the g*PROMS* software (Process System Enterprise Ltd, 1999) is used to solve each *NLP* optimisation.

E.3.2 Binary variables

Binary variables (y) are introduced to the problem definition to identify whether a heat exchanger (y_h) and compressor (y_c) unit should exist on a given stream. A value of 0

means that the unit is deselected and a value of 1 means that it is present. This is necessary when using *NLP* solvers in order to prevent discontinuous functions. If the unit is not present, then the optimiser is forbidden from adjusting the state (S) of the stream by the following constraint

$$0 \leq \Delta S \leq y\Delta S^{max} \tag{E.6}$$

and the fixed unit cost (Eq. 4.1) is rewritten

$$C_{fixed} = yf_1(\Delta S) \tag{E.7}$$

To apply the branch and bound search method, it is necessary to relax the discrete variables to continuous variables. Heat exchanger and compressor units are selected/deselected using binary variables. When relaxed, the binary variable, y, can assume any value between 0 and 1. The number of modules connected in parallel within a stage is described by an integer variable, this is similarly relaxed and can therefore assume any value between 0 and n^{max}.

The process of relaxing the integer variables converts the *MINLP* optimisation problem into a *NLP* which can be solved using gradient based optimisation methods (g*OPT* is used in this case). This is now considered.

E.3.3 Relaxed solution

To solve the design problem outlined in Section 6.3, a process superstructure of eight stages is generated (see Section 6.2.1). The result of the superstructure optimisation for the fully relaxed problem (i.e. when all of the integer variables are relaxed) is shown in Table E.2, this gives the lower bound on the objective function (the minimum total cost). This *NLP* optimisation took just over 20 minutes of computational time. The upper bound on the objective function is obtained by rounding the integer variables to the nearest integer values, and carrying out a second optimisation in order to determine the best values for the remaining continuous variables (see Table E.2). The results show that the optimal solution must be between \$5377/yr and \$5400/yr.

Table E.2 *Lower and upper bounds on the optimal solution*

	Variable	Lower bound	Upper bound
Stage 1	Number of modules, N^m	1.018	*1*
	Heater binary variable, y^h	1	*1*
	Normalised heater temperature, D^T	1	1
	Compressor number, $D^{P\prime}$	1	1
Stage 2	Number of modules, N^m	1.226	*1*
	Heater binary variable, y^h	1	*1*
	Normalised heater temperature, D^T	1	1
	Compressor number, $D^{P\prime}$	1	1
Stage 3	Number of modules, N^m	1	*1*
	Heater binary variable, y^h	1	*1*
	Normalised heater temperature, D^T	1	1
	Compressor number, $D^{P\prime}$	1	1
Stage 4	Number of modules, N^m	0.753	*1*
	Heater binary variable, y^h	0	*0*
	Normalised heater temperature, D^T	0	0
	Compressor number, $D^{P\prime}$	2	2
Stage 5	Number of modules, N^m	0.7499	*1*
	Heater binary variable, y^h	0	*0*
	Normalised heater temperature, D^T	0	0
	Compressor number, $D^{P\prime}$	2	2
Stage 6	Number of modules, N^m	0.745	*1*
	Heater binary variable, y^h	0	*0*
	Normalised heater temperature, D^T	0	0
	Compressor number, $D^{P\prime}$	2	2
Stage 7	Number of modules, N^m	0.803	*1*
	Heater binary variable, y^h	0	*0*
	Normalised heater temperature, D^T	0	0
	Compressor number, $D^{P\prime}$	2	2
Stage 8	Number of modules, N^m	0.793	*0*
	Heater binary variable, y^h	0	*0*
	Normalised heater temperature, D^T	0	0
	Compressor number, $D^{P\prime}$	2	2
Compressor 1	Compressor binary variable, y^P	0.738	*1*
	Normalised pressure, D^P	0.262	0.221
Compressor 2	Compressor binary variable, y^P	0.979	*1*
	Normalised compressor pressure, D^P	0.021	0.013
Compressor 3	Compressor binary variable, y^P	0	*0*
	Normalised compressor pressure, D^P	0	0
Compressor 4	Compressor binary variable, y^P	0	*0*
	Normalised compressor pressure, D^P	0	0
	Annualised cost \$/yr	**5377**	**5400**

Values in italics were specified prior to optimisation.

E.3.4 Branch and bound search

The relaxed solution of the superstructure optimisation problem contains approximately seven modules. This is easily shown to be a tight constraint, as relaxed optima for six and eight modules exceed the current upper bound (not shown). Therefore, we can add the following constraint to the problem definition

$$\sum_{S=1}^{N^s} N_S^m = 7 \tag{E.8}$$

The main search is carried out by selectively fixing the binary and integer variables. After each variable has been fixed, the relaxed optimum solution is calculated using the *NLP* solver. If this solution exceeds the current upper bound, then the branch is terminated. If not, then another integer or binary variable is fixed. This is repeated until all the integer and binary variables hold integer values. It should be noted that a guarantee of global optimality is not possible so each optimisation is repeated (somewhat subjectively) from two or three different initial conditions.

In total, 40 *NLP* optimisations were required to confirm that the optimal solution corresponds to the original upper bound on the solution given in Table E.2. However, due to the need to repeat the optimisations, over 100 *NLP* optimisations were actually performed, taking a total of 35 hours of computational time.

The best design found is shown in Figure E.2. The annualised cost of this design ($5377 per year) appears to be lower than that found in Chapter 6 ($5863 per year). However, if the design is recalculated with the more accurate 2-D model that was used in Chapter 6 then the actual annualised cost is $5927 per year which is inferior to that found using the genetic algorithm approach.

The divergence from the previous design is most likely a consequence of the over simplified mathematical model used in this case. A comparison of the two designs (Figs E.2 & 6.4) reveals only small differences: the equipment requirements of the two designs are identical and there is only a slight change in the process configuration (the last four modules are connected in series rather than in parallel). The compressor pressures show the biggest difference but in both cases, a much higher vacuum is used at the end of the process than for the initial stages.

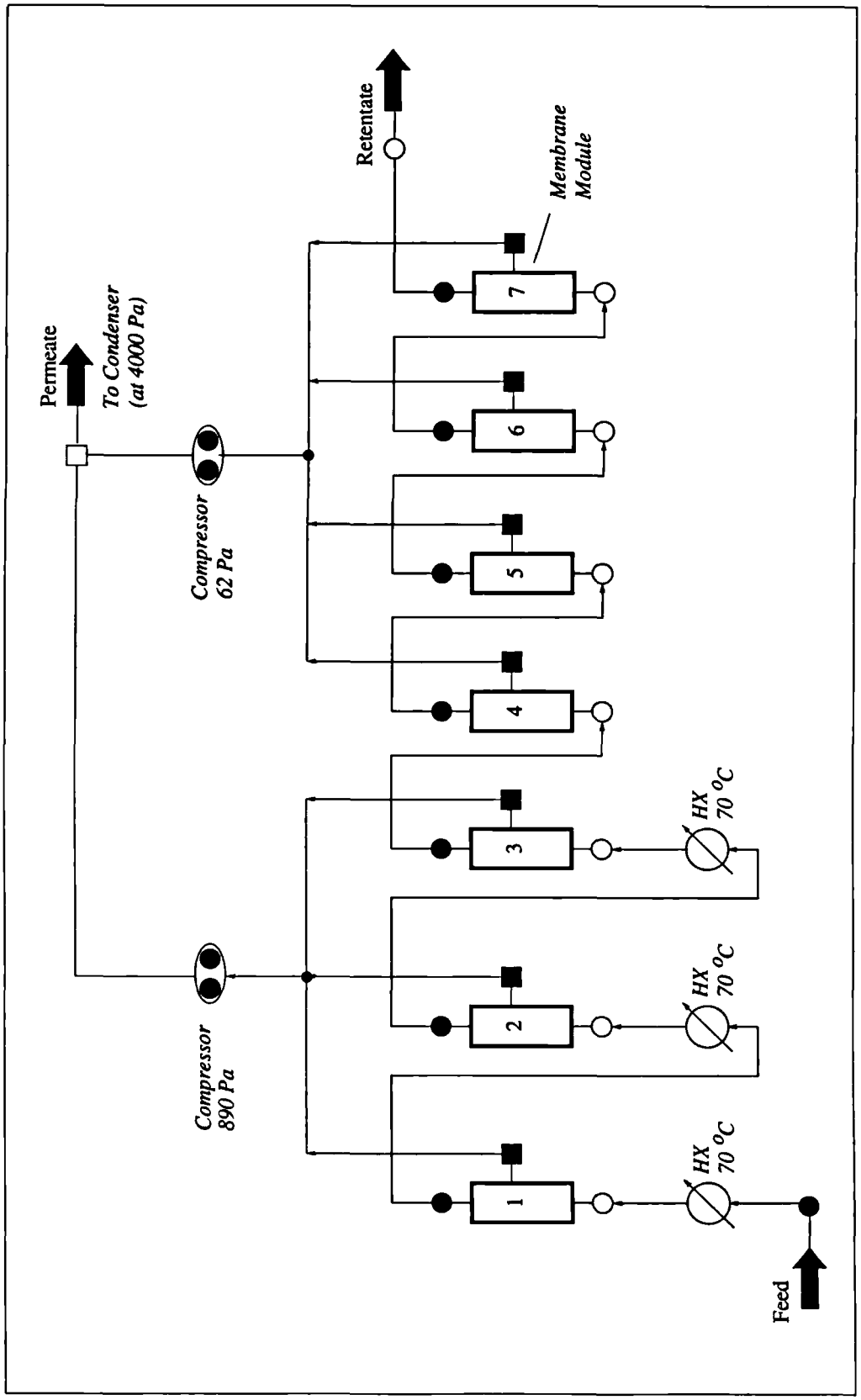

Figure E.2 *Best plant design identified using a MINLP solution technique*